Alma Mater Studiorum · University of Bologna

School of Science
Department of Physics and Astronomy
Master Degree in Physics

An exposure indicator of population classes to the electric field generated by RF telecommunications systems

Supervisor:
Prof. Giuseppe Baldazzi

Co-supervisor:
Dr.ssa Chiara Pedroli
Dr.ssa Sara Adda

Submitted by:
Elena Fusillo

Academic Year 2022/2023

Abstract

The so-called *electromagnetic pollution* generated by high frequency fields (RadioFrequencies RF, 10 kHz - 300 GHz), i.e. non-ionising radiations, is a topic of increasingly current interest given the continuous evolution of mobile network technologies.

This master thesis takes place within a ministerial project financed by the MATTM *(Ministero dell'Ambiente e della Tutela del Territorio e del Mare*) with the abbreviated title "*Programma ricerca CEM*", the "*EXP-1*" study aims to "evaluate EMF emissions from various sources, exposure scenarios and levels of exposure from new and emerging technologies and from changes in the use of established technologies". The work has been possibile through the collaboration between the ARPA (*Agenzia Regionale per la Protezione Ambientale*) Piemonte and ARPAE (*Agenzia Regionale per la Prevenzione, l'Ambiente e l'Energia*) Emilia-Romagna.

The thesis, according to the DPSIR (*Drivers, Pressures, State, Impacts, Responses*) model, realized calculations and validation of an *indicator of population exposure to electromagnetic fields generated by cellular telephone systems* (BTS – *Base Transceiver Stations*) and the consequent estimate of the population exposed to different levels of electric field.

BTS simulated electric field values from some areas of Torino, population data and building height data were analyzed. Python scripts, R scripts, QGIS and other ARPA in-house softwares were used for this purpose. The evaluation height of the simulations and the value of the electric field used, the resulting indicator calculation and the presentation of the results were justified.

Finally, an experimental validation was carried out using existing measurements to validate the results obtained and to identify possible correction factors to be applied to make the indicator estimates closer to the real exposure.

Sommario

Il cosiddetto *inquinamento elettromagnetico* generato dai campi ad alta frequenza (RadioFrequenze RF, 10 kHz - 300 GHz), ovvero radiazioni non ionizzanti, è un argomento di crescente interesse attuale, considerata la continua evoluzione delle tecnologie delle reti mobili.

Questa tesi di laurea fa parte di un progetto ministeriale finanziato dal MATTM (*Ministero dell'Ambiente e della Tutela del Territorio e del Mare*) dal titolo abbreviato "*Programma ricerca CEM*". Lo studio "*EXP-1*" mira a valutare le emissioni di campi elettromagnetici da varie fonti, scenari di esposizione e livelli di esposizione derivanti da nuove ed emergenti tecnologie e dai cambiamenti nell'uso delle tecnologie consolidate. Il lavoro è stato reso possibile grazie alla collaborazione tra ARPA (*Agenzia Regionale per la Protezione Ambientale*) Piemonte e ARPAE (*Agenzia Regionale per la Prevenzione, l'Ambiente e l'Energia*) Emilia-Romagna.

La tesi, secondo il modello DPSIR (*Drivers, Pressures, State, Impacts, Responses*), ha realizzato dei calcoli e la validazione di un *indicatore dell'esposizione della popolazione ai campi elettromagnetici generati dai sistemi di telefonia cellulare* (SRB - *Stazioni Radio Base*) con la conseguente stima della popolazione esposta a diversi livelli di campo elettrico.

Sono stati analizzati i valori simulati del campo elettrico delle SRB in alcune aree di Torino, insieme ai dati sulla popolazione e all'altezza degli edifici. Per questo scopo sono stati utilizzati script in Python, script in R, QGIS e altri software interni ad ARPA. È stata giustificata l'altezza di valutazione delle simulazioni e il valore del campo elettrico utilizzato, insieme al calcolo dell'indicatore risultante e alla presentazione dei risultati.

Infine, è stata effettuata una validazione sperimentale utilizzando misurazioni già esistenti per convalidare i risultati ottenuti e identificare eventuali fattori correttivi da applicare al fine di rendere le stime dell'indicatore più vicine all'esposizione reale.

Contents

Introduction

The so-called *electromagnetic pollution* generated by high frequency fields (RadioFrequencies RF, included in the range between 10kHz and 300 GHz), i.e. deriving from non-ionising electromagnetic radiation, is a topic of increasingly current interest given the continuous evolution of mobile network technologies (see various generations 2G, 3G, 4G and 5G).

In order to quantify the impact that the presence of these sources (called *Base Transceiver Stations* - BTS) has on the population in terms of exposure, it is necessary to resort to the definition of an appropriate environmental indicator, which takes into consideration the BTS sources, the distribution of buildings, the electric field values estimated at a chosen point of each building and the distribution of the resident population in the area.

This is done by ARPA (*Agenzia Regionale per la Protezione Ambientale*), which is an environmental and technical body present in each Italian region that supports local authorities to protect people health, ecosystems and territorial safety.

In this regard, within a ministerial project financed by the MATTM (*Ministero dell' Ambiente e della Tutela del Territorio e del Mare*) with the abbreviated title "*Programma ricerca CEM*", the "*EXP-1*" study aims to "evaluate EMF emissions from various sources, exposure scenarios and levels of exposure from new and emerging technologies and from changes in the use of established technologies" [1].

The work of this master thesis is part of this study through the collaboration between the "*Dipartimento Rischi Fisici e Tecnologici - Struttura Semplice Radiazioni non ionizzanti e servizio tarature*" of ARPA Piemonte, the "*Centro Tematico Regionale Agenti Fisici*" and the "*Unità Coordinamento CEM Area Est (Area Prevenzione Ambientale)*" of ARPAE Emilia-Romagna.

The thesis aims to carry out evaluations for the calculations and validation of an indicator of population exposure to electromagnetic fields generated by cellular telephone systems (BTS) and the consequent estimate of the population exposed to different levels of electric field.

The thesis will be structured in the following chapters:

- **Radio frequencies**: introduction to the topic of the radio frequency electromagnetic field, brief description of the functioning and technologies used by mobile telephony sources, description of the calculation methods in order to estimate the electric field for this type of sources;
- **Regulatory framework**: brief summary of the sector regulations at national and regional level with indication of the legal values to be respected, relationship between these and the exposure of the population and ICNIRP studies;
- **Study of the environmental status indicator**: introduction of the concept of indicator according to the DPSIR model, explanation of the procedure necessary for calculating the indicator of exposure to EM RF fields, description of collected data. Presentation of the problem relating to the choice of a representative value of the estimated electric field to be used: study of the distribution of estimated electric field values in the volume of typically exposed buildings, study of the buildings characteristics in the major urban centers. Justification of the evaluation height of simulations and electric field value used, consequent calculation of the indicator and presentation of the results;
- **Experimental validation**: use of existing measurements to validate the results obtained and identification of possible correction factors to be applied to make the indicator estimates closer to real exposure, calculation of the indicator on a *validation area*;
- **Discussion of the results**: brief discussion of the results obtained.

Chapter 1

Radio frequencies

In order to be able to introduce the discussion from a radiation protection point of view, a brief introduction to the physical quantities involved is necessary: electric field strength (**E**), magnetic field strength (**H**) , magnetic induction (**B**) and power density (**S**) and the plane wave approximation using Maxwell's equations for time-varying electromagnetic fields (electromagnetic waves).

1.1 The Radiofrequency ElectroMagnetic Field - RF EMF

1.1.1 Electric field

A (vector) field can be seen as a disturbance of space, such that when placed at any point in time, an object sensitive to this disturbance experiences a force. An example of this is the Earth's gravitational field.

Similarly, in analogy to the gravitational example, an electric charge Q placed in space generates an electric field, such that if a second test charge q is placed at a distance r from the first charge, it experiences a force that is attractive for charges of opposite sign or repulsive for charges with the same sign. The intensity of this force is given by *Coulomb's Law*:

$$F = \frac{1}{4\pi\varepsilon} \cdot \frac{Qq}{r^2} \tag{1.1}$$

ε is a constant that depends on the properties of the medium in which the charges are immersed, known as the *dielectric constant*. In vacuum and, with a good approximation, in air, this constant has the value: $\varepsilon_0 = 8.85 \cdot 10^{-12}\ C^2/Nm^2$

The intensity of the electric field is defined as the force acting on a unit charge placed at that point, and therefore:

$$E = \frac{F}{q} \tag{1.2}$$

Therefore, the value of the electric field generated by the charge Q at a distance r is given by:

$$E = \frac{1}{4\pi\varepsilon} \cdot \frac{Q}{r^2} \tag{1.3}$$

Assuming a positive test charge and considering that the electric field has the same direction as the Coulomb force, the field will be attractive if Q is negative and repulsive if Q is positive (Figure 1.1).

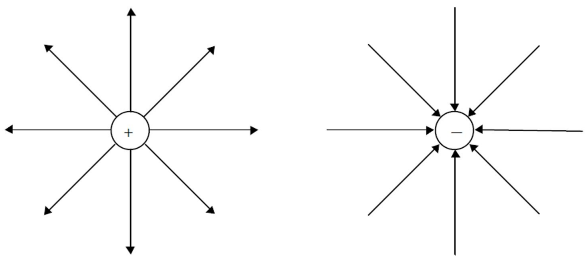

Figure 1.1: Field lines exiting/entering for the electric field produced by a positive/negative charge in space.

As can be seen from Figure 1.1, electric fields are typically represented using "field lines" (or "lines of force"). These field lines have the property that the tangent at any point indicates the direction of the force that would act on a charge placed at that point. The unit of measurement for electric field intensity E is Newton per Coulomb (N/C), but operationally, Volt per meter (V/m) is often used.

1.1.2 Magnetic field

While the electric field, as seen above, is generated by electric charges, the magnetic field is generated by magnetic dipoles or by moving electric charges. When electric charges move (such as electrons in a copper wire), an electric current is formed, which means a certain amount of charge is transported from one end to the other in a given amount of time. The amount of charge ΔQ that passes through the cross-section of the conductor in unit time Δt is defined as the *current intensity*:

$$i = \frac{dq}{dt} \tag{1.4}$$

The unit of measurement for current intensity I is the Ampere (A). If two straight wires carrying constant currents I_1 and I_2 are placed at a very small distance r relative to their length, it is observed that an attractive force occurs between the two conductors when the two currents flow in the same direction (concordant), and a repulsive force occurs when they flow in opposite directions (contrary). The intensity of the force acting on a segment l of one of the two wires is:

$$F = \frac{\mu}{2\pi} \cdot \frac{I_1 I_2 l}{r} \tag{1.5}$$

μ is a constant called *magnetic permeability* that depends on the properties of the intervening medium. In vacuum and, with a good approximation, also in air, this constant has the value of: $\mu_0 = 4\pi \cdot 10^{-7}\ N/A^2$

The magnetic field can, at this point, be introduced as a disturbance created by a wire carrying current in the surrounding space, similarly to what has been seen for the electric field. Consequently, it can therefore be defined the vector *magnetic induction*, whose intensity is:

$$B = \frac{\mu}{2\pi} \cdot \frac{I}{r} \tag{1.6}$$

The magnetic field H is a quantity related to the magnetic induction B according to the relationship:

$$\overrightarrow{B} = \mu \cdot \overrightarrow{H} \tag{1.7}$$

The field lines for a straight conductor can be observed in Figure 1.2.

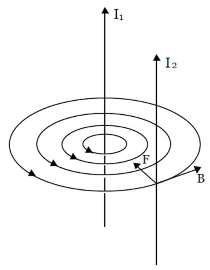

Figure 1.2: Magnetic field lines for a straight conductor.

In Figure 1.2 it can be observed that, unlike what occurs in the case of electric fields, in a magnetic field, the direction of the tangent to the field lines does not coincide with the direction of the force vector because it is perpendicular to the field direction. As mentioned earlier, a magnetic field can also be generated by magnetic dipoles. Magnets (or magnetic poles) consist of a South pole (field lines entering) and a North pole (field lines exiting) and generate a field pattern identical to that created by a circular current loop (Figure 1.3).

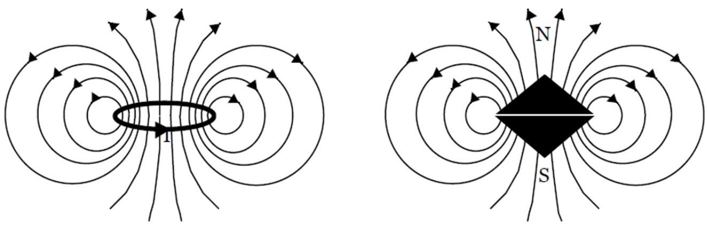

Figure 1.3: Magnetic field lines generated by a circular current loop (left) and by a magnet (right).

The close analogy between the field generated by a magnet and that generated by a circular loop of current led to the hypothesis, later confirmed, that the magnetic field is actually always produced by moving electric charges, even in the case of permanent magnets. The unit of measurement for magnetic field is Ampere per meter (A/m), while the unit of measurement for magnetic induction is the Tesla (T). Occasionally, the Gauss (G) is also used as a unit of measurement for magnetic induction. Below are the conversions applicable for fields in vacuum or air:

$$1\,T = 7,958 \cdot 10^5\,\frac{A}{m} \cdot 1\,T = 10^4\,G \tag{1.8}$$

1.1.3 Electromagnetic waves

Up to this point, static electric and magnetic fields have been considered, meaning fields that do not change over time. However, when one starts to consider time-varying fields, it is discovered that the magnetic field and the electric field are related. In other words, any change in the electric field gives rise to a magnetic field, and vice versa. In this way, magnetic and electric fields generate each other and can propagate through space independently of the charges and currents that generated them [2].

This propagation has a wave-like character (hence the term *electromagnetic waves*) and occurs at a speed equal to:

$$v = \frac{1}{\sqrt{\varepsilon \cdot \mu}} \tag{1.9}$$

In vacuum, and with good approximation, also in air, this speed corresponds to the *speed of light* c, where:

$$c = \frac{1}{\sqrt{\varepsilon_0 \cdot \mu_0}} \approx 3 \cdot 10^8 \; m/s \tag{1.10}$$

The mathematical relationships that describe the behavior of electromagnetic waves are the *Maxwell's Equations*:

$$\begin{cases} \vec{\nabla} \cdot \vec{D} = \rho \\ \vec{\nabla} \cdot \vec{B} = 0 \\ \vec{\nabla} \times \vec{E} = -\dfrac{\partial \vec{B}}{\partial t} \\ \vec{\nabla} \times \vec{H} = \vec{j} - \dfrac{\partial \vec{D}}{\partial t} \end{cases}$$

where $\overrightarrow{E}$ and $\overrightarrow{H}$ are the electric field and magnetic field vectors, $\overrightarrow{D}$ and $\overrightarrow{B}$ are the electric ($\overrightarrow{D} = \varepsilon \cdot \overrightarrow{E}$) and magnetic ($\overrightarrow{B} = \mu \cdot \overrightarrow{H}$) induction vectors and finally $\overrightarrow{j}$ and ρ are the current density and charge density, respectively.

Through these equations, in theory, it is possible to fully determine the electric and magnetic fields generated by any type of source in any transmitting medium. However, in practice, the treatment becomes quite complex. Therefore, simplifications are often used that approximate the real situation well and are relatively easier to work with. One of the most important simplifications, especially for the purpose of controlling electromagnetic pollution, is that of the *uniform plane wave*.

At large distances from the sources, or more precisely, in the region located at a distance equal to the greater of the two quantities λ and $2d^2/\lambda$ (where λ and d are the wavelength and the maximum dimension of the source, respectively), called the *far-field zone*, the electric and magnetic fields become, with a good approximation, sinusoidal, in phase with each other, and orthogonal to the direction of propagation, forming a uniform plane wave (Figure 1.4).

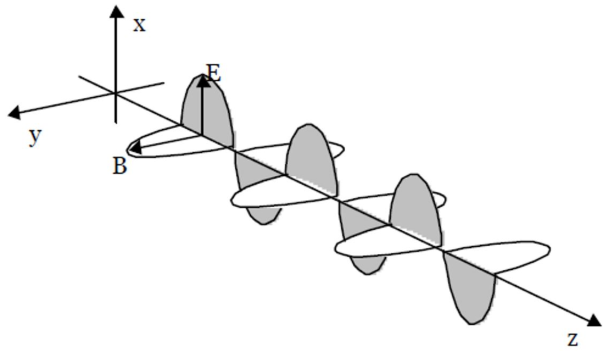

Figure 1.4: Example of uniform plane wave. Electric and magnetic fields are sinusoidal, in phase and orthogonal.

In this case, there is a constant ratio between the intensities of the electric and magnetic fields, known as the *wave impedance* Z_0, which in the case of the propagation medium being vacuum or air is given by:

$$Z_0 = \frac{|E|}{|H|} = \sqrt{\frac{\mu_0}{\varepsilon_0}} = 377\ \Omega \tag{1.11}$$

The energy carried by such a wave per unit time and per unit area perpendicular to the direction of propagation is given by the *total power density* S , which is measured in Watts per square meter (W/m^2). Its expression, in vacuum or air, is as follows:

$$S = \frac{E_{eff}^2}{Z_0} = \frac{E_{eff}^2}{377\ \Omega} = 377 \cdot H_{eff}^2 \tag{1.12}$$

where E_{eff}^2 and H_{eff}^2 are the effective values of the electric and magnetic fields which, in the case of a sine wave, are equal to $\frac{E_{max}}{\sqrt{2}}$ and $\frac{H_{max}}{\sqrt{2}}$, respectively.

The power per unit area carried by the wave is given by the magnitude of the *Poynting vector*, which is perpendicular to the vectors of the two fields and aligned with the direction of radiation propagation:

$$\mathbf{S} = \mathbf{E} \times \mathbf{H} \tag{1.13}$$

The plane determined by the direction of propagation and the vector $\mathbf{E}$ is called the *plane of polarization*. If this plane remains unchanged, the wave is called *linearly polarized*. If, on the other hand, the vector $\mathbf{E}$ rotates, the wave is said to have *elliptical polarization*. *Circular polarization* is a special case of elliptical polarization in which the magnitude of $\mathbf{E}$ remains constant during the rotation.

The conservation of energy implies that the intensity of the fields decreases as the wave moves away from the source. In other words, as the distance r increases, the surface area of the wavefronts grows proportionally as r^2, and the power density S decreases as $1/r^2$.

All of this is true when we are in the *far-field region*. As we approach the source, electromagnetic fields undergo substantial changes in structure and properties. Instead of the configuration we had in the far-field zone, where the electric and magnetic fields depended on each other, the fields have a configuration determined by the distribution of charges and currents on the source. This distribution, in turn, depends on the geometry of the source, the electrical properties of its components, and the type of connection between the source and generator.

These fields are commonly referred to as *reactive fields*. The critical distance at which the aforementioned changes occur is on the order of the wavelength λ. The transition is not abrupt but gradual. It can still be asserted that the reactive component is certainly predominant at points that are much closer than one wavelength (less than 0.1λ) to the charges and currents from which the fields originate.

Regarding the *reactive electric field*, the field lines do not form closed loops around the magnetic field lines but start from charges of one sign and terminate on those of the opposite sign; furthermore, the field intensity varies over time.

It essentially oscillates in phase with the generator's voltage; the energy stored in reactive fields does not leave the source, meaning it is not radiated but continuously emitted and reabsorbed. Emission is maximum when the generator reaches its peak and is completely reabsorbed a quarter of a period later when the generator voltage crosses zero, and the fields have zero intensity. Similarly, the magnetic field is localized around the currents flowing through the various metallic elements that make up the radiator, and its field lines form loops around the currents [2].

Due to their behavior, which is very similar to that of static fields (from which they practically only differ because their intensity oscillates over time), reactive fields are also referred to as *quasi-static fields*. Furthermore, reactive fields possess some unique properties compared to static fields, including:

- The reactive field is essentially confined near the source within a volume that extends to distances on the order of fractions of λ (typically $\lambda/10$);
- It is not associated with radiated power, and its maintenance does not require the generator to deliver real power. Only if there are objects within the reactive field capable of absorbing energy, some real power flows from the generator to these objects;
- The electric and magnetic fields typically have very complex configurations. These configurations depend specifically on the geometric and electrical structure of the conductors making up the source, as summarized in the following two points:
  - The electric field, at each instant, has a spatial distribution and intensity equal to what it would have if the set of conductors forming the source were powered by an electric generator of the same current as the instantaneous value of the actual generator. Electric field lines originate from positive charges and terminate on negative charges. The field has higher values near the conductors where there is a higher charge density, particularly near edges, points, or regions with a small radius of curvature. This is especially true where conductors with a high potential difference approach each other;
  - The magnetic field is concentrated primarily near conductors with intense currents flowing through them and has a distribution similar to that described in the case of steady currents. The field decreases rapidly as one moves away from the conductors, especially if the outgoing and returning conductors are close to each other;

- In the *near-field region*, the amplitudes E and H are not related by a constant ratio, and there is no simple way to deduce one from the other. Therefore, when both fields are present, it is necessary to separately measure their respective intensities and directions.

Other fundamental parameters of an electromagnetic wave are the frequency f, the wavelength λ, and the period T, which are defined as follows (Figure 1.5):

- f (unit of measure Hertz - Hz) = number of oscillations/second = 1/T
- λ (unit of measure meters - m) = distance between two maxima (or minima) of the sinusoid
- T (unit of measure seconds - s) = time needed to move a length λ

f, T and λ are linked to the speed of propagation of the wave (in vacuum equal to the speed of light c, equal to $3 \cdot 10^8$ m/s) by the relation:

$$c = \lambda \cdot f = \frac{\lambda}{T} \tag{1.14}$$

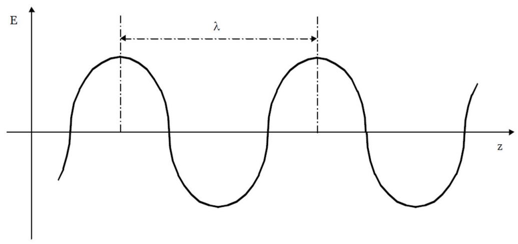

Figure 1.5: Schematic of an electromagnetic wave: indication of the wavelength.

1.1.4 Radio frequency (RF) radiations

The electromagnetic spectrum (Figure 1.6) includes various types of radiation, whose physical nature consists of the space-time oscillation of an electromagnetic field at specific frequencies (f) or wavelengths (λ). Frequency and wavelength are two physical quantities that can be interchangeably used to identify different types of radiation in

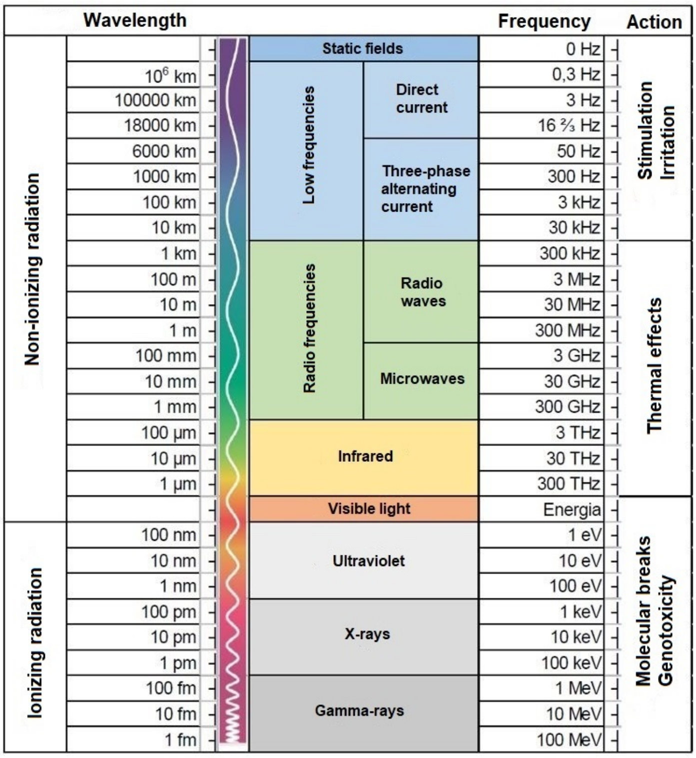

Figure 1.6: Electromagnetic spectrum.

the electromagnetic spectrum because they are closely related by the aforementioned relationship.

The term *radiofrequency (RF) radiation* (or electromagnetic fields, or waves) refers to the part of the electromagnetic spectrum that falls within the frequency range between 100 kHz and 300 GHz. RF, like visible light, belong to the *non-ionizing* region of the electromagnetic spectrum. These types of radiation do not have enough energy (expressed in electronvolt eV) to break atomic or molecular bonds. Therefore, their interaction with matter is less destructive compared to ionizing radiation, such as X-rays or gamma rays.

Unlike ionizing radiation and optical radiation, which are largely present in the environment due to natural sources, RF radiation is widespread, especially in urban environments, almost exclusively from artificial sources. RF electromagnetic fields can penetrate the body (with penetration depth decreasing as the frequency increases) and cause vibrations of electrically charged or polar molecules. This results in friction and, consequently, the production of heat. Tissue heating is the only critical effect of RF exposure relevant to health and safety that has been scientifically demonstrated to date [3].

1.1.5 Radio frequencies and information

RF electromagnetic waves carry both energy and information. There are numerous technological applications of RF, primarily in telecommunications (radio and television broadcasting, radar, cell phones, WiFi), in medicine (MRI *Magnetic Resonance Imaging*, shortwave or microwave diathermy, radiofrequency ablation) and for heat generation in domestic (cooking and heating food) or industrial (welding plastic sheets or melting metallic objects in jewelry and mechanical industries) uses [3].

For the majority of the population, exposure to RF electromagnetic fields is primarily due to two main types of sources:

- Installations that emit signals used in telecommunications (broadcasting antennas for radio and TV, BTS *Base Transceiver Stations*, WiFi installations), which can be termed *fixed environmental sources*;
- Personal devices (cell phones, cordless phones, laptops and other wireless devices).

Fixed environmental sources result in prolonged exposures over time that affect the entire body, whereas personal devices are sources of non-continuous exposures that specifically affect a part of the body.

A third category of sources found in household or common use environments includes microwave ovens (which, despite being equipped with shielding, can emit RF radiation) and various devices that transmit RF signals over short distances (security systems, toll collection devices and remote controls). These sources emit low-intensity and short-duration RF fields, so they do not result in significant levels of exposure [4].

Telecommunication installations, such as radio and television signal transmitters and Base Transceiver Stations, are designed to ensure signal reception by users of the service within a certain area. For this reason, these installations generate RF electromagnetic signals that need to be ubiquitous, thus creating a background level of RF radiation across the entire territory. The intensity of radiation emitted by these installations, in terms of the electric field level, decreases as $1/d$ thus being inversely proportional to the distance from the source.

When assessing the impact of these sources on population exposure, it is also important to consider that RF radiation is shielded by building structures, significantly reducing its intensity inside them (up to approximately 10 times, depending on the construction materials used). This factor is of great importance for the average exposure of the population, given that most of the time during a day is spent indoors, either at home or in workplaces.

In Table 1.1, for illustrative purposes, some values of RF radiation attenuation for different types of buildings are provided. The attenuation values are expressed in decibels (dB) and correspond to factors that reduce electric field levels ranging from 1.4 (3 dB) to 10 (20 dB).

		Attenuation	
Typology	**Structure (material)**	**(dB)***	**(dB)****
Sheds in open area	Corrugated sheet metal, metal framed windows	20	–
Commercial buildings or offices	Reinforced concrete, metal framed windows	15	19.5
Buildings with predominant glass	Reinforced concrete and glass	12.5	17
Buildings in urban area	Reinforced concrete and/or masonry (very thick walls)	10	14.5
Buildings in suburban area	Bricks (medium thickness), fiber cement	6	7.5
Isolated buildings in open area	Bricks (medium thickness), wood	3	4.5

* Average attenuation values for rooms adjacent to the external wall; **Average attenuation values for more internal rooms

Table 1.1: Attenuation factors of radiofrequency electromagnetic fields for some types of buildings (indicative values of the order of magnitude) [5].

Human exposure to RF electromagnetic fields is determined not only by signal intensity but also by its frequency. As the frequency increases, the penetration depth of the electromagnetic field into the human body decreases, and consequently, the absorption of electromagnetic energy is limited to more superficial tissues. For example, at the typical frequencies of radio signals (88-108 MHz), the penetration depth is approximately 10 cm, while it reduces to values on the order of 1 cm at the frequencies used for mobile phones (800-2500 MHz) and WiFi systems (around 1-5 GHz).

1.2 Territorial Coverage: Base Transceiver Stations (BTS) and Cells

1.2.1 Environmental fixed sources

Fixed telecommunication installations are designed to achieve targeted coverage of a specific area, ensuring signal reception for as many users as possible while avoiding unnecessary energy dispersion and limiting potential interference with signals from other installations. To guarantee coverage of more distant areas, these installations must transmit signals by orienting the emission along a vertical direction with a slight angle of inclination relative to the horizon, avoiding irradiation of closer areas. To clarify how this affects exposure, the radiation emitted by the antenna can be compared with the beam of light emitted by a lighthouse that illuminates a part of the territory propagating within a cone, with a gradual loss of intensity along the direction of radiation: the level of the electromagnetic field in the "illuminated" area by the beam will be higher than that in the "shadow" zone.

The intensity of the electromagnetic field near a telecommunications installation depends on various factors: the distance from the installation, the RF power it is powered with, its height above ground, the radiation pattern (*radiation diagram*), and the downward tilt angle of the radiation beam (*antenna tilt*).

Figure 1.7: Exposure modes at different distances from a BTS.

As an illustrative example, Figure 1.7 shows an apparently paradoxical case. The highest levels of the electromagnetic field emitted by the telecommunications installation are found in house A, which is the farthest from the antenna. This is because house A is in the direction of maximum radiation from the antenna, while house B, despite being closer to the antenna, is in a shadow zone with significantly lower radiation. On the other hand, house C, located at the same distance from the antenna as house B, is not exposed at all because it is in an area where there is no radiation of the electromagnetic field. Many antennas used in the telecommunications sector are "directional", meaning they are designed to primarily radiate the electromagnetic field toward the area in front of the installation.

The distance from the transmitting antenna, considered in isolation, is not a reliable indicator of exposure. This also can be qualitatively understood from Figure 1.8, which highlights the radiation lobe within which values above a predefined threshold are recorded. Consequently, a building at a greater distance may still have higher electric field values.

Figure 1.8: Example of the vertical extension of the radiation lobe.

To accurately assess the level of exposure, measurements (environmental or personal) or theoretical calculations based on geospatial propagation models are required. These calculations take into account factors beyond just transmission power and source-receiver distance. They also consider other relevant factors like antenna height, tilt, radiation pattern, as well as absorption and reflection by obstacles such as trees, vegetation, metal structures, and building walls [3]. These theoretical calculations will be addressed in Section 1.4.

1.2.2 Radio-TV transmitters and Base Transceiver Stations for mobile telephony

In *broadcasting*, the service requires the transmission of information from a transmitting system (the transmitter) to multiple receiving systems (the antennas of television or radio devices), and it is important to cover the largest possible territory with a single system, while remaining compatible with interference from signals coming from other installations. This explains the high power levels of broadcasting systems, which can reach several tens of kilowatts (kW). In reality, the highest power values are now typical of radio systems, as the transition to digital technology and the resulting increased "signal robustness" have led to a reduction in the power of television installations.

As for mobile telephony, the user is not a passive receiver of information but also transmits signals to communicate with fixed installations (*base stations*) located in the area and, through them, with other users. For this type of service, it is necessary to divide the territory into regions (called *cells*) of radio frequencies dedicated to communication between users (users of mobile devices), with each cell having a single transceiving antenna. The term *cellular telephony* derives from this division of the territory into cells (Figure 1.9).

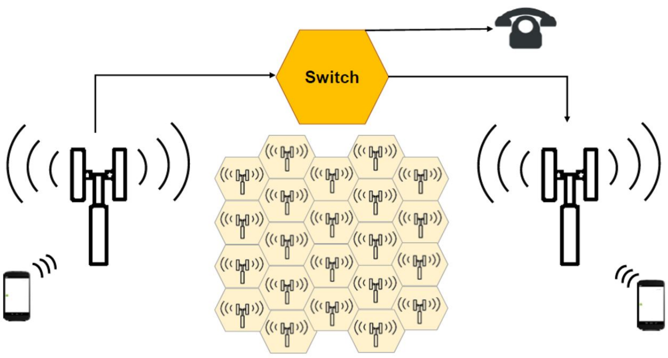

Figure 1.9: Schematic representation of how *cellular telephony* works.

Due to the limited size of the cells, which in densely populated urban areas have a coverage radius of 300-400 meters, mobile telephony installations are characterized by power levels that reach at most a few hundred watts, much lower than those of radio and television transmitters.

The highest levels of RF electromagnetic field from *fixed environmental sources* can therefore be detected in areas affected by radio and television transmitter sites. However, since these sites are often located in non-urban areas, such as on the tops of hills or elevations, residents in areas with high levels of RF signals emitted by radio and TV transmitters represent a small fraction of the population.

Mobile phone *base stations*, mainly distributed in urban areas, can lead to higher levels of electromagnetic fields in the immediate vicinity, i.e., on the upper floors of buildings facing the antennas. Greater height above the ground corresponds to higher field levels due to both the closer proximity to the *base stations* and the reduced shielding provided by buildings, which, in densely built areas, results in a significant attenuation of signals at ground level.

RF electromagnetic field levels in urban areas have often been the subject of experimental investigations by ARPA Piemonte in the city of Turin, since 2001 [6] and up to the present days (see Chapter 4). In investigations carried out in 2001, the RF electromagnetic background was characterized at various points, located in different districts of the city, at different heights above ground, with frequency-selective measurements in order to assess the contributions due to radio and television signals and those of mobile telephony. The results not only showed a prevalence of contributions due to television signals, but also lead to values that were always well below the *attention value* of 6 V/m.

1.3 Mobile Communication Technologies (TACS, GSM, UMTS, LTE, 5G)

All telecommunications services based on the free propagation of the electromagnetic field require the existence of a transmitting site from which the field radiates into the surrounding environment. With some variations depending on the application, transmitting sites can be thought of as essentially consisting of three fundamental elements: the *transmitter*, the *transmission line*, and the *transmitting antenna* [7].

The *transmitter*, in particular, includes a carrier generator that produces a sinusoidal signal oscillating at the working frequency assigned to the transmitter; a modulator that overlays the information to be broadcast on the carrier, and an amplifier that raises the modulated signal to the desired power level.

The *transmission line* is a guiding structure that connects the transmitter to the antenna, allowing the transfer of power generated by the transmitter to the antenna, which will radiate it into space. It is important to note that losses of the generated power occur along the connecting line, and these losses can be significant, especially at high frequencies.

The *transmitting antenna* is the component responsible for radiating into space the energy received from the transmitter through the connecting line. As will be shown later, the characteristics of the antenna determine the main directions in which the signal is directed and the ways in which the signal is distributed in space.

Different communication systems using electromagnetic waves for signal transmission operate in different frequency ranges. Taking cellular telephone systems into consideration, we can refer to Figure 1.10 to highlight their main technical characteristics.

		Frequency [MHz]		Channel width [kHz]	Power [kW]	Gain G_{max}	Signal encoding	Modulation	Multiple access
		Downlink	*uplink*						
Base stations for mobile telephony	**TACS**	917÷950	872÷905	25	Up to 0.3	Up to 70	analog	Frequency	FDMA
	GSM	925÷960	880÷915	200			digital	Frequency GMSK	FDMA÷ ÷TDMA
	DCS	1805÷1880	1710÷1785						
	UMTS earth asymmetric	1900÷1920 and 2010÷2025		5000				Phase QPSK	TD-CDMA
	UMTS earth symmetric	2110÷2170	1920÷1980						W-CDMA
	UMTS satellite	2170÷2200	1980÷2010						
	4G-LTE	832÷862 1710÷1785 1920÷1980 2500÷2570	791÷821 1805÷1880 2110÷2170 2620÷2690					QPSK e QAM Amplitude	SC-FDMA
	5G	main 758÷803 3600-3680 26500-27500	main 703÷748 3600-3680 26500-27500	**[MHz]** 5,10,15,20 Up to 100				F-OFDM	NOMA

Figure 1.10: Main characteristics of mobile telephony systems.

Considering the entries in Figure 1.10, it can be seen that the frequency range within which cellular telephony installations operate is further subdivided into *downlink* and *uplink* frequencies (Figure 1.11). This division is related to the necessity for bidirectional telephone communication. In this context, downlink frequencies are used for communication from the transmitting antenna to the mobile device, while uplink frequencies are used for communication from the mobile device to the antenna. The cellular phone system is undoubtedly much less powerful than the more potent installations found in the category of broadcasting stations.

Continuing with reference to the entries in Figure 1.10, it is worth noting that *modulation* is the technique used to enable an electromagnetic wave to carry information. A perfectly sinusoidal waveform, in which amplitude, frequency, and phase remain constant over time, is unable to carry any type of information. To make this possible, one of the three parameters of the sine wave must be varied over time in such a way that this variation is uniquely associated with the information to be transmitted. In par-

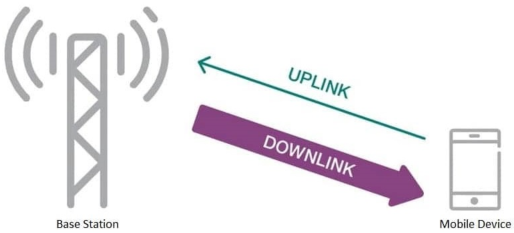

Figure 1.11: Downlink and uplink between a device and the network.

ticular, the sinusoidal waveform (called the *carrier*) is modulated in one of the three mentioned parameters by the *modulating signal*, which is the electrical signal derived from the information to be transmitted.

Depending on which parameter is modified, it can be achieved *amplitude modulation*, *phase modulation*, or *frequency modulation*. When the modulated signal reaches the receiver, it will need to undergo the reverse process of modulation, i.e., it will need to be *demodulated*, in order to extract the contained information [7].

Also, regarding the entries in Figure 1.10, *multiple access* refers to the technique used in various systems to ensure the possibility of multiple communications of the same type coexisting in the same geographic area. For example, a single radio or television device must be able to receive multiple different programs without them overlapping, multiple mobile phone users (from the same operator or different operators) must be able to make calls simultaneously without interfering with each other, even when they are very close to each other, and so on. To make this possible, various distinct techniques have been developed, known by the English acronyms FDMA, TDMA, CDMA and OFDMA.

In short, the FDMA (*Frequency Division Multiple Access*) technique involves dividing the frequency range assigned to a particular service into a certain number of channels (i.e., narrower frequency intervals), each of which is allocated to a specific broadcaster. The simplest case is that of *Frequency Modulation* (FM) radio broadcasting, which is allocated the frequency range between 88 and 108 MHz. This band is divided into 100 channels, each with a width of 200 kHz. Each broadcaster in a given area will have access to one of these channels. This allows up to 100 FM broadcasts to coexist simultaneously in each geographical area. For example, if a broadcaster operates at a frequency of 91.5 MHz, it actually uses the channel between 91.4 and 91.6 MHz. The channel width is particularly related to the amount of information per unit of time that can pass through it, and therefore, the quality of the transmission. A 200 kHz channel, typical of FM radios, provides high-fidelity stereo audio quality, while a 25 kHz channel, typical of TACS (1G) telephony technology, allows for acceptable voice transmission only.

With TDMA (*Time Division Multiple Access*) technique, communications of the same type use the same frequency but in distinct small time intervals or slots. A combination of FDMA and TDMA techniques is used in GSM (*Global System for Mobile Communications*) technology.

The CDMA (*Code Division Multiple Access*) technique allows communications to coexist at the same frequency all the time, making them distinct through the use of digital codes. This access technique is used in UMTS (*Universal Mobile Telecommunications System*) technology.

A graphical representation of these three access techniques is shown in Figure 1.12.

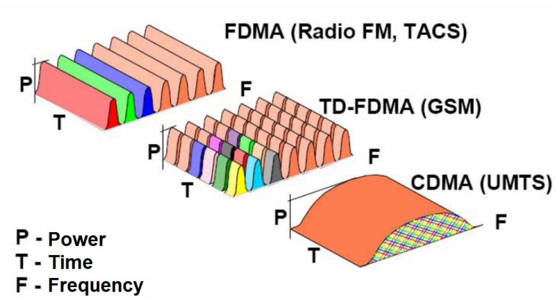

Figure 1.12: Different multiple access techniques used in radio and telephony technologies up to 3G.

Finally, the OFDMA (*Orthogonal Frequency Division Multiplexing Access*) technique transmits multiple closely spaced orthogonal subcarrier signals with overlapping spectra, with each carrier modulated with bits from the incoming stream so multiple bits are being transmitted in parallel. Multiple access is achieved by assigning subsets of subcarriers to individual users, thus allowing simultaneous low-data-rate transmission from several users. This technique is used in LTE (*Long Term Evolution*) and 5G technologies, achieving much lower latency and greater flexibility.

Finally, in Figure 1.10, there is an indication of the *gain* of the antennas used in the various systems under consideration. In technical terms, an antenna has a *maximum gain* (G_{MAX}) if the power density it produces at a certain distance in the direction of maximum radiation is greater by a factor of G_{MAX} than what would be produced at the same distance by an isotropic antenna fed with the same power. An *isotropic antenna* is one that radiates in all directions with equal intensity. The gain of an antenna is, by definition, a dimensionless quantity. However, for practical reasons, it has become customary to express gain in decibels (dBi).

With the following relationships, it is possible to convert between the value in dBi (G_{dBi}) and the natural value G_{MAX}, and vice versa:

$$G_{dBi} = 10 \cdot Log_{10}(G_{MAX}) \tag{1.15}$$

$$G_{MAX} = 10^{\frac{G_{dBi}}{10}} \tag{1.16}$$

Now, since any antenna radiates in the direction of maximum gain more than an isotropic radiator, it must necessarily radiate less in other directions if the total radiated power is to remain the same. Therefore, the higher the maximum gain, the more the radiation is concentrated around the direction of maximum radiation.

The detailed information on how the radiated power from an antenna is distributed in various directions and in the far field is typically contained in the *horizontal* and *vertical radiation patterns*. Such patterns, an illustrative representation of which is provided in Figure 1.13 for a cellular antenna, specify, for each direction, the intensity of the emitted radiation in that direction, relative to the value in the direction of maximum radiation.

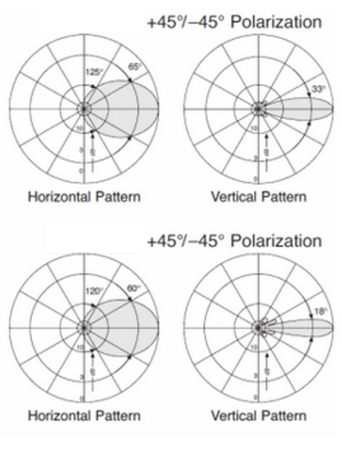

Figure 1.13: Examples of horizontal and vertical radiation diagrams or patterns.

An additional piece of practical information, related to the determination of the spatial distribution of power radiated from an antenna, concerns the HPBw (*half-power beamwidth*) in the horizontal and vertical planes. These values are typically provided by the manufacturer for each antenna, but they can also be approximately deduced from the dimensions of the antenna in the horizontal and vertical planes, relative to the wavelength of the emitted radiation.

If we denote the horizontal and vertical dimensions of the antenna as D_h and D_v, respectively, and express the angles Δ_h and Δ_v in sexagesimal degrees, the first approximation is as follows:

$$\Delta_h \cong 57\frac{\lambda}{D_h} \tag{1.17}$$

$$\Delta_v \cong 57\frac{\lambda}{D_v} \tag{1.18}$$

In other words, if, for example, an antenna is vertically extensive (relative to the wavelength), it produces a very narrow radiation beam in the vertical plane. Similarly, an antenna that is relatively narrow in the horizontal direction produces a proportionally wide beam in the same plane [7].

1.3.1 Cell phone antennas

The cellular mobile communication system has evolved over time, starting with TACS (analog), then transitioning to GSM, UMTS, LTE, and finally reaching 5G. In principle, however, the construction of communication networks for these different systems follows the same general logic. In particular, the territory is divided into *cells*, with varying sizes based on certain characteristics, each served by a *Base Station* (BS) capable of transmitting signals to mobile phones and receiving signals transmitted by them.

In order to meet all the call requests from users, the transmitters of telephony signals must cover the entire territory to ensure coverage almost everywhere. Each antenna, called a *Base Station* (BS), can emit a signal at a maximum power that cannot be infinite; for this reason, the territory is divided into smaller portions called *cells* (Figure 1.14), whose size depends on the power and sensitivity of the BS and the obstacles present. Beyond the virtual boundaries of the cell, a new cell generated by a subsequent BS is ensured to exist so that the connection is not lost.

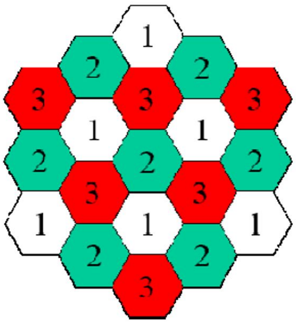

Figure 1.14: Cell coverage of the territory served by Base Stations.

The *handover* from one cell to the next, which occurs when a user in conversation moves around the territory, poses some challenges in handling that call. The probability of having a handover increases with the duration of the conversation and the size of the cell. In urban areas, where cells usually have a smaller diameter, users change cells multiple times during a conversation. For this reason, it is necessary to establish a procedure, called *Handover*, capable of managing these transitions between cells.

Figure 1.15: Actual examples of BTS installations in an urban environment.

Indeed, the need to establish bi-directional communications and ensure an adequate number of concurrent communications has led to the deployment of Base Stations (BS) even within urban areas. Figure 1.15 shows some examples of BS installations in urban environments.

The antennas typically used in Base Stations consist of various radiating elements arranged vertically and spaced equally apart. In the rear and along the vertical axis of the antenna, there is a metallic surface with a reflecting function. The antenna is then covered with plastic material for protection against atmospheric agents. Figure 1.16 shows a representation of a typical antenna with its respective horizontal and vertical radiation patterns.

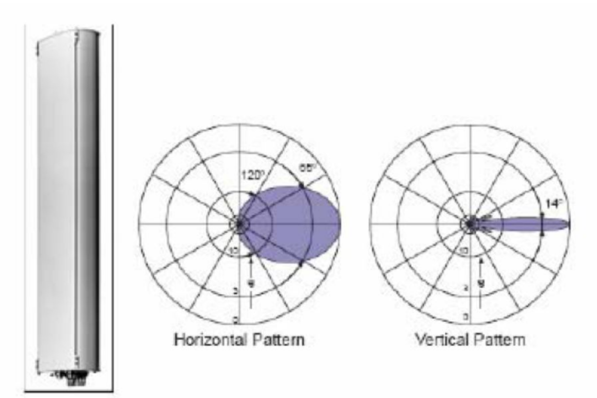

Figure 1.16: Representation of a typical Base Station with the relative horizontal and vertical radiation diagrams.

Panel antennas typically have a vertical length ranging from 1 to 2 meters, which is relatively large compared to the wavelength of the emitted radiation. The horizontal width is usually between 15 and 30 cm. Because of this, the radiated beam is relatively narrow in the vertical plane and wider in the horizontal plane. Typical half-power beamwidth values can be between 5° and 15° in the vertical plane and between 60° and 90° in the horizontal plane. The potential vertical tilt of the radiation beam, known as *tilt*, is also in the range of 0° to 15°. Tilt can be achieved by either adjusting the position of the panel during installation (*mechanical tilt*) or by modifying the vertical radiation pattern during antenna design (*electrical tilt*). These types of antennas are typically powered with wattages ranging from 100 to 300 Watts.

Regarding the values of the electric field that these antennas can generate in the environment, let's consider for illustrative purposes only the case of an antenna powered with 20 Watts and with a gain of 17 dBi (common gain values for BTSs range from 7 to 20 dBi). Referring to the values specified by regulations (6 and 20 V/m) and considering the direction of maximum radiation, it can be calculated (by means of the formulas in Section 1.4) that these values are reached at distances of approximately 29 and 9 meters, respectively. If directions other than the direction of maximum radiation are considered, it has to be taken into account the mentioned radiation patterns of the antenna to quantify the attenuation of the resulting electric field.

1.3.2 Cellphone telephony generations

At this point, it is appropriate to clarify in more detail the meaning and historical evolution of the various acronyms used in explaining access technologies [8].

1G (TACS)

Analog standards like TACS (*Total Access Communication System*) and ETACS (*Extended TACS*, an extended version of TACS with additional frequencies) mainly used in Europe, AMPS (*Advanced Mobile Phone System*) mainly used in America, and NMT (*Nordisk Mobil Telefoni*) mainly used in Northern Europe. The 1G networks transmitted data using an analog standard, which required very bulky devices due to the size of the transceiver module and the volume of the lead-acid battery, needed to compensate for the high power consumption of the device. Additionally, 1G networks had very low security levels, making intercepts and hacking possible. 1G networks became obsolete with the advent of GSM, the first 2G standard.

2G (GSM, CDMA, EDGE)

The 2G is the standard supported by all telecommunications operators, it is entirely digital which ensures full encryption of transmissions, it has better spectral efficiency and the possibility to use data services like SMS (*Short Message Service*). The coverage of the GSM network (*Global System for Mobile Communications*) uses the 900 MHz and 1800 MHz bands in Italy and most of the world, except in North America where it uses the 850 MHz and 1900 MHz bands. A cell phone that supports only the GSM frequency might not work in the USA if it's not *dual band* (meaning it doesn't support the different GSM bands). EDGE (*Enhanced Data rates for GSM Evolution*) is the standard for data transfer on the GSM network: when the "E" icon appears on the cellphone, it means the phone is connected to the internet on GSM, which is so slow that it practically prevents you from doing anything on modern smartphones.

3G (UMTS, HSPA, HSPA+)

The 3G (UMTS - *Universal Mobile Telecommunications System*) was the first revolution in cellular frequencies, with a standard that uses the 2100 MHz frequency worldwide. Thanks to 3G and HSPA and HSPA+ connections, there was a significant increase in data transmission speed, allowing not only internet browsing but also streaming videos, making video calls, and downloading applications and photos. When the phone is connected to 3G, it is visible the "H" or "H+" icon on the mobile, indicating an HSPA (*High-Speed Packet Access*) or HSPA Evolution (HSPA+) data connection.

4G (LTE)

Today, 4G is widespread almost worldwide, but it uses different frequency bands: 800 MHz, 1800 MHz, 2100 MHz and 2600 MHz. The maximum data transmission speed for LTE (*Long Term Evolution*) connections is 326.4 Mbit/s for download and 86.4 Mbit/s for upload, which is more than enough for streaming HD videos. LTE utilizes new technologies that allow it to have higher spectral efficiency, including MIMO (*Multiple Input Multiple Output*) which specifically refers to a class of techniques for sending and receiving more than one data signal simultaneously over the same radio channel by exploiting the difference in signal propagation between different antennas (e.g. due to *multipath propagation*) [9].

5G

5G is the fifth generation of mobile networks, a significant evolution from today's 4G LTE networks. 5G has been designed to meet the massive growth in data connectivity in today's modern society, especially to enable fast connections with various smart devices, not just smartphones and PCs. In the initial early phase, 5G operates alongside existing 4G networks before evolving into fully independent networks in subsequent versions, expanding coverage. In addition to providing faster connections and greater capacity, the main advantage of 5G is its rapid response time or, in more technical terms, lower latency. *Latency* is the time it takes for devices to communicate with each other over a wireless network. 3G networks have a typical response time of 100 ms, 4G is about 30 ms, but with 5G, this latency is just 1 ms, practically instant response, opening up a new world of connected applications. 5G will enable instant connectivity to billions of devices, with any object that can be connected ready to respond without delays. When a 5G connection is established, the device will connect to the 4G network to provide control signaling and to the 5G network to deliver fast data connectivity in addition to the existing 4G capacity. Like other cellular networks, 5G networks use a system of cell sites that divide the territory into sectors and transmit encoded data via radio waves. Each cell site must be connected to a network, either through wired or wireless connections. 5G is also designed to operate on much larger channels than 4G. While most 4G channels are 20 MHz, combined up to 160 MHz at a time, 5G channels can go up to 100 MHz, with up to 800 MHz combined at once.

1.3.3 Telecommunications developments: 5G systems

The 5G technology represents a development in telecommunications that may bring significant changes to the infrastructure of antenna networks installed in the territory in the near future.

There are three main categories of use cases for 5G (Figure 1.17):

1. *Massive machine to machine communications*, also known as IoT (*Internet of Things*), which involves connecting billions of devices on a large scale without human intervention. This has the potential to revolutionize modern industrial processes and applications, including agriculture, manufacturing, and commercial communications, as well as applications involving communication between sensor-equipped objects, such as smart home appliances in home automation;

2. *Extremely reliable low-latency communications* for real-time control of smart home devices, industrial robotics, automobiles, security systems, autonomous driving, and safer transportation networks. Low-latency communications open up a new world where remote medical care, procedures, and treatments are possible;

3. *Mobile broadband enhancement*: 5G's data transmission speed is significantly faster and has greater capacity to keep the world connected. New applications will include

wireless fixed internet access for homes and increased connectivity for people on the move.

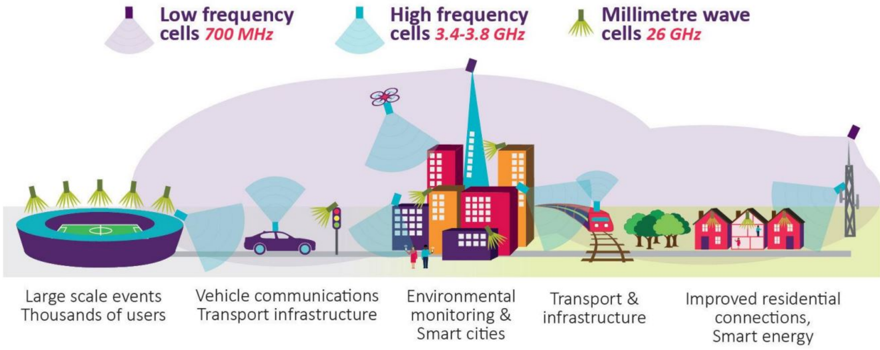

Figure 1.17: Possible applications of 5G technology.

The performance offered by 5G technology is made possible, in part, thanks to *beam-forming*, which is the ability to direct the radiation beam emitted by the base station towards the user (Figure 1.18) [3]. The greater directivity of the radiation beam coverage will be associated with a greater spatial and temporal variability of exposure to these systems.

Based on the expected characteristics of the radiating systems used, in order to correctly assess exposure, it will be necessary to consider not only the average values of the electromagnetic field but also the maximum values reached for short exposure periods. This aspect will require an adaptation of national regulations, which currently

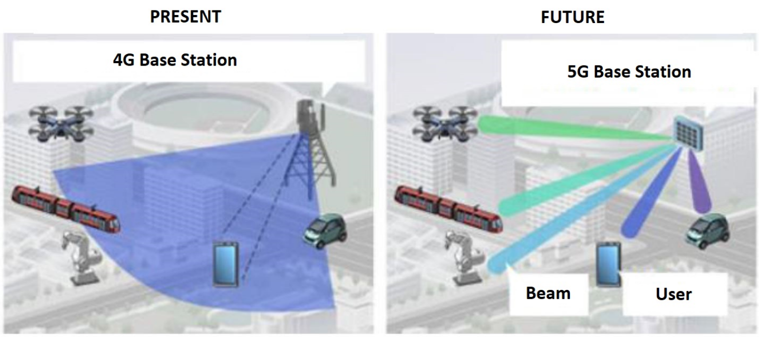

Figure 1.18: Comparison between the radiation beam emitted by 4G base stations (fixed radiation diagram) and 5G (dynamic and user-directed radiation diagram).

do not consider short-duration exposures but only continuous exposures, establishing limits based on averaged electromagnetic field values over 6 minutes or 24 hours.

In Italy, the 5G systems operate in the frequency bands of 694-790 MHz, 3.6-3.8 GHz and 26.5-27.5 GHz [10]. The 26.5-27.5 GHz band corresponds to the so-called *millimeter waves*, which, due to their high attenuation during propagation, result in areas of very limited coverage. This characteristic, along with the multitude of applications for 5G technology (human-to-human, human-to-machine, machine-to-machine connectivity), will lead to a significant increase in the number of installations across the territory [11].

The introduction of 5G technology could lead to complex exposure scenarios with highly variable levels of electromagnetic fields in terms of time, space, and frequency band resource usage. Consequently, a single value (average or peak) assessed over an area or time interval might not be a valid metric to effectively describe an exposure characterized by unprecedented uncertainty and variability. Traditional methods for exposure estimation will need to be complemented with other techniques, such as stochastic methodologies, to address this complexity [12].

The *International Electrotechnical Commission* (IEC) has already considered a statistical method for assessing exposure near Base Stations for telecommunications in the IEC 62332 standard from the third edition published in 2022 [13]. The application of this method to specific case studies involving antennas emitting 5G signals is described in the second edition of the IEC 62669 standard, published in 2019 [14].

According to the approach described in the IEC standards, the average levels of electromagnetic fields emitted by the antenna are theoretically estimated, in a prudent but realistic manner, based on a spatial statistical distribution of users within the coverage area. The statistical average level of electromagnetic emission will then be assessed on a radiation diagram of the 5G antenna, similar to the one illustrated in Figure 1.19, consisting of an envelope (black peripheral graph) of various diagrams (central graphs) associated with possible configurations due to *beam-forming*.

To the diagram thus obtained, which represents the maximum possible electromagnetic field emission from the antenna in each direction of radiation, a *statistical reduction factor* is applied, taking into account the probability of being exposed to the beam in a given position. When evaluating exposure to 5G signals, it will be necessary to consider not only the average levels of the environmental electromagnetic field estimated using

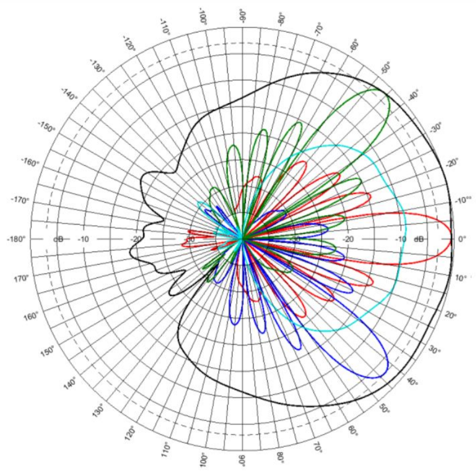

Figure 1.19: Envelope diagram of a 5G antenna.

statistical methods but also the possible peak levels for very short periods, less than a minute, which are typical of the fluctuations inherent to these signals [3].

Currently, the deployment of 5G networks, with the implementation of various services envisaged by the *Internet of Things* (IoT) and the resulting proliferation of a large number of transmitting antennas for 5G signals, is approaching a mature phase. Yet, studies support that the provisioning of 5G service over mid-band frequencies is effective in improving the throughput levels, while maintaining the exposure levels substantially unchanged compared to the pre-5G scenario. Moreover, the provisioning of 5G over sub-GHz bands does not introduce a substantial increase in the traffic levels (*throughput*), mainly because such spectrum is in reality employed to provide coverage and to carry background 4G traffic [15].

1.4 Calculation method of the radiofrequency electric field

In the case of a new installation, it is necessary to perform a series of calculations and simulations to understand whether the field emitted by this new source, when added to the existing fields, still complies with regulatory limits or if it is necessary to change the technical data or the geographical location of the installation. These simulations are essential for the operator to dimension all parameters in order to achieve the desired coverage objectives, as well as for all the authorities responsible for authorizing the creation of such an installation.

In general, it is possible to perform a theoretical evaluation of power density, electric field, or magnetic field using numerical techniques. The distribution of radiated field can be described using an integral expression that can be numerically solved. Numerical methods for solving electromagnetic problems related to antennas are based on calculating currents on the antenna with appropriate modeling and their subsequent integration.

These methods can be divided into three groups: the *method of moments* (MOM), the *finite element method* (FEM), and the *finite-difference time-domain method* (FDTD) [16].

To evaluate the electromagnetic field at a generic point in space, a simplification is employed that utilizes the far-field conditions and neglects reflections from the ground, infrastructure, and vegetation. However, it is important to consider that this calculation procedure is prudent because the field values are overestimated due to the simplifications described above. At large distances from the source, the *far-field conditions* occur, and power density at a specific point in space defined by angles θ and φ can be calculated if the antenna gain function $G(\theta, \varphi)$ and the feeding power P_{alim} are known:

$$S(r, \theta, \varphi) = \frac{P_{alim}\, G(\theta, \varphi)}{4\pi r^2} \tag{1.19}$$

Applying the impedance relationship shown in Equation 1.12, the effective values of the electric field and the magnetic field are obtained [17]:

$$E(r, \theta, \varphi) = \frac{\sqrt{30\, P_{alim}\, G(\theta, \varphi)}}{r} \tag{1.20}$$

$$H(r, \theta, \varphi) = \frac{\sqrt{\frac{P_{alim}\, G(\theta,\varphi)}{30}}}{4\pi r} \tag{1.21}$$

where

$$P_{alim}(dBm) = P_{BTS}(dBm) + G(dB) - A(dB) \tag{1.22}$$

$P_{BTS}(dBm)$ is the power output from the BTS, $G(dB)$ is the overall gain of any amplifiers placed between the BTS and the antenna and $A(dB)$ is the sum of all attenuations of passive components.

We recall that:

$$G(\theta, \varphi) = G_{MAX} \cdot D_V(\theta) \cdot D_H(\varphi) \tag{1.23}$$

where $D_V(\theta)$ and $D_H(\varphi)$ are the vertical and horizontal radiation patterns, and G_{MAX} is the gain value in the direction of maximum radiation.

The assessment of electromagnetic field levels can be carried out following these steps:

- Calculation of the local reference system of the antenna in spherical coordinates (r, θ, φ) as a function of the global reference system:

$$\begin{bmatrix} x_L \\ y_L \\ z_L \end{bmatrix} = \begin{bmatrix} \cos\alpha\cos\beta & \sin\alpha\cos\beta & -\sin\beta \\ -\sin\alpha & \cos\alpha & 0 \\ \cos\alpha\sin\beta & \sin\alpha\sin\beta & \cos\beta \end{bmatrix} \begin{bmatrix} x_G - x_A \\ y_G - y_A \\ z_G - z_A \end{bmatrix} \tag{1.24}$$

$$r_L = \sqrt{(x_G - x_A)^2 + (y_G - y_A)^2 + (z_G - z_A)^2} \tag{1.25}$$

$$\theta_L = a\sin\left(\frac{z_L}{r_A}\right) \tag{1.26}$$

$$\varphi_L = a\sin\left(\frac{y_L}{\sqrt{r_L^2 - z_L^2}}\right) sgn(x_L) + \frac{\pi}{2} sgn(y_L)(1 - sgn(x_L)) \tag{1.27}$$

- Calculation of the gain function $G(\theta, \varphi)$ (Equation 1.23);
- Power calculation $P_{alim}(dBm)$ (Equation 1.22);
- Calculation of the power density value of the electric and magnetic field (Equations 1.20 and 1.21).

In the vast majority of installations, there are multiple transmitting antennas that cover the same sectors or have radiation patterns with overlapping main lobes. In this case, it is necessary to perform electromagnetic field assessments by simultaneously considering the emissions from all antennas contributing to the field value. Considering that the M sources are uncorrelated, the field contributions are summed in quadrature:

$$E = \sqrt{\sum_{i=1}^{M} E_i^2} \qquad (1.28)$$

$$H = \sqrt{\sum_{i=1}^{M} H_i^2} \qquad (1.29)$$

$$S = \sum_{i=1}^{M} S_i \qquad (1.30)$$

To visualize variations in field levels in space, *iso-level curves* are drawn on significant sections of the space around the antennas (horizontal planes at different heights and vertical planes containing the pointing axis). In addition to these curves, the use of the so-called *volume of compliance* is useful for assessing the extent of the field for certain intensity values (Figure 1.20).

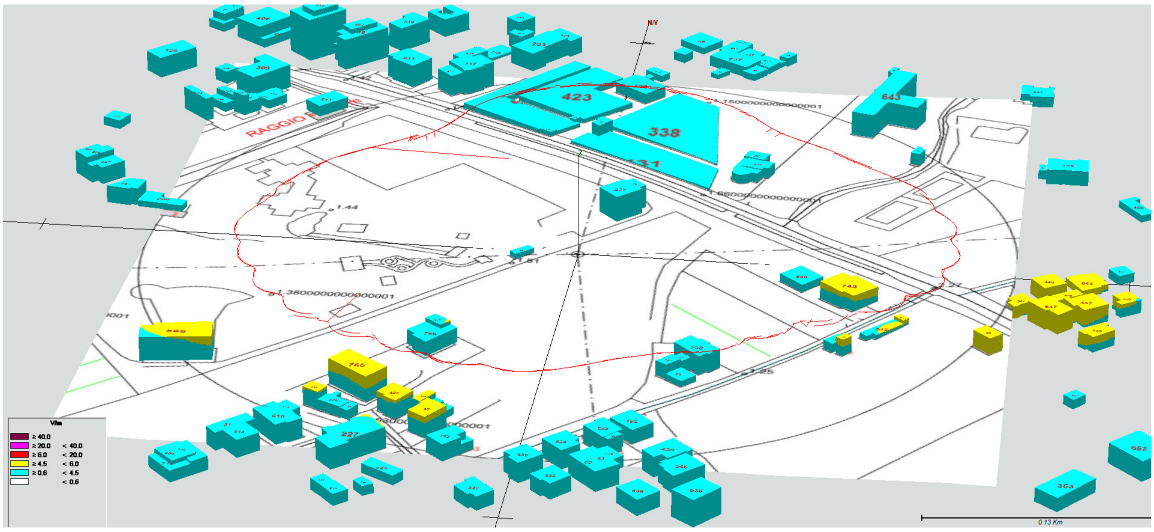

Figure 1.20: Example of a simulation using the 6 V/m *volume of compliance* (red line). The simulated electric field values are color coded and projected onto the surface of the surrounding buildings.

The *volume of compliance* is the region of space around the antenna, outside of which the electromagnetic field is lower than the considered limit value. In the presence of multiple transmitting antennas, it is not possible to use simple relationships to determine the volume of compliance. It is recommended to construct an *isosurface* at a constant field by calculating the field at a suitable set of points and connecting the isolevel points (Figure 1.21).

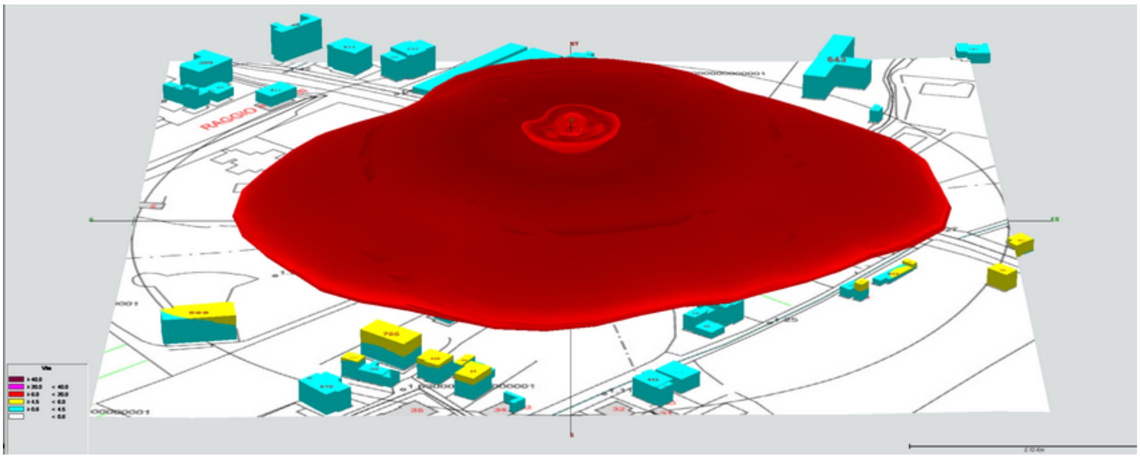

Figure 1.21: Example of a simulation using the 6 V/m *isosurface* (red solid). The simulated electric field values are color coded and projected onto the surface of the surrounding buildings.

The relationships and techniques described above are correctly applicable only at large distances from the source when the conditions of *far-field* are met. However, the power density equation S provides conservative values even for distances shorter than the far-field distance. It is possible to calculate the field distribution in the *near-field* zone of the antenna using approximate methods, given the physical dimensions and radioelectric characteristics already used in the far-field formulation. In this case as well, the limits of applicability and margins of error are difficult to verify. It is therefore advisable to perform checks through comparison with numerical methods.

Geometric optics can accurately describe the interaction of an electromagnetic field source with an object of any shape, but its validity is limited to direct and reflected fields, and it does not cover wave regions. This limitation is overcome by using the *Geometrical Theory of Diffraction* (GTD), which takes into account the diffracted field from edges, which is scattered over large regions of space. To simulate the multipath effect, *ray-tracing* algorithms are used. These algorithms aim to calculate the rays that connect a transmission point T to a reception point R, considering that these rays can be reflected and diffracted any number of times [16]. For calculation methods imposed by recent technological and regulatory developments, see Section 2.1.5.

Chapter 2

Regulatory framework

2.1 National and regional legislation - Exposure of the population - ICNIRP

It is clear that analyzes must be conducted within a regulatory framework, which is the Italian one. It is derived from the ICNIRP standards, but as far as reference values are concerned, it is strongly influenced by the principle of *prudent avoidance* [18].

2.1.1 Radiation protection and fundamental quantities

As mentioned earlier, in the electromagnetic spectrum, it is possible to distinguish between non-ionizing radiations and those that are capable of ionizing matter. While the ionizing radiations are known to be carcinogenic, there is still no clarity regarding the latter, and for this reason, they deserve a more in-depth examination. In the context of fundamental quantities related to non-ionizing radiations, the ICRU (*International Commission on Radiological Units*) introduced the physical quantity SAR.

In medical physics, SAR (*Specific Absorption Rate*) is the measure of the rate at which energy is absorbed by the human body when exposed to radiation and is expressed in Watts per kilogram (W/kg) [19].

The SAR is defined by the equation:

$$SAR = \frac{\sigma \left|\mathbf{E}\right|^2}{\rho} \tag{2.1}$$

where the following quantities are denoted:

- σ is the equivalent electrical conductivity of the sample;
- $|E|$ is the root mean square (rms) value of the incident electric field intensity;
- ρ is the sample density.

Typical reference volumes for SAR evaluation are:

- Volumes of 1g of mass (SAR_{1g});
- Volumes of 10g of mass (SAR_{10g});

$$SAR_{10g} = \frac{(Total\ power)_{V_{10g}}}{(Total\ mass)_{V_{10g}}} = \frac{\left[\int_{V_{10g}} \sigma \left|\mathbf{E}\right|^2 d\nu\right]_{V_{10g}}}{\int_{V_{10g}} \rho d\nu} \tag{2.2}$$

- The head (SAR-head, SAR_H);
- The whole body (SAR-whole-body, SAR_{WB}).

$$Whole - body\ average\ SAR = \frac{(Total\ power)_{WB}}{(Total\ mass)_{WB}} = \frac{\left[\int_{WB} \sigma \left|\mathbf{E}\right|^2 d\nu\right]_{WB}}{\int_{WB} \rho d\nu} \tag{2.3}$$

Estimating the SAR induced by exposure to electromagnetic fields is a very complex problem because it depends on many factors such as:

- Proximity to the source;
- Wavelength/body size ratio;
- Polarization of the field relative to the body's position;
- Body shape;
- Position relative to a ground plane;
- Electromagnetic properties of tissues;

- Thermal/biological properties of tissues (for example, the eyes have limited blood flow and are therefore more susceptible to heating).

For these reasons, analytical models are used to approximate the human body with homogeneous volumes of various shapes (spheres, prolate spheroids, ellipsoids, cylinders) and the absorbed power is calculated under the assumption of irradiation from a uniform plane wave. This allows for qualitative estimates of the dependence of the phenomenon on various parameters [20].

Another noteworthy quantity for estimating SAR is the *penetration depth*, defined as the distance through a material at which the magnitude of the electric field decreases by a factor of $1/e$ compared to the value at the surface.

The *penetration depth* parameter is given by the relationship:

$$\delta_S = \frac{1}{\alpha} = \frac{1}{\sqrt{\pi f \mu \sigma}} \cdot \frac{1}{\sqrt{\sqrt{1 + \left(\frac{\omega\varepsilon}{\sigma}\right)^2} - \frac{\omega\varepsilon}{\sigma}}} \tag{2.4}$$

where it can be identified a first term as that of the good conductor approximation and a second term that represents a correction factor when the previously mentioned assumption is not valid. The *penetration depth* is measured in meters (m).

The tissues of the human body can be approximated as good conductors up to frequencies of a few tens of MHz, but for higher frequencies, this is no longer valid. Therefore, it is necessary to use the complete expression of the attenuation constant α [21].

Figure 2.1 confirms the analysis related to the *penetration depth*, highlighting the inadequacy of the good conductor approximation for bodily tissues, starting from frequencies of several tens of MHz. In this case, a significant increase in *penetration depth* is observed, particularly concerning adipose tissue (blue line).

From Figure 2.2, it can be observed that there is nearly total reflection of the incident electric field by the major body tissues up to frequencies of the order of MHz. For higher frequencies, a progressive decrease in the reflection coefficient is observed, especially in adipose tissue, which reflects less than half of the radiation for frequencies of the order of GHz [20].

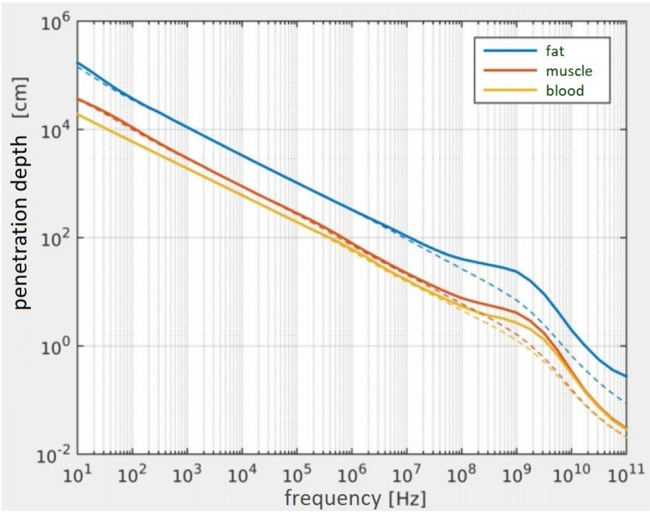

Figure 2.1: Penetration depth calculated for normal incidence as a function of frequency; the dashed curves refer to the approximate formula for good conductors [21].

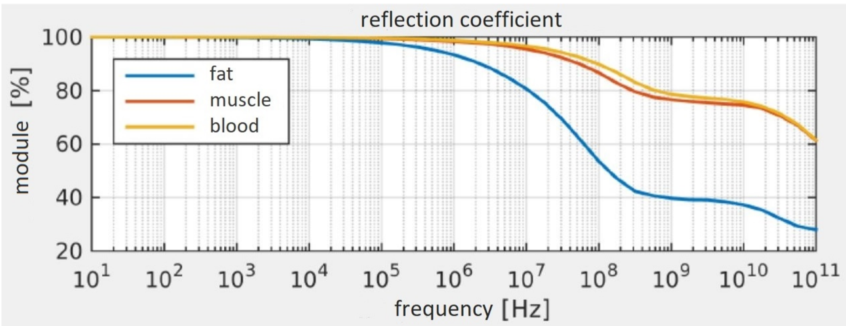

Figure 2.2: Coefficient of reflection of the electric field for normal incidence as a function of frequency [21].

2.1.2 Effects of RF radiation exposure

Analyzing the health effects on humans of electromagnetic radiation at radio frequencies that have been confirmed or hypothesized, the following effects can be identified:

- Acute thermal effects;
- Chronic effects at low exposure levels, once referred to as non-thermal effects;
- Presumed effects with a long latency period, such as tumorigenic effects.

Acute thermal effects

This category of effects can be observed following a significant increase in induced currents in the body or a prolonged increase in temperature, which can lead to localized damage to heat-sensitive organs such as the lens of the eye (cataracts) and the testicles (sterility). Well-established and reliable dosimetric studies allow for a correspondence to be established between these increases in induced current and temperature and the intensity of external electromagnetic fields, through two physical quantities: current density j and SAR.

High-intensity radiofrequency electromagnetic fields, as mentioned, can lead to well-documented and well-understood acute effects. However, the typical levels of exposure to which the population is exposed in living environments are far below the threshold levels for these types of effects.

For example, in the case of Base Stations used for mobile telephony, the low radiated powers and the highly directional characteristics of the emissions, which relatively shadow (i.e., unexpose) the areas accessible near the antennas, certainly exclude any tissue heating effect under any exposure conditions. To induce effects of this kind, significant exposures to the target organs (SAR values of at least several tens of W/kg) for rather extended periods of exposure are required [22].

Chronic effects from low-level exposure (non-thermal effects)

These effects are characterized by biological alterations, transient changes in electrical and magnetic properties of molecules and cells without demonstrable or attributable effects to biophysical phenomena. Some studies have reported conditions such as headaches, depression, drowsiness, and epileptic seizures, all attributed to *electricity hypersensitivity*, but there is no clear link to radiofrequency electromagnetic field exposure.

The *International Scientific Community* has therefore concluded that the scientific data available so far do not provide adequate evidence of a real cause-and-effect relationship between electromagnetic fields and the development of electricity hypersensitivity. Additionally, knowledge about the possible mechanism(s) underlying these conditions is entirely inadequate. Therefore, as of now, this syndrome is not associated with exposure to electromagnetic fields.

The only evidence of the effects of radiofrequency radiation, on the other hand, has been identified in some categories of workers exposed to radar, radio, and telecommunications, affecting the central nervous system, the autonomic nervous system, and the cardiovascular system, but only for prolonged exposures over many years to electromagnetic field intensities of several tens of V/m [22].

Suspected effects with a long latency period of a tumorous nature

In a limited number of epidemiological studies [23], a connection has been suggested between exposure to radiofrequency electromagnetic fields in living and working environments and an increased risk of cancer. These studies hypothesize that radiation emitted by cell phones, and to a lesser extent by Base Stations, may act as promoters of neoplasms when combined with proximity to the source and prolonged exposure over time. Epidemiological studies on the tumorigenic effects of radiofrequency exposure published to date, however, do not allow for conclusive assessments due to the heterogeneity of research designs, shortcomings in exposure assessments, and insufficient sample sizes in the studied populations [22] [24].

In 2013, the IARC (*International Agency for Research on Cancer*) classified RF-EMF as “possibly carcinogenic to humans”, allocating them to *Group 2B* of its classification system [23].

The first category described above represents the *physical effects* that can be measured, while the other two can be grouped into the so-called *biological effects*, for which it is much more difficult to draw objective and reliable conclusions. For this reason, it becomes important to distinguish biological effects into stochastic and deterministic effects.

Stochastic effects are characterized by a probability of occurrence that depends on the dose received and the absence of any threshold dose for their manifestation. For these effects, it is not possible to establish an individual causal relationship between the observed effect and the dose received.

Deterministic effects, on the other hand, only occur when the dose exceeds certain values, and their severity depends on the dose received. The threshold values for various deterministic effects are usually known and are generally quite high compared to the dose levels typically encountered in practical situations [25].

2.1.3 Exposure limits established by the ICNIRP

As the use of devices emitting electromagnetic fields below the ionization threshold becomes increasingly widespread, there has been a need to regulate exposure to these lower-frequency radiations as well.

One of the international organizations dedicated to protection from non-ionizing radiation is ICNIRP (*International Commission on Non-Ionizing Radiation Protection*), established in 1992. The ICNIRP is an independent international organization responsible for providing evidence-based guidelines and recommendations to limit human exposure to non-ionizing radiation, ensuring safety and public health protection.

The definition of dose limits for non-ionizing radiation established by ICNIRP follows a sequential scientific approach, which is outlined below:

1. Systematic literature review;
2. Identification of adverse effects;
3. Determination of the critical effect;
4. Application of reduction factors;
5. Establishment of basic restrictions;
6. Derivation of reference levels.

To define exposure standards with documented efficacy, it is essential that there are scientifically proven adverse effects with well-characterized dose-response relationships in both qualitative and quantitative terms. Scientifically proven effects are those documented by reliable epidemiological and/or experimental evidence (not attributable to errors or distortions), reproducible (replicated independently and/or consistent across studies with different designs), understandable in terms of interaction mechanisms, and consistent with other relevant scientific knowledge [20].

In light of these considerations, two types of limits can be distinguished:

- For *deterministic effects*, a threshold exposure value is identified;
- For *stochastic effects*, an acceptable level of risk is defined.

These limits are calculated by applying appropriate reduction factors to the exposure level associated with the critical effect (the adverse effect observed at the lowest exposure level). This takes into account the inevitable uncertainty in risk estimates and individual variability in biological responses. Since international standards for radiofrequency fields are aimed at preventing established harmful effects, only *deterministic effects*, for which a threshold value could be identified, have been considered. The critical level of exposure for these effects corresponds to a specific absorption rate averaged over the whole body equal to 4 W/kg.

The *ICNIRP guidelines*, in particular, include basic restrictions in terms of SAR and reference levels in terms of electric field intensity in volts per meter (V/m) (Table 2.1).

	Whole body SAR [W/kg]	**Local SAR [W/kg]**
Workers	0.4	10
Population	0.08	2

Table 2.1: Basic restrictions in terms of SAR according to the ICNIRP guidelines [3].

The basic restrictions for workers correspond to SAR values of 0.4 W/kg for whole-body exposures and 10 W/kg for localized exposures, while for the general population, the corresponding SAR values are 0.08 W/kg and 2 W/kg. Please note that the whole-body SAR limit for the public corresponds to one-fiftieth (1/50) of the critical value.

These restrictions are independent of the frequency band because they directly refer to the absorbed energy which, when converted to heat inside the body, can cause general or localized overheating damage.

Due to the mechanisms of electromagnetic field coupling with the human body, however, at the same level of external field, the absorption of energy varies depending on the frequency, and for this reason, the guidelines provide variable reference levels of electric field intensity by frequency (Figure 2.3) [3] [26].

Despite the guidelines previously outlined, ICNIRP has given individual states the freedom to establish their own limits for their areas of jurisdiction.

In particular, the European Union has adopted the aforementioned standards for the prevention of health risks arising from exposure to radiofrequency fields, both for the general population (Recommendation 1999/519/EC) and for workers (Directive 2013/35/EU). Countries like Italy, on the other hand, have chosen to implement more restrictive measures, as described in Subsection 2.1.4.

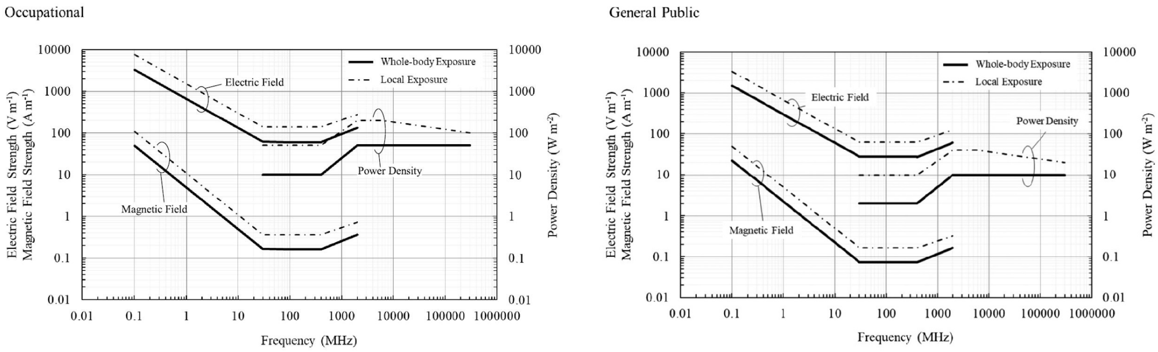

Figure 2.3: Reference levels for time averaged exposure (occupational and general public) of ≥ 6 min, to electromagnetic fields from 100 kHz to 300 GHz [26].

2.1.4 Exposure limits for the population in Italy

Regarding the general population, with the D.P.C.M. of July 8, 2003 [27], concerning electromagnetic fields at frequencies between 100 kHz and 300 GHz, Italian regulations adopted the ICNIRP standards for most sources of radiofrequency exposure, except for fixed radio and television sources and telecommunications. For these specific sources, stricter *exposure limits* (in Italian "limite di esposizione") were set at 20 V/m in the frequency range between 3 MHz and 3 GHz, as well as *attention values* (in Italian "valori di attenzione") and *quality objectives* (in Italian "obiettivi di qualità").

The *attention values* consist of a reference level of 6 V/m that should not be exceeded in areas with prolonged exposure (> 4 hours). *Quality objectives*, on the other hand, require the same reference value of 6 V/m to be met in heavily frequented outdoor areas, such as places intended for social activities (Table 2.2).

Frequency [MHz]	**ICNIRP Reference Level**	**Italy Limit Value**	**Italy Attention Value and Quality Objective**
10-100	28 V/m	20 V/m	6 V/m
915	42 V/m		
1800	58 V/m		
2000-2700	61 V/m		

Table 2.2: Comparison between ICNIRP reference levels and the current limits in Italy for the frequency bands used by radio and television transmitters and telecommunication facilities [3].

Following the amendments to the D.P.C.M. of July 8, 2003, introduced by L. 221/2012 [28], both the *attention values* and *quality objectives* are no longer to be understood as values averaged over six minutes but as values averaged over a 24-hour period.

The choice made by the Italian legislator to establish attention values and quality objectives in terms of electric field levels lower than those set for the limits is based on a *prudent avoidance approach*, aiming to limit potential long-term effects. Therefore, the reduction factor is entirely arbitrary [3].

In light of the values mentioned above, it should be noted that the attention value of 6 V/m as stipulated by Italian regulations must be applied in all homes and offices, making it the valid reference level in urban areas as well.

Taking into account the typical variability of emission levels from facilities such as Base Stations, the maximum exposure levels allowed by national regulations are, in urban areas, significantly lower than those set by ICNIRP, being ten times lower at frequencies around 2 GHz (2000 MHz), which are typical of some mobile phone systems [3].

Regional laws in the sector establish the authorization procedures for mobile and telecommunications installations in general. The "Legge quadro" on the protection from exposure to electric, magnetic, and electromagnetic Fields, L. n° 36 of February 22, 2001 [29], defines the competencies of the various involved entities and provides definitions for *exposure limits*, *attention values*, and *quality objectives*.

2.1.5 Regulations and standards on electric field calculation

Law n° 221/2012 [28], which converted into law, with amendments, Decree-Law No. 179 of Oct. 18, 2012, established that for measurement techniques, the technical standard CEI 211-7 [30] must be followed and for predictive calculation techniques, the technical standard CEI 211-10 [17] or subsequent ones.

The text introduces important novelties going to modify what was established by the D.P.C.M. July 8, 2003, that are:

- the field levels to be compared with the *exposure limits* in Table 1 of Annex B of the D.P.C.M. July 8, 2003, understood as RMS values (i.e. *Root Mean Square*), must be measured at a height of 1,50m above the floor level only and must be averaged over any 6-minute interval;

- the field levels to be compared with the *attention values* in Table 2 of Annex B of D.P.C.M. July 8, 2003, understood as effective values, are to be measured at the height of 1,50 m above the floor level only and are to be averaged over any 24-hour interval;
- the field levels to be compared with the *quality objectives* in Table 3 of Annex B of the D.P.C.M. July 8, 2003, understood as effective values, are to be measured at a height of 1,50 m above floor level only and are to be understood as the average of the values over 24 hours.

It is also specified that the *attention values* must be applied inside buildings used as living environments with continuous stays of not less than four hours a day and in their *outdoor appurtenances*. Regarding outdoor appurtenances, please refer to the definition given in the Guidelines prepared by ISPRA and ARPA/APPA (D.M. 7/12/2016) [31].

For the purpose of verification through forecast estimation of the attention value and quality objective, the instances provided for in D. Lgs. No. 259/2003 (in Italian "Codice delle comunicazioni elettroniche") [32] will be based on values averaged over the 24-hour period, evaluated on the basis of the reduction of the maximum power at the antenna connector with appropriate factors that take into account the temporal variability of the emission of the installations over the 24-hour period.

In addition, where external building appurtenances are absent, the forecast calculations should take into account the electromagnetic field absorption values by building structures. The power reduction factors and attenuation values by building structures mentioned above will be defined within the ISPRA-ARPA/APPA Guidelines.

To take into account the temporal variability of installation emission over 24 hours [33], the factor α_{24h} defined as follows is introduced (Formula 2.5):

- for each electromagnetic signal generated by an installation corresponding to a service type (GSM, UMTS, LTE, 5G...);
- emitted in a specific sector;
- on a particular frequency band (BTS or radio/TV installations) i.e. *signal*.

$$\alpha_{24h} = MAXIMUM\ VALUE\ on\ an\ annual\ basis\ of\ the\ daily\ coefficient\ \alpha_{24h}^{day} \tag{2.5}$$

$$\alpha_{24h}^{day} = \frac{1}{m}\sum_{i=1}^{m}\frac{P_i}{P_{max}} \tag{2.6}$$

$$E_{24h} = E_{max}\sqrt{\alpha_{24h}} \tag{2.7}$$

Where:

- m: number of time intervals of duration equal to 60 minutes included in a day (that are 24);
- E_{max}: maximum electric field value of the *signal* evaluated on the basis of P_{max}, maximum power deliverable at the antenna terminals;
- the value α_{24h} must be uniquely fixed for each *signal.*

For new 4G technologies and especially for 5G, the calculation of the electric field must now proceed differently from the Equation 1.20 [17]. The *uplink/downlink* separation can take place in the frequency range (4G) or following a strict time alternation scheme (5G).

Therefore, in the IEC 62232:2022 standard [13], evaluation methodologies are introduced for:

- the Massive MIMO;
- the LTE TDD signals.

Since the massive MIMO antennas of 5G synthesize beams of time-varying shape (Figure 2.4), it is necessary to define the radiation pattern of a time-varying active antenna. It can be defined, conservatively and deterministically, through the *envelope diagram*, regardless of the actual utilization of the beams (Figure 2.5 and Figure 2.6). The envelope diagram is obtained by considering, for each direction, the highest value among the gains of all possible traffic beams synthesizable by the antenna in that direction.

The *horizontal compliance distance* would depend on the maximum EIRP (*Equivalent Isotropic Radiated Power*) of a single beam. The *vertical* and *transverse compliance*

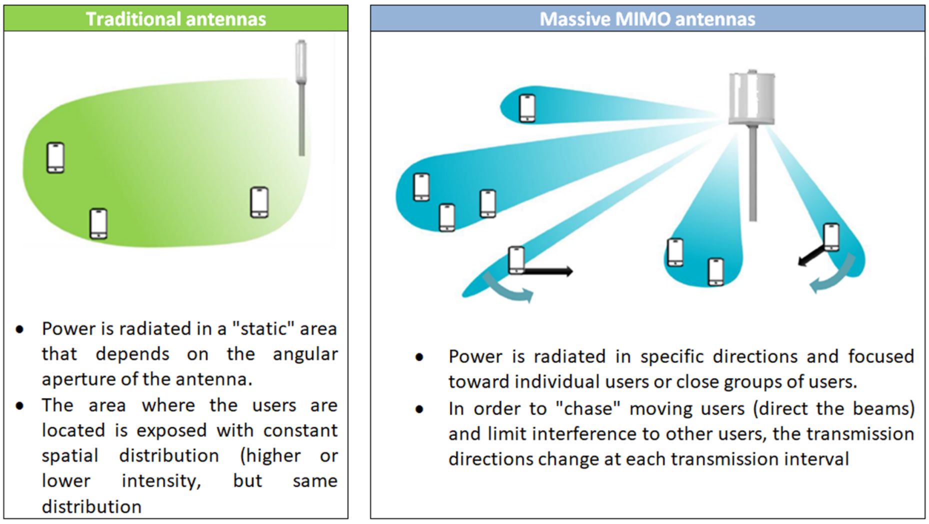

Figure 2.4: Differences between traditional antennas and massive MIMO antennas.

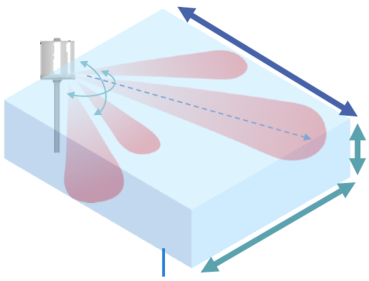

Figure 2.5: Radiation envelope diagram (theoretical, not real).

distances would depend on the maximum angles at which the antenna is able to direct traffic beams.

IEC Technical Report 62669:2019 [14] defines the following formulation for the statistical evaluation of the average EIRP over a time interval T for beam-time variant antennas:

$$EIRP\left(\vartheta,\varphi\right) = P_{TXM} \cdot F_{TDC} \cdot F_{PDL}\left(\vartheta,\varphi\right) \cdot G_{MLB} \cdot F_{G}\left(\vartheta,\varphi\right) \tag{2.8}$$

Where:

- P_{TXM}, deterministic component: maximum power downlink;
- F_{TDC}, deterministic component: duty-cycle of the technology, equal to 1 for FDD,

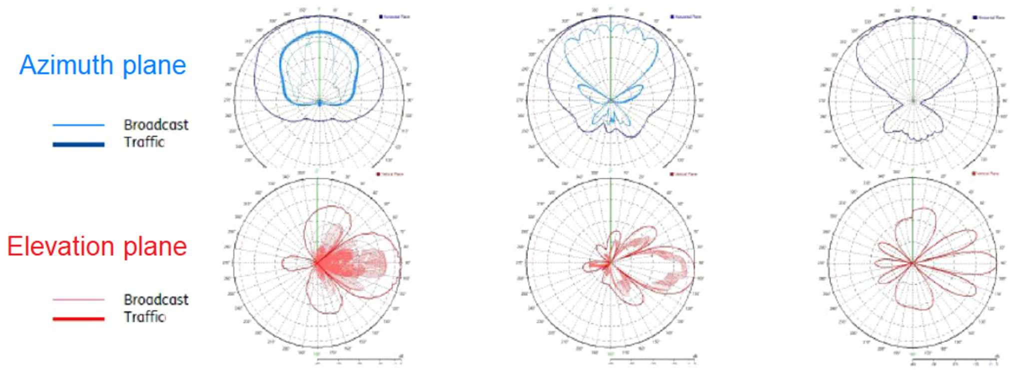

Figure 2.6: Radiation envelope diagram (practical real example).

< 1 for TDD;

- $F_{PDL}(\vartheta, \varphi)$, statistical component: normalized downlink power $F_{PDL}(\vartheta, \varphi, t)$ averaged over observational interval T;

- $G_{MLB}\ F_G(\vartheta, \varphi)$, statistical component: maximum gain G_{MLB} and normalized gain $F_G(\vartheta, \varphi, t)$ averaged over observational interval T.

Rewriting Equation 2.8 in the equivalent "static" form:

$$EIRP = P_{eff} \cdot G_{inv}(\vartheta, \varphi) \tag{2.9}$$

$$Effective\ power \qquad P_{eff} = P_{TXM} \cdot F_{TDC} \cdot F_{PR} \tag{2.10}$$

$$Envelope\ diagram \qquad G_{inv}(\vartheta, \varphi) = G_{MLB} \cdot \widehat{F_G}(\vartheta, \varphi) \tag{2.11}$$

Where:

- P_{eff}: maximum effective power at the antenna connector;

- F_{PR}: power reduction factor, derived from the statistics of the spatiotemporal distribution of normalized power $F_{PDL}(\vartheta, \varphi, t)$;

- Traffic envelope radiation diagram: $G_{inv}(\vartheta, \varphi) \geq G_{MLB}\ \widehat{F_G}(\vartheta, \varphi)$, conservatively and deterministically describes the use of beams in time and space.

IEC Technical Report 62669:2019 [14] provides that the power reduction factor can be either calculated by the mobile operator using node meters to monitor (direct or indirect) the average transmitted power or ensured by average transmitted power control features implemented by the antenna manufacturer (also based on node meters).

The mobile operator will use the power meters to determine:

- the power reduction factor F_{PR} (construction/estimation of the cumulative distribution function and extraction of the 100th percentile);
- the α_{24h} power reduction coefficients (see Law No. 221/2012);
- F_{PR} and α_{24h} are overestimated in the case of using only the total power meter: it does not contain the information about its spatial distribution.
- the exposure limit: $P_{EFF} = P_{TXM} \cdot F_{TDC} \cdot F_{PR}$;
- the quality objective value: $P_{EFF} = P_{TXM} \cdot F_{TDC} \cdot \alpha_{24h}$;

  where $\alpha_{24h} \leq F_{PR}$

So for the electric field is:

$$E(\vartheta, \varphi) = \sqrt{\frac{377 \cdot P_{eff} \cdot G_{inv}(\vartheta, \varphi)}{4\pi r^2}} = \sqrt{\frac{377 \cdot P_{TMX} \cdot G_{MLB}}{4\pi r^2}} \cdot \sqrt{A_h \cdot A_v} \cdot \sqrt{F_{TDC} \cdot F_{PR}} \tag{2.12}$$

Recalling that F_{TDC} accounts for the duty-cycle of TDD, F_{PR} accounts for mMIMO reduction and beamforming and A_h, A_v account for the envelop diagram.

For the 24-hour electric field is:

$$E_{24h}(\vartheta, \varphi) = \sqrt{\frac{377 \cdot P_{TMX} \cdot G_{MLB}}{4\pi r^2}} \cdot \sqrt{A_h \cdot A_v} \cdot \sqrt{\alpha_{24h}} \tag{2.13}$$

With the α_{24h} coefficient (computed according to Equation 2.6) leading to daily power reduction due to: TDD, statistical factor and data traffic.

2.2 The ARPA system

A regional agency for the protection of the environment (acronym ARPA - *Agenzia Regionale per la Protezione dell'Ambiente*) is an agency of the Italian public administration, where each Italian region has established its own agency. The 19 regional ARPAs, the two APPAs of the autonomous provinces of Trento and Bolzano, and ISPRA (*Istituto Superiore per Protezione e la Ricerca Ambientale*) make up the SNPA (*Sistema Nazionale per la protezione dell'ambiente*) established by L. n° 132/2016 [34].

Among the various institutional tasks, the Environmental Agencies (ARPA and APPA) operate in the area to verify compliance with the legal limits established by the regulations in force regarding the protection from low and high frequency electromagnetic fields. This activity is mainly carried out through the exercise of the following functions:

- assessment and expression of opinion on requests for new installations or modifications to existing installations, made by operators of radio and telecommunications systems and power lines;

- control and monitoring carried out through measurements with broadband instruments and with selective instruments for the assessment of complex situations or risks of exceeding the limits, or on reports of critical issues and environmental problems;

- creation and updating of the register of low and high frequency systems and communication of data to ISPRA;

- training, information and dissemination actions regarding the assessment of electromagnetic fields and exposure.

The Agencies also carry out activities to improve knowledge on the effects of exposure to electromagnetic fields, homogenize methods and procedures and activities aimed at improving the quality and reliability of the data produced, through participation in joint projects, studies collaborative and intercomparison campaigns [1].

Chapter 3

Study of the environmental status indicator

3.1 Necessity of an environmental status indicator relating to RF EMF (DPSIR model)

The DPSIR model, which stands for *Drivers, Pressures, State, Impacts, Responses*, is a relational framework that allows for a proper understanding of the relationships between society and the environment. Specifically, it can be said that the DPSIR model, developed in the context of EEA-Eurostat [35], is the most suitable tool for analyzing socio-economic-environmental problems based on cause-effect relationships and for expressing both the quality of the environment and project alternatives for improvement through indices.

For this reason, all environmental reporting processes, at any level, are or should be guided by this model in order to thoroughly and comprehensively analyze every environmental issue, including all relevant aspects. In fact, the "Rapporto sullo Stato dell'Ambiente" published by various ARPA and by the ISPRA adopt this approach.

As the acronym suggests, the model consists of five elements, each of which must find a representation through numerical indices when analyzing an environmental theme (Figure 3.1). These indices should be representative, measurable, based on solid scientific assumptions, easy to interpret, sensitive to changes and capable of highlighting the trend of the phenomenon over time [36].

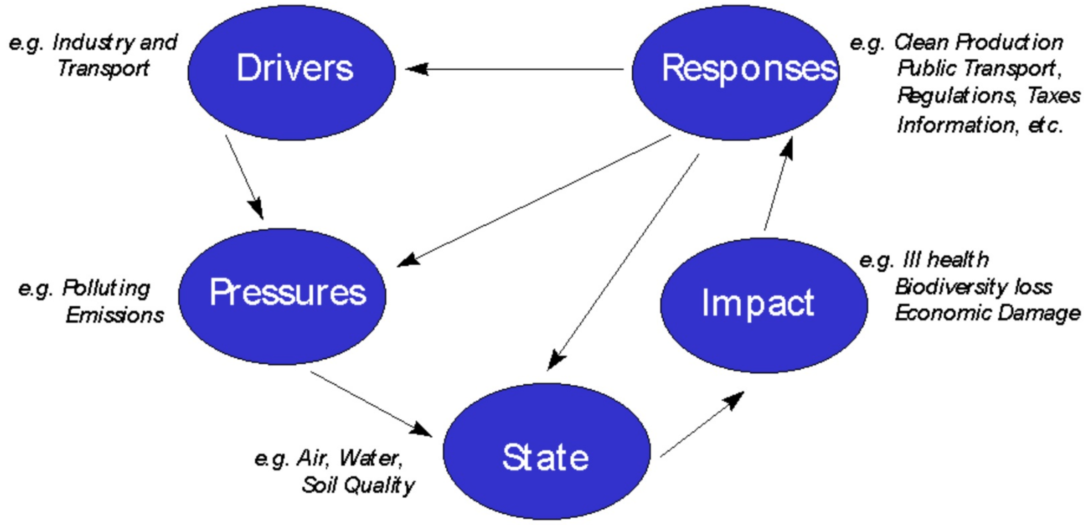

Figure 3.1: The *Driver-Pressure-State-Impact-Response* framework.

D – *Drivers*

The *drivers* represent the "indirect causes", often interacting with each other, of adverse effects on the environment. Depending on the phenomena studied, they include: the density and lifestyle of the population residing in an area, the methods of agricultural and industrial production, the type of urbanization, but also natural factors such as the topography, hydrology, and climate of a region, marine currents, etc.

P – *Pressures*

They are the anthropogenic *pressures* exerted directly on the environment, which can be quantified and controlled. For example: atmospheric emissions, noise, electromagnetic fields, waste production, industrial discharges, soil sealing, deforestation, etc.

S – *State*

The *state* of the environment, characterized by specific quality indicators that can be monitored over time.

I – *Impacts*

Significant changes (i.e. *impacts*) in the state of the environment that manifest as alterations in ecosystems, their ability to support life, human health, and society.

R – *Responses*

These are government actions implemented to protect the environment; *responses* can act on all elements of DPSIR and can take the form of controls, programs, funding plans, direct interventions, etc.

Regardless of where the description of the model begins, it is important to keep in mind that all assessments in the analysis of a problem using the DPSIR model must be rigorously based on "numbers". They must be carried out, read and interpreted based on the values assumed by the indices used to represent each element of the model.

In the radiofrequency electromagnetic fields sector, the DPSIR model leads to these examples of environmental pressure-state-response indicators [37]:

Pressure indicators

Telecommunications systems density ($number/km^2$): the number of telecommunications systems present per square kilometer of territory;

Total power of telecommunications systems (Watt): algebraic sum of the powers of the systems that provide the same type of service;

State indicators

Levels of electromagnetic field in the vicinity of radio and television installations and base stations (percentage): distribution of levels in percentage classes;

Levels of radiofrequency electromagnetic field exposure for the population (percentage): distribution of levels in percentage classes;

Exceedance of limits for radiofrequency electromagnetic field exposure (number): number of measurement points with levels of field exceeding the limits;

Variability of radiofrequency electromagnetic field levels (percentage): temporal variation of radiofrequency electromagnetic field levels, assessed with prolonged measurements carried out with monitoring stations. It is calculated as the ratio between the standard deviation of the measured average field level and the field level itself.

Response indicators

Opinions and statements issued for the installation or modification of telecommunication systems (number): the population of this indicator is possible thanks to the activities of the ARPA system;

Control and monitoring actions for radiofrequency fields (number): the population of this indicator is possible thanks to the activities of the ARPA system.

Regarding the aforementioned environmental indicators in the radiofrequency electromagnetic field sector, with the RINDEC-2018-0000156 [38] decree dated 11.16.2018, the MATTM (*Ministero dell'Ambiente e della Tutela del Territorio e del Mare*) defined a "Program for the promotion of technical-scientific research and experimentation activities aimed at studying the risks associated with exposure to low and high frequency electromagnetic fields", briefly addressed as *Programma di ricerca CEM*, in line with the priorities that emerged from the recent critical review of the literature on the potential effects of EMFs on health [39] and the renewed research needs in this area at an international level, linked to new technologies.

It lists both the research activities to be investigated and those of technical-scientific experimentation for emerging technologies and the financial coverage provided for the direct beneficiaries: the agencies of the agency system and ISPRA have been defined in detail. With this, it was understood that the MATTM wanted to encourage the Agencies, given their degree of knowledge of the territory from the point of view of emissions and exposure to EMFs, to participate "in the deepening of scientific knowledge relating to the effects on health, in particular the long-term ones, deriving from exposure...", provided for by the Legge Quadro (n. 36 of 2/22/2001) [29], activities which, for the Agencies, are often subordinate to those of supervision and control, of in situ measurements and monitoring and preventive assessments to provide technical support to local administrations.

This finalized project, entitled "Campi elettromagnetici e salute: studi di valutazione dell'esposizione e approfondimento sui possibili rischi delle esposizioni a lungo termine" constitutes the proposal for carrying out the research activities that the agency system intends to undertake for the satisfaction of the *Programma di ricerca CEM*, consistent with the current guidelines of research on EMF at an international level.

In particular, this thesis work was developed within the scope of the "Exp-1: Exposure Evaluation Studies" aspect of the aforementioned project. The *Exp-1* studies are aimed at evaluating EMF emissions (RF, IF, ELF, static NMR fields) from various sources, exposure scenarios and exposure levels from new and emerging technologies and changes in the use of already established technologies evaluating, throughout the country, the effective levels of exposure of the population to the complex of electromagnetic sources, through the analysis of individual exposures.

To do this, it was necessary to develop a methodology for determining synthetic exposure indicators based on data from sources of electric, magnetic and electromagnetic fields (telecommunication systems) contained in digital archives managed at regional level and on GIS cartographic tools which allow associating the estimated levels of exposure the population residing in certain areas of the territory.

A further element for the development of the methodology will be made up of the measurements on the territory which will allow the introduction of proposals for corrective factors to the theoretical estimates to take into account the real operating conditions of the sources of electromagnetic fields. Following the sharing of the methodology and the tools to be adopted to implement it, it will be possible to proceed with the population of the indicators chosen on a supra-regional basis.

These analyzes will allow the determination of exposure trends in order to evaluate the contribution of new technologies and the changes inherent to technologies already in use. Beyond, therefore, carrying out studies and replications that help reduce the persistent scientific uncertainties in this regard, the main benefit will be that of producing indicators and exposure data representative of the national situation thanks to a shared and coordinated approach [1].

3.2 Calculation method of the environmental indicator

The chosen environmental state indicator within the *Programma Ricerca CEM - Exp-1* was the indicator "levels of radiofrequency electromagnetic field exposure for the population". **This indicator involves providing, categorized into classes, the distribution of electric field levels to which the population is exposed**. Through the data analysis, information about the threshold values of electric field below which a certain percentage of the population is exposed is also available. Typically, the 50th and 95th percentiles are considered to provide a measure of radiofrequency electromagnetic field exposure for respectively half and the majority of the population.

The indicator was developed and calculated with reference to the APAT RTI CTN_AGF 2/2005 document [40], which outlines the methodological procedures for populating the indicator, accompanied by applicative criteria for determining the percentage of the population exposed to electromagnetic fields produced by mobile telecommunication systems [41], [42]. Evaluating this indicator involves addressing issues related to estimating electric field levels in the area, assessing the actual power radiated by Base Stations and defining the population distribution within buildings.

It is evident, therefore, that data collection is necessary for various aspects.

To estimate the electric field levels and the actual power radiated by the BTSs, knowledge of radioelectric data, the technologies in place, the power levels and the positions of the BTSs is essential. Indeed, given the technical characteristics of the sources, a large-scale assessment of field levels in the environment can be obtained using software (with a theoretical approach) that allows the determination of exposure levels over an entire defined territory, referred to as the calculation area.

In this way, specific electric field values can be associated with the population and thus populate the indicator. The electric field value used for indicator calculations should be a characteristic and representative value of population exposure: we will later discuss the possibility of choosing from the various statistical indicators that can fulfill this role.

Furthermore, it is certainly necessary to gather data regarding the distribution and division of the population across the territory, as the indicator is aimed at studying this subject.

Finally, since the 6 V/m prudent value applies within buildings used for daily stays of not less than four hours, as well as their external areas usable as living spaces, it is possible eventually to narrow the focus of the indicator study only to those places that meet this condition, namely the buildings for which information will be collected.

3.2.1 Indicator calculation steps and population distribution procedures

Before delving into the details and describing how the data was collected and its characteristics, it's important to outline the logic and steps that lead to the assessment of the indicator.

The indicator is calculated for the exposed population, where this population comprises all individuals exposed for non-professional reasons to electromagnetic fields.

The reference database for the population is represented by the information derived from the censuses conducted by ISTAT (*Istituto Nazionale di Statistica*), where information about the resident population is available at the census section level. Therefore, detailed information at the individual building level and even the resident population per floor is not available. In order to calculate the indicator, it is necessary to assign to each resident a value of the electric field to which they are exposed and, as a result, display the population distribution as a function of the electric field. The electric field values are calculated inside the buildings, which are the places where people spend more than four hours daily.

Two distinct procedures can be defined (based on the availability of three-dimensional data on building volumes) to establish models for the distribution of exposed individuals: one that is more general and one that is more detailed.

The *general procedure*, simplified model involves identifying, for each reference territorial unit (e.g., census section), an indicative average height of the built volumes (e.g., the ratio between the total built volume and the total covered area) and defining an adequate number of calculation surfaces parallel to the ground of individual buildings and placed at significant elevations. For the sake of simplicity, considerations will be made later to consider only one of these elevations, chosen as statistically representative. At this point, for each territorial unit, the resident data is divided equally among these surfaces [41]. In the case where a single evaluation elevation is chosen as significant, the resident data will be directly assigned to the entire territorial unit.

The *detailed procedure*, on the other hand, assumes that there is a thematic layer available regarding the precise distribution of built volumes, and it is possible to refine the analyses presented above in a way to "concentrate" the presence of exposed individuals in indoor spaces. The database associated with the thematic layer should be organized to contain the following information for each building E_i:

- identifying code;
- covered area SE_i;
- height hE_i;
- volume VE_i;
- population related to the entire reference territorial unit P_{tot};

- built volume related to the entire reference territorial unit V_{tot}.

For each reference territorial unit, it is necessary to distribute the resident population data among the various buildings present; for this purpose, it is assumed that this operation can be carried out by considering a direct proportionality with the volume of individual buildings [40]:

$$P_{E(i)} = P_{tot} \cdot \frac{V_{E(i)}}{V_{tot}} \tag{3.1}$$

Therefore, the *detailed procedure* redistributes, in a uniform manner for each territorial unit, the information about the resident population within the volume occupied by the individual building relative to the total volume of the buildings. By doing this, for each building, it is possible to assert with a certain degree of certainty the associated number of residents, and consequently, the simulated characteristic electric field value of each building will be assigned to them. It is worth noting that this procedure is very refined and is also very useful for managing the census sections that are on the border of the area of interest possibly taken into consideration for the calculation of the indicator. In this way, only the population of those buildings falling within the area of interest would be considered.

However, the indicator is a tool for assessing the environmental status over large areas of territory. In fact, very extensive areas of interest are considered, encompassing a large number of census sections (i.e. dozens of census sections for areas with a 300m radius, several hundred for areas with a 1500m radius). Therefore, it is clear that this level of detail is not strictly necessary for the evaluations because it would affect data processing times without leading to significant differences and improvements compared to the *general procedure*. For this reason, it can be stated that the *detailed procedure* can be used for small study areas, while the *general procedure* is preferable when considering very large areas of interest.

In this study, the calculation of the indicator "levels of radiofrequency electromagnetic field to which the population is exposed" has been limited to an urban context, considering three areas of interest in the metropolitan city of Turin. These three areas will be referred to by the main street that runs through them, namely: "Corso Belgio", "Via Vigliani", and "Via Togliatti". They consist of circular areas with a radius of 300 meters, with the center corresponding to a specific Base Station. These three areas were chosen because they have a varying presence of Base Stations and different building characteristics: "Corso Belgio", "Via Vigliani", and "Via Togliatti" have, respectively, high, medium, and low building density, roughly speaking.

The first part of the study was focused on determining the levels of electric field generated by radiofrequency electromagnetic field sources. For this study, the selection was limited to only the Base Stations (BS) located within the areas of interest, applying a calculation model for electric field in free space (*far-field*).

Within the areas of interest, the existing buildings were considered, and for each of them, points were identified for simulating the electric field. For each building, there were two possibilities: either a three-dimensional grid of points with a horizontal step of 3 meters (X, Y) and a vertical step of 1 meter (Z), or a single point at the centroid on the horizontal plane with an associated elevation (a.g.l.) considered representative of the building (hereinafter referred to as the *centroid*).

At these points, whether considering a three-dimensional grid or a single representative point, an electromagnetic field model in free space is used to assess the electric field levels generated by each individual BTS as well as by all the BTS simultaneously. In this work, only the simulated total electric field value was considered because in the context of population exposure to electromagnetic fields, it's not possible to separate individual contributions and exposure is cumulative from all present sources.

For the calculation of the indicator, two approaches can be outlined depending on whether the area of interest considered has a small or large radius since it can affect, as seen earlier, the procedure used to obtain a representative population distribution in territorial units.

In the case of areas of interest with a small radius (e.g., 300 meters), it is preferable to use the *detailed procedure* for assigning the population to buildings. By doing so, each building is assigned a number of residents, and they will be associated with an electromagnetic field value derived either from a representative value of the three-dimensional grid of simulated points or by direct assignment of the point value at the centroid.

In the case of areas of interest with a large radius (e.g., 1500 meters), the *general procedure* for assigning the population to buildings is used. As mentioned earlier, if this procedure chooses to consider a single statistically representative a.g.l. level, it translates into the direct assignment of the resident population to the entire census section, without considering the granularity of individual buildings. Given the level of approximation, it is reasonable to associate an aggregated simulated electromagnetic field value with this information. This value is identified as the average of the choosen simulated electromagnetic field values of buildings throughout the territorial unit, whether it is entirely or partially within the area of interest.

This way, for each census section, you obtain the values of simulated electromagnetic fields to which the resident population is exposed. From these values, considering the entire areas of interest, you can derive the distributions of the population exposed to different average electromagnetic field values (divided into appropriate field strength classes) calculated in free space. From these distributions, characteristic values can be derived, including: the median (or 50th percentile), which is the electromagnetic field value to which half of the population is exposed and the 95th percentile, which is the electromagnetic field value below which the majority of the resident population is exposed.

3.3 Data collection

In the context of the thesis work, it was necessary to collect various types of data from different sources. Below, the source of the data and their characteristics are described for each of them.

3.3.1 Buildings

Arpa reports on frequencies of buildings' heights in major urban centers

To evaluate an indicator of population exposure to the electric field generated by BTSs, it is necessary to reasonably determine the above-ground level of buildings to which centroids' point calculations must refer. This entails analyzing and understanding the main features of the buildings in the urban areas of the cities of greatest interest, namely the most densely populated ones. For this purpose, Arpa Piemonte has made available PDF reports prepared by Arpa technicians from various regions regarding analyses conducted on the buildings in some of the major cities in northern Italy, including Turin, Novara, Biella, Aosta, Trento, and the provincial capitals in the Veneto region.

The purpose of these analyses is to assess the frequency of the number of buildings with a specific height (and correspondingly, a certain number of floors) and to identify the most common number of above-ground floors. By "above-ground floors", it is meant the total number of floors that make up a building above the ground, including the ground floor but excluding the number of basement floors. Therefore, the number of above-ground floors is equal to the number of the last floor plus one [43].

In this way, based on the Agencies that have data on the buildings in their major cities, other regional Agencies that do not have building data in digital format or do not have the means to conduct these analyses can represent the population's exposure with justified confidence.

Since the thesis topic revolves around the metropolitan city of Turin, we will proceed to explain in detail the report on the buildings in that city. Briefly, the conclusions of the studies concerning other cities will be mentioned, and then the data collection carried out within ARPAE Emilia-Romagna will be presented to include analyses for the cities of Bologna and Cesena (developed in detail in Subsection 3.6.1).

The report regarding the analysis of the buildings in the metropolitan city of Turin used building data in *shapefile* format for the year 2015 and the year 2017, extracted from the regional geoportal. Where necessary, the data source was modified. This results in an approximate database, but considering that the purpose of this study is a broad statistical evaluation, it was decided that this database could be sufficient, as long as it is not affected by systematic errors.

Data cleaning was performed, excluding:

- Buildings with a eave height of 0 meters. These elements cannot be considered as valid buildings since they lack height;
- Buildings with a eave height exceeding 40 meters, which are typically associated with structures having a high number of floors and/or bell towers of religious buildings. For the purpose of conducting a general analysis of the buildings, it was decided not to consider such elements;
- Buildings with an area less than $50m^2$, indicating places where the presence of people is highly unlikely (as the habitability threshold is $28m^2$);
- In the Turin 2017 building dataset, given the availability of information about the specific use of each building, those with a daily stay duration of less than 4 hours were excluded. Specifically, the following building types were excluded: "campanile", "cappella", "chiosco", "dehor stabile", "edicola funeraria", "edificio

cimiteriale", "galleria non sovracostruita", "garage box auto", "serra", "tendone pressurizzato", "parcheggio", "torre porta".

An analysis of the distribution of *eave heights* (h) for this data was then conducted, using height classes of 3 meters (Figure 3.2). The choice of these height classes is justified by the fact that an internal floor of a building is typically around 270 cm to 300 cm in height, to which the thickness of the flooring must be added. It is reasonable to assert, on average, that one floor corresponds to 3 meters.

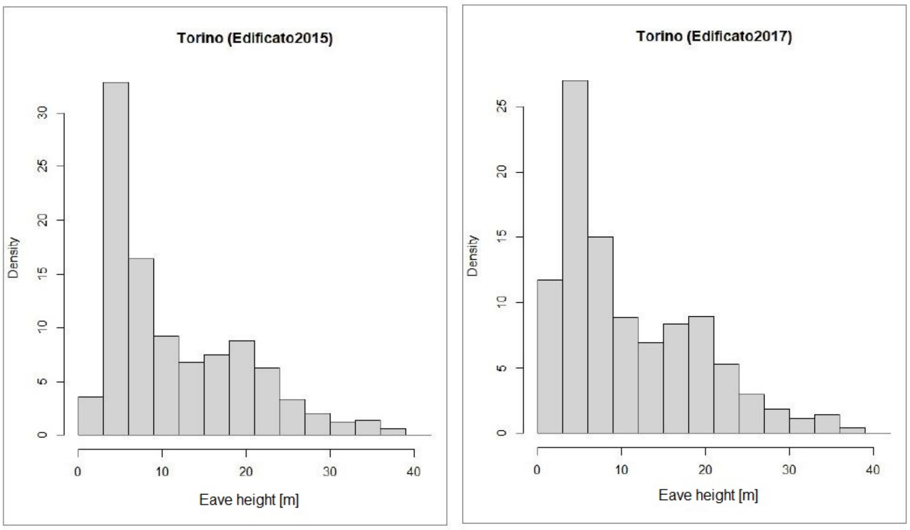

Figure 3.2: Distribution of eave heights (h) in the metropolitan city of Turin, with height classes of 3 meters.

It can be observed that the mode of the eave heights distribution falls within the 3-6 meter bin for both data sources in Turin's building dataset.

An analysis of the distribution of *areas* (A) was also performed, where the histogram displays area classes of 50 m^2 up to an area value approximately corresponding to the 95th percentile of the area distribution (Figure 3.3).

As expected, from Figure 3.3 it can be noticed that the trend is strongly decreasing, with the most frequent area classes certainly in the first bins ($50 \div 100$ m^2).

The *weighted height* (h/A) was then calculated and divided into classes with a width of 0.05 m^{-1} (Figure 3.4).

These frequency histograms both exhibit similar trends, that is, a rapid decrease with the mode corresponding to the $0 \div 0.05$ m^{-1} bin. Consequently, it was possible to

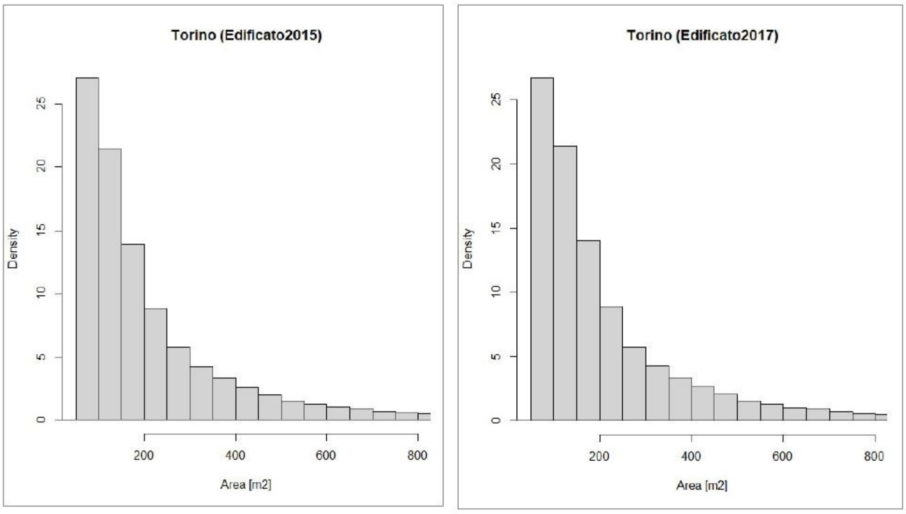

Figure 3.3: Distribution of areas (A) in the metropolitan city of Turin, with area classes of 50 m^2.

make considerations regarding the values with higher probability in the histograms in Figure 3.3 and Figure 3.4. In other words, it was possible to infer the most probable above-ground floor height through the distributions of areas and weighted heights.

In this regard, for the metropolitan city of Turin:

$$\tilde{h} = \tilde{A} \cdot (\widetilde{h/A}) = 100\ m^2 \cdot 0.05\ m^{-1} = 5\ m \tag{3.2}$$

This height corresponds to the most frequent *eave height* through this analysis. An eave at 5 meters above the ground, in turn, corresponds to the second/third level above-ground, indicated in the future as *2nd/3rd L.A.G.*.

In the Arpa Piemonte report, an analysis of the distribution of *volumes at the eave* (V) of the considered buildings was also conducted, modeling them as parallelepipeds, meaning the volume was calculated as a simple $h \cdot A$ product.

The histogram in Figure 3.5 displays volume classes of 500 m^3 up to a volume value approximately corresponding to the 95th percentile of the volume distribution.

The trend of the eave volume distributions for the city of Turin is decreasing, with the mode corresponding to the first bin ($0 \div 500\ m^3$).

Similar to the previous step, considerations were made regarding the values with higher probability in the histograms in Figure 3.3 and Figure 3.5. In other words, it was

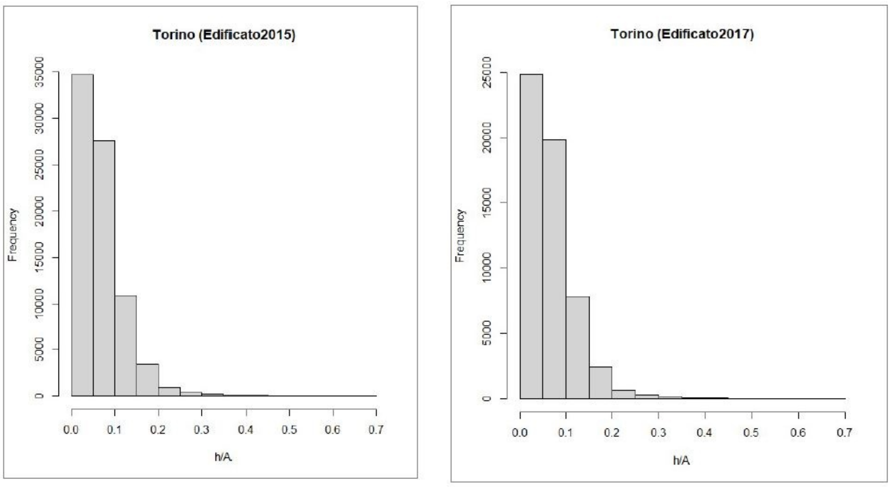

Figure 3.4: Distribution of weighted eave heights (h/A) in the metropolitan city of Turin, with weighted height classes of 0.1 m^{-1}.

possible to infer the most probable above-ground floor height through the distributions of areas and eave volumes.

In this regard, for the metropolitan city of Turin:

$$\tilde{h} = \frac{\tilde{V}}{\tilde{A}} = \frac{500\ m^3}{70\ m^2} \approx 7m \tag{3.3}$$

These heights correspond to the most frequent eave heights through this analysis. An eave at 7 meters above the ground, in turn, corresponds to the third/fourth level above-ground, indicated in the future as *3rd/4th L.A.G.*.

As previously mentioned, reports with similar analyses conducted by other ARPA/APPA agencies have been provided, particularly from Valle d'Aosta, Veneto, and the Autonomous Province of Trento. Below are the conclusions of these studies:

- *Aosta*: the study conducted on the buildings in the municipality of Aosta highlighted the prevalence of buildings with *2/3 levels above-ground*. The analysis that considered eave heights also confirmed that the most frequent height falls between approximately 4 meters and 10 meters above ground level. In the analyses that took building areas into account, the total number of counted buildings and the absolute number in their respective frequency classes naturally change, but this does not substantially alter the initial results;

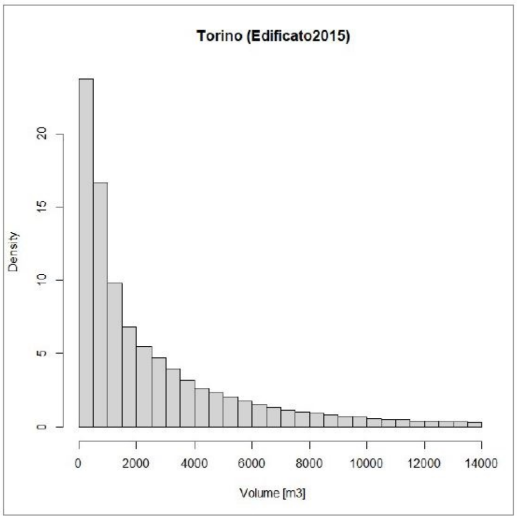

Figure 3.5: Distribution of volumes (V) in the metropolitan city of Turin, with volume classes of 500 m^3.

- *Trento*: in the case of the municipal territory of Trento, the analysis conducted highlighted the prevalence of buildings with *3/4 levels above-ground*, corresponding to 6-12 meters above ground level. The two different files considered in the analysis, despite referring to the same territory, yielded slightly different results, attributed to various factors: different file ages, varying levels of detail and building characterization. Unlike other ARPA agencies, the altitude used for the analysis is not the eave height, but the altitude obtained as the mean value of the pixel altitudes composing the roof, calculated from the DSM (*Digital Surface Model*) raster file;

- *Veneto*: using the ISTAT 2011 building data for all seven provincial capitals (Belluno, Padova, Rovigo, Treviso, Venezia, Verona, Vicenza), it is noted that the mode of the above-ground floor distribution always corresponds to the *2nd L.A.G.*.

Bologna and Cesena buildings data - csv

From the analysis of building heights in the municipalities of Turin, Aosta, Trento and Veneto, it can be seen that the mode regarding above-ground floors, i.e., the value that appears most frequently, varies depending on the city but generally falls around the *2nd/3rd L.A.G.*.

In order to expand the sample and include the largest urban centers in the Emilia-Romagna region, it was decided to carry out the same analysis conducted by Arpa Piemonte on the data obtained for the municipalities of Bologna and Cesena.

For the Municipality of Bologna, building data was acquired through its Open Data portal, using the dataset "Carta Tecnica Comunale (CTC) - Edifici volumetrici" [44] in *CSV* format, updated daily, and distributed under a CC BY 4.0 license.

The CTC is a technical cartography at a 1:2000 scale that the *Geographic Information System* (SIT - Sistema Informativo Territoriale) of the Municipality of Bologna had created in 2001 using direct photogrammetric methods. In the return, among other alphanumeric information, the eave height and base height of the volumetric buildings were included, with a tolerance of 54 cm.

From 2001 onwards, the update of the CTC, especially regarding the eave heights of volumetric buildings, has been carried out using, as the primary source, the project documentation from building permit applications submitted for new constructions or significant modifications to existing structures. As secondary sources, for support and verification, high-resolution precision orthophotos and libraries of oblique images were utilized. These oblique images consist of aerial, oblique, and ortho-rectified images with substantial overlap. The Municipality of Bologna has accumulated a substantial series of such image libraries since annual surveys have been conducted starting in 2005. Recently, an aerial survey was performed with a new sensor that acquired both images and LiDAR data simultaneously. The LiDAR data has become an important source for updating the eave heights in the Carta Tecnica Comunale. The update of the main layers in the CTC, particularly the layer in question, is carried out in a continuous process.

The .csv file for the buildings in the Municipality of Bologna contains one row for each building, totaling 66,124 rows. Each of these rows has 14 features, or columns, with the following characteristics:

- CODICE_OGGETTO, Geo Point, Geo Shape: they contain a unique identifier for each building and information regarding the geolocation of these buildings;
- ORIGINE, DATA_ISTITUZIONE, DATA_VARIAZIONE, NOTEOGG: they indicate the data source (e.g., from orthophoto or topographic survey), the date of insertion and modification, as well as any additional information;
- QUOTA_PIEDE, ALTEZZA_GRONDA, QUOTA_GRONDA: for each building,

they provide the following information in meters: the base height above sea level (a.s.l.), the eave height above ground level (a.g.l.) and above sea level (s.l.m.);

- DESCRIZIONE: the intended use of the property. The various possible categories are, in Italian: "Baracca", "Cabina ENEL", "Campanile", "Carcere", "Chiesa", "Chiosco alimentari", "Chiosco fiori", "Chiosco giornali", "Cimitero", "Collegamento in quota", "Edificio ad uso agricolo", "Edificio diroccato", "Edificio generico", "Edificio per centrale termica", "Edificio scolastico", "Edificio sportivo", "In costruzione", "Mura storiche", "Ospedale", "Portico", "Serra", "Servizi", "Silos", "Stabilimento industriale", "Stazione di rifornimento", "Tettoia/pensilina";

- PERIMETRO, AREA_OGG, VOLUME: for each building, respectively, the perimeter in meters, the area in square meters, and the volume in cubic meters.

Similarly, for the Municipality of Cesena, building data was acquired through the Open Data portal of the Union of the Municipalities "Valle del Savio", using the dataset "Edifici" [45] in *CSV* format. This dataset is managed by the SIT of the "Union Valle del Savio", updated daily and distributed under a CC BY - free reuse by citing the source.

The base cartography of the Municipality of Cesena is derived from the digitization of the CTR (*Carta Tecnica Regionale*), updated with a survey conducted in 1995. Subsequently, the GIS department (SIT) implemented increasingly computerized updating procedures, currently carried out through the "SIT ONLINE" system. These procedures use data submitted by external technicians. Providing updated data is mandatory for projects that modify territorial objects both at the beginning and at the end of works.

Similarly to Bologna, the .csv file for the buildings in the Municipality of Cesena contains one row for each building, totaling 62,616 rows. Each of these rows has 28 features or columns containing information about the data source, the type of construction, its shape, and population-related data. For the subsequent data analysis, the following features were used:

- STATO, TIPO_EDIL: information regarding the building's condition (in Italian: "in costruzione", "in disuso-diruto", "in esercizio") and its intended use (in Italian: "campanile", "chiesa/basilica", "chiosco", "cimitero", "edificio industrialeartigianale", "edificio monumentale", "edificio rurale", "generica", "minareto-moschea", "serra fissa", "tempio", "tribuna di stadio", "villa", "villetta a schiera");

- Q_BASE, Q_ALTEZZA, Q_GRONDA: for each building, respectively, in meters, the base height above sea level (a.s.l.), the eave height above ground level (a.g.l.), and the eave height above sea level (s.l.m.);
- SHAPE_AREA: for each building, the area in square meters.

Turin building data - shapefile

The assessment of human exposure to radiofrequency electromagnetic fields is carried out by ARPA in order to evaluate the impact of sources on the territory and compare the levels with the limits set by regulations for the protection of human health. This assessment is done through measurements (monitoring, source control, response to exposed individuals and requests from local and regional authorities) or calculations. The latter, which involve the use of predictive models, are particularly important in the preventive phase, such as in the issuance of technical opinions within the procedures for authorizing the installation and modification of telecommunications facilities.

When it comes to radiofrequency electromagnetic fields, we refer to those generated by the aforementioned sources, at frequencies that vary depending on the implemented telecommunications services. The intensity of these fields depends on two sets of factors: the emission characteristics of the device generating them and the distance from the point of interest. Points of interest include all those places where the population can stay for a continuous period of not less than four hours per day. Specifically, this includes residential and/or commercial buildings and their external areas, as indicated by D.M. 07/12/2016 [31].

In order to assess the indicator of population exposure to radiofrequency electromagnetic fields at the relevant points of interest, it was necessary to obtain both the volumetric and geographic characteristics of the selected buildings for the three selected areas of interest.

Arpa Piemonte thus provided three georeferenced *shapefile* files (which have an attached .dbf database) using the EPSG:32632 reference system, containing the buildings for the three areas of interest in the metropolitan city of Turin, namely "Corso Belgio", "via Togliatti" and "Via Vigliani" (Figure 3.6). The buildings in these three files are the result of the intersection between the buildings in Turin and the entire ISTAT census sections that fall within the areas of interest. The building layer of Turin used by Arpa Piemonte combines a base created by the city of Turin [46] under a CC BY 4.0 license, updated and integrated with the information collected by Arpa technicians during various surveys and inspections conducted during measurement campaigns.

Figure 3.6: In orange: building layer in "Via Vigliani" area of interest (visualization via QGIS software).

These shapefiles, essential for calculating the indicator, were visualized using the open-source software QGIS (*Quantum Geographic Information System*) [47], allowing for the extraction of information regarding the shape and geolocation of the buildings. Associated with this spatial information is the so-called "attribute table", which corresponds to the associated .dbf database. In this table, each row corresponds to a building, i.e., a geometry present in the respective shapefiles: "Corso Belgio" contains 605 buildings, "Via Vigliani" contains 938 buildings, and "Via Togliatti" contains 461 buildings.

All three "attribute tables", although of different lengths, have five columns:

- CIT_AR: unique code identifier of the building;
- QT_SUOLO, ALTEZZA_VO, QT_GRONDA: for each building, respectively, in meters, the base height a.s.l., the eave height a.s.l. and a.g.l.;
- NUM_PIANI: information about the number of floors in the building.

Finally, the BDTRE (*Base Dati Territoriale di Riferimento degli Enti*) [48] of the Piemonte region was used to visualize the map of the city of Torino in QGIS. This provided a cartographic background for locating the three areas of interest and obtaining a comprehensive overview.

The BDTRE is the geographic database of the Piemonte region, promoted by the Regione Piemonte, with the typical contents of technical cartography, structured according to the "Technical rules for defining the content specifications of national geotopographic databases". It is primarily aimed at supporting planning, governance, and territorial protection activities. Since 2014, "the reference cartographic base for the Region and for all public and private entities interfacing with it is derived from the BDTRE" (Article 10 of Regional Law No. 1 of February 5, 2014).

The Regional Law No. 21 of December 1, 2017, establishes the Regional Geographic Infrastructure, with the aim of integrating geographically related information from various sources, including regional offices, local authorities, and other public and private entities. It ensures the validity, accuracy, consistency, completeness and up-to-date nature of this information, reaffirming what was determined in 2014. The BDTRE thus assumes the role of a shared "container" for all geospatial data, from which the regional reference cartographic base is derived.

To allow its full use by the various interested parties, ranging from Piemonte's public administration entities to professionals, university and research institutions, and citizens, the Piemonte Region makes the BDTRE available in an open mode. All the data and services published on the BDTRE are made available under a Creative Commons license - BY 2.5, progressively being replaced with version 4.0.

The BDTRE is published in various formats and through different types of services following the main standards. The vector data (discrete geometries such as points, lines, and polygons) of BDTRE, along with their associated alphanumeric information, were obtained from the aggregated structure, accessible via a WFS (*Web Feature Service*) connection. For the meaning of this acronym, please refer to Subsection 3.3.3.

3.3.2 Population data and census sections

To calculate the indicator of population exposure to radiofrequency electromagnetic fields, it is evident that access to data regarding the population residing in the selected areas of interest is necessary. This information can be obtained through the ongoing population and housing census made available by ISTAT (*Istituto Nazionale di Statistica*), which allows for the understanding of the demographic and social structure of Italy and its territories at the municipal level [49].

On June 9, 2023, ISTAT published the initial results of the ongoing population census for exclusive statistical purposes [50]. The data is available at the following sub-municipal territorial levels:

- census sections, for all Italian municipalities;
- sub-municipal administrative areas of the first level, for the 14 provincial capital municipalities (including the metropolitan city of Turin).

It is worth noting that the data obtained in this way pertains to the population counted on 31/12/2021, while the territorial reference bases (i.e., the census sections) are from 2011 [51]. In this release, the first digits of the census section code refer to the municipalities that were present during the 2011 census.

A *census section* is defined as the smallest unit for data collection within a municipality, upon which the census survey is organized. It consists of a single area enclosed by a closed broken line. Starting from the census sections, higher-level geographical and administrative entities (inhabited places, sub-municipal areas, electoral districts, and others) can be reconstructed through aggregation. Each census section must be entirely contained within one and only one inhabited place. The municipal territory must be comprehensively divided into census sections; the sum of all census sections reconstructs the entire national territory [52].

The new permanent census is based on the integration of data from administrative sources and data collected through annual surveys involving a representative sample of municipalities and households. However, it's important to note that the ISTAT data obtained are related to the *resident population* and do not take into account the portion of the population that, for work or study purposes, may have their usual residence in the respective census sections.

As part of this thesis work, the population data used pertains to the sub-municipal area of the capital of the metropolitan city of Turin [50]. These data are provided in .xlsx format, where each row in the file is identified by the corresponding census section code, totaling 3,509 sections for the metropolitan city of Turin.

The information contained in the columns of this .xlsx file includes the total resident population as well as population breakdown by variables such as gender, age, citizenship, education, occupation, and families, along with some cross-referencing of these variables. For the calculations to be performed later, only the information regarding the total resident population was used. However, given the availability of data broken down by categories, there is the possibility, in the future, to further refine the research presented in this thesis.

It should be emphasized that, for the permanent population census of the year 2021, there is no available distribution of the resident population divided by above-ground floors of buildings, unlike in previous permanent censuses.

To address this issue, with the aim of calculating an indicator that also takes into account the distribution of the population in places where it is legally required to assess exposure to electromagnetic fields (i.e., in places with more than 4 hours of daily presence), in certain cases it was necessary to distribute the population of each of the census sections within the buildings in those sections. To do this, considerations were made regarding the volume of the buildings themselves (seeking a redistribution of the population that takes into account the number of floors/height of the building). These considerations are described in detail in Section 3.2.1, to which reference is made.

More generally, the use of this type of information requires attention to issues related to data representativeness:

- there can be significant local differences between the average data and the actual distribution of exposed individuals, depending on the location and use of the built volumes;

- the data is related to the resident population and may not accurately represent the actual presence of exposed individuals, which can vary, for example, during working hours.

An additional issue with ISTAT data is related to updates, which are tied to censuses (usually conducted every 10 years, with occasional intermediate censuses). These sources of imprecision are difficult to control but can be tolerated in a study on a large territorial scale and conducted on a statistical basis, as is the case here. More detailed information would require specific analyses in areas affected by radio installations [40].

As mentioned, the 2021 population data is divided by 2011 census sections, also known as *territorial bases*.

The 2011 *territorial bases* were retrieved from the ISTAT page dedicated to "Basi territoriali - dati definitivi (1991-2011)" [51], where the geographical data of the 2011 territorial bases for all statistical territorial partitions and zoning of Italian territory are published. The geographical data for the census sections, mosaicked at the national level, are available in .xls format and in dual geographic projection (ED50 UTM Zone 32N - EPSG code: 23032 and WGS84 UTM Zone 32N - EPSG code: 32632) in *shapefile* format. The 2011 data is also available in .kmz format. As known, shapefile data can be viewed using open-source GIS software, such as QGis.

The regional geographic files for the 2011 census sections are named *Rxx_aa_pppp.zip*, where *xx* represents the region code. Inside these files, the necessary data for the geographical representation of polygons can be found. The .xls and .dbf files can be accessed with software other than geographical visualization tools.

For the purposes of this thesis, the corresponding shapefile for the 2011 census sections of the entire Piedmont region, "R01_11_WGS84.shp", was downloaded with the WGS84 UTM Zone 32N reference system - EPSG code: 32632.

The information associated with the census sections used in this study includes their geometries (viewable through QGis) and the unique identification code "SEZ2011". This is a numeric code that uniquely identifies the 2011 census section within the national territory. It was used to associate the total resident population with each geometry of the census sections in QGis.

In practice, out of all the census sections in Piedmont (a total of 35672), only those corresponding to the intersection with the three areas of interest were considered (Figure

3.7). Consequently, for each of them, it is obtained that "Corso Belgio" intersects 19 sections, "Via Vigliani" intersects 18 sections, and "Via Togliatti" intersects 10 sections.

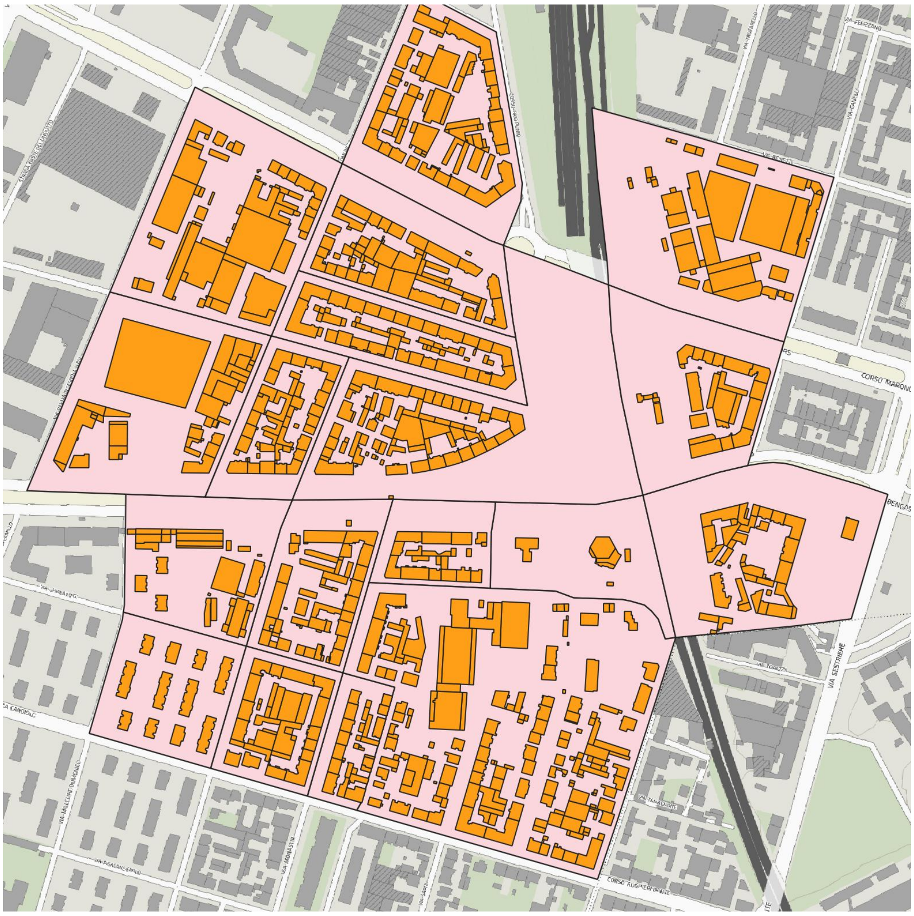

Figure 3.7: In light pink: census sections layer in "Via Vigliani" area of interest.

3.3.3 Base transceiver stations BTSs (location, technologies)

One of the main subjects of this study is the base stations, also referred to as sources of electric field. The data can be obtained from the "Portale CEM - campi elettromagnetici in Piemonte" [53], which contains geographical data and in-depth technical sheets [54] regarding the theoretical evaluation of the electric field generated by telecommunications installations. In particular, the technical sheets contain data derived from the documentation submitted to Arpa Piemonte in the context of the request for an opinion issued by the Agency in accordance with current regulations. These data relate to both telecommunications installations - Radio and TV transmitters - and base stations for mobile telephony.

The installations are distinguished based on the technology used into the following categories:

- Telephony and Radio TV installations;
- Telephony 2G-3G installations;
- Telephony 4G installations;
- Telephony 5G installations;
- Telephony 5G temporary installations;
- Other type of telecommunications system.

On the portal, each installation is associated with a set of information that can be accessed with a click on the map. Under the "Details" section, it can be found the list of installations and their respective sources on the same support structure. This card includes the following information necessary for building a hypothetical model of the installation:

- *Technical features*: source identifier, system name, direction, mechanical tilt, electrical tilt, total power (W), reduced power (W)*, gain (dBi), carriers, height (m);
- *Administrative process leading to the issuance of an opinion by Arpa Piemonte*: request protocol, request date, release protocol, release date, opinion;
- *Diagram*: data sequence to reconstruct the antenna radiation solid.

Note that the *tilt* is the inclination of the main radiation direction of the antenna relative to the case where it is broadside, meaning orthogonal to the plane in which the antenna lies. This change in the main radiation direction can be achieved either mechanically by physically tilting the antenna on its support, or electronically by modifying the antenna's own characteristics, which remains mechanically in the same position [16]. Detailed information about the installations is available in the "Sources", "Emission Calculation" and "Complete Map" sections.

In this distribution, data accessibility is not automated, as it requires clicking on the icon of each individual base station to obtain the listed information. Moreover, of these details, what is actually desired is a limited subset, namely the geographic location, to complete the visualization on the map. In fact, there is no need to use the technical specifications and the horizontal and vertical radiation diagrams (essential for performing electric field simulations) because, as will be explained later, such simulated values were provided directly by Arpa Piemonte.

Therefore, it was preferred to make use of the *open data* services available on the portal itself. In fact, the services that power the Portal are also available according to the interoperable OGC (*Open Geospatial Consortium*) protocols, which can be used for data querying and download through open GIS tools.

The "Radio Frequency Installations" service includes:

- the location of TLC ()*telecommunications*) installations for which requests for opinions/pronouncements have been received by ARPA Piemonte in accordance with current regulations (daily updates). These installations include: Radio and TV transmitters (e.g., AM and FM radio, DAB, UHF, VHF, DVB-T, DVB-H TV transmitters) and Base Transceiver Stations (e.g., GSM, DCS, UMTS, Wi-Fi, Wi-Max);

- estimation of the electric field at a height of 1.5 meters a.g.l., generated collectively by the telecommunications installations that have authorization to transmit in the regional territory, as maintained by ARPA Piemonte. This estimation is performed at the headquarters of the *Centro Tematico Regionale Agenti Fisici* for forecasting and protection purposes. It is obtained by theoretically evaluating each individual installation using the *free space* and *far-field* model. The calculation is based on the maximum power at the antenna, and the contributions from each individual installation are summed up in quadrature to obtain the overall electric field level. This level represents the maximum achievable electric field value around the installations;

- the results of the monitoring of electromagnetic fields generated by TLC (Telecommunications) installations, with daily updates. These measurements are conducted through field surveys by operators equipped with portable instruments or by monitoring stations that continuously collect information. In the case of point measurements, the maximum value of the electromagnetic field measured in the survey area is reported. As for monitoring stations, the reported values include the minimum, average, and maximum values measured, along with the time period to which these values refer;

- density and number of installations (radio-TV transmitters or mobile telephony base stations) installed in each municipality in Piedmont (daily updates).

The source dataset is fed from the EMITEM database, the regional registry of electromagnetic sources, maintained through ARPA's technical activity. Each source is georeferenced with a pair of coordinates, derived from cartography or GPS surveys. From the metadata [55], it can be inferred that the data is recorded in the WGS84/UTM 32N coordinate system and distributed under the Creative Commons Attribution 4.0 International License.

From the *open data* portal, there is the option to access data on base stations as both WMS (*Web Map Services*) and WFS (*Web Feature Services*), where:

- the Web Map Service (WMS) standard provides a simple HTTP interface for requesting map images from one or more servers distributed on the internet. A WMS request defines which geographic layers and the area of interest to process. The response to the request is one or more map images (in formats like JPEG, PNG, etc.) that can be displayed in a web browser. The standard also supports the ability to specify whether the returned image should be transparent, allowing you to combine layers from different servers;

- the Web Feature Service (WFS) standard, similar to WMS, provides a simple HTTP interface for directly requesting geographic objects (not map images) from one or more servers distributed on the internet. The request and response mechanisms are similar to WMS, with the difference that it doesn't return images but rather descriptions of individual spatial objects within the area of interest to be processed (spatial coordinates and any alphanumeric attributes).

Of the two, the WFS service of RF sources was used, specifically the "Tutti_gli_impianti" layer (Figure 3.8). In the *attribute table* of this layer, it contains the following columns:

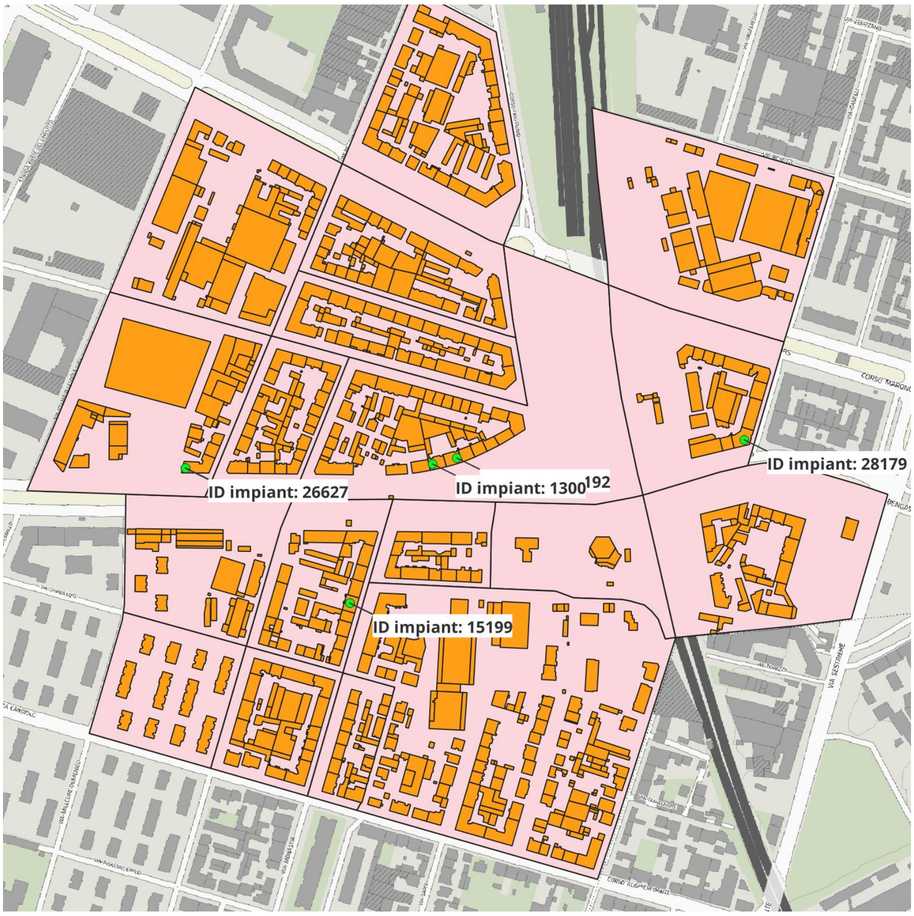

Figure 3.8: In green: base stations locations layer in "Via Vigliani" area of interest.

objectid, comune (municipality), indirizzo (address), id_impianto (plant ID), id_sostegno (supporting structure ID), provincia (province), quota_slm (base height a.s.l.) and tipo_impianto (plant type).

Using the built-in *Field Calculator* in QGIS, longitude and latitude coordinates of the geographical objects representing the sources have been calculated as columns in the attribute table. The expressions *$x* and *$y* were used to perform this calculation. These data will be useful for calculating the relative distance between individual sources and the buildings in the area of interest.

In particular, the *Field Calculator* in QGIS is a tool that allows you to perform calculations based on existing attribute values or predefined functions. For example, you can calculate the length or area of geometric features. The results can be written to a new attribute field, a virtual field, or can be used to update values in an existing field. The *Field Calculator* offers over 400 functions, with nearly half of them being geometric functions.

3.3.4 Estimated values of electric field emitted by BTSs

In order to calculate the population exposure indicator to the electric field generated by BTSs, it is necessary, first and foremost, to focus on selected areas of interest. For these areas, you need to have the simulated electric field values inside buildings since these are the areas where daily exposure exceeds four hours.

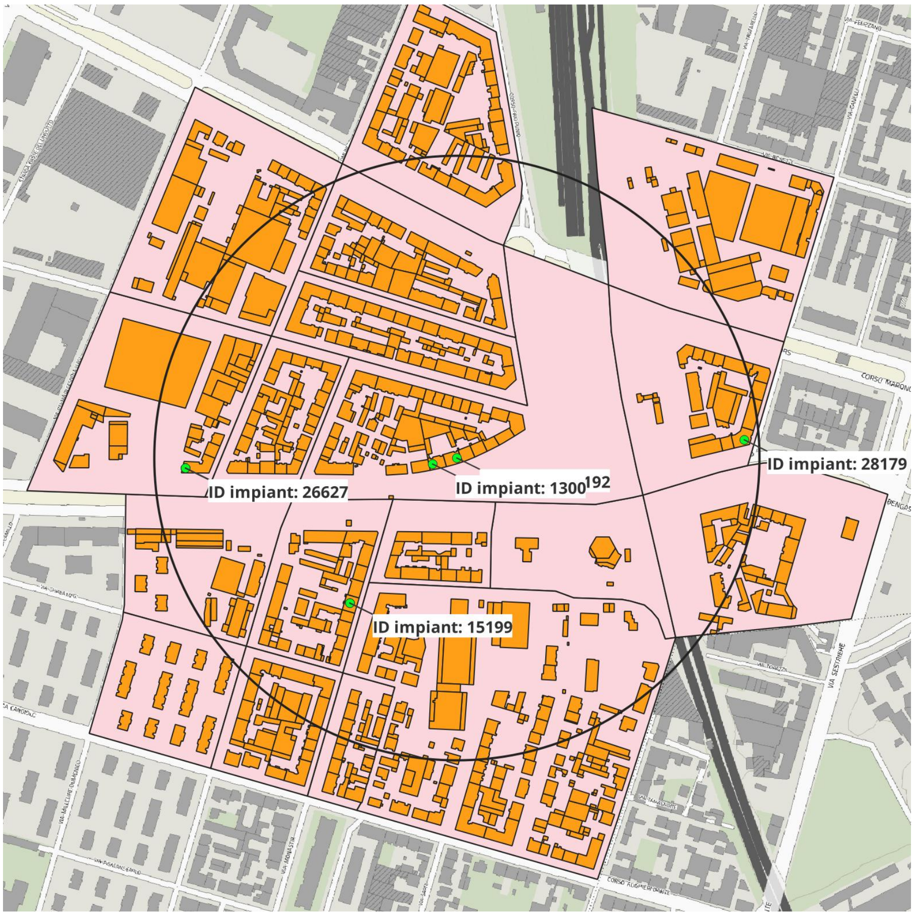

Figure 3.9: In black: circular area of interest layer of “Via Vigliani” area of interest.

As previously said, three areas of interest were selected within the metropolitan city of Turin, namely “Corso Belgio”, “Via Vigliani” and “Via Togliatti”. These areas are circular areas with a radius of 300 meters, and the center corresponds to a specific BTS (Base Transceiver Station), as shown in Figure 3.9.

For the calculation of electromagnetic field levels (in free space), all the BTSs within the areas of interest were considered, meaning within a radius of 300 meters from the central BTS. It's evident that by considering only the base stations within the area of interest, not all significant electromagnetic field contributions will be taken into account. Nevertheless, in many common cases, this is a reasonable approximation because it is likely that the installations outside the area of interest are not in line of sight from the evaluation points due to many obstacles in the way (given the urban environment). This compromise is reasonable because, for the purpose of exposure assessment in a situation closer to reality, these additional considerations would be redundant.

ID impiant	Address	Technologies
12654*	Torino - Corso Belgio, 120	GSM, UMTS, LTE, LTE DSS
15248	Torino - Corso Belgio, 95	LTE, 5G
26375	Torino - Corso Belgio, 95	UMTS, LTE
1197*	Torino - Via Togliatti, 24	GSM, UMTS, LTE, LTE DSS, 5G
8214	Torino - Via Togliatti, 26	UMTS, LTE, 5G
10257	Torino - Via Pavese, 20	GSM, LTE, 5G
19129	Torino - Via Pavese, 20	GSM, LTE, 5G
21056	Torino - Via Palmiro Togliatti, 22-24	LTE, 5G
1192*	Torino - Via Onorato Vigliani, 195	GSM, UMTS, LTE, LTE DSS, 5G
1300	Torino - Via Onorato Vigliani, 193	UMTS, LTE, 5G
10145	Torino - Via Onorato Vigliani, 161	GSM, UMTS, LTE, 5G
15199	Torino - Via Monastir, 10	LTE, 5G
24802	Torino - Via Onorato Vigliani, 161	LTE
26627	Torino - Via Onorato Vigliani, 161	LTE, 5G
26647	Torino - Via Monastir, 10	LTE
28179	Torino - Via Canelli, 130	UMTS, LTE, 5G

Table 3.1: Base transceiver stations considered for each area of interest. The asterisk indicates the BTSs considered as the center of the circular areas.

By doing this, the corresponding installations to be considered during the simulations were identified for each of the three areas: 3 for "Corso Belgio", 8 for "Via Vigliani", and 5 for "Via Togliatti". Some of these include all transmission systems (GSM, UMTS, LTE, LTE DSS, 5G), while others have only some of them. The presence or absence of different technologies is indicated for each installation in Table 3.1. Additionally, the

BTSs considered as the center of each area of interest are marked with an asterisk.

The calculation models of ARPA Piemonte

To calculate the electric field, ARPA Piemonte uses two different software programs, both developed and maintained internally by the agency, called *Cemview* and *ValutaEdifici*.

Cemview

The *Cemview* software has been developed in the National Instruments *LabVIEW* environment and allows for estimating the calculation of the electric field produced by an electromagnetic source according to the *free space* and *far-field* model in two different modes:

- for a list of points with coordinates (x, y, z);
- for an entire area, defined by a spatial origin, a radius (with variable steps), and an altitude relative to the ground (flat or following the orographic profile).

For both modes, the calculation of the electric field is performed in the same way: for each point provided in the list or belonging to the identified area, the contribution produced by each individual source of all the telecommunications installations in the area is calculated. By summing the square of all the contributions calculated for each point, an estimate of the overall electric field value is obtained.

Cemview interfaces with a management software to obtain all the necessary data for the theoretical evaluation. In addition to the x, y, and z coordinates of all the involved installations, all the technical data of the sources present are provided: the height of the electrical center, radiating system power with applied reduction coefficients, the pointing direction, electrical and mechanical tilts, gain of the radiating system, and antenna radiation pattern. Additionally, the DTM (*Digital Terrain Model*) is used.

At the end of the evaluation, it's possible to view the results in both tabular and graphical form (Figure 3.10) and export them in CSV format to potentially feed into GIS software for a geographic context visualization.

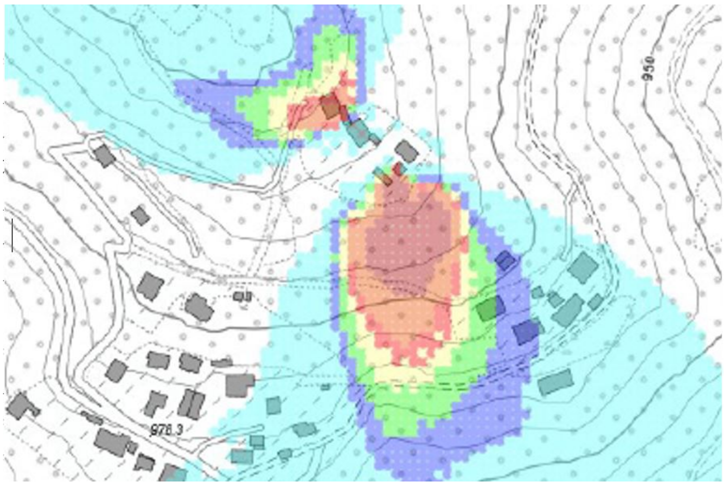

Figure 3.10: Example simulation output for an entire area of the *Cemview* software.

ValutaEdifici

The *ValutaEdifici* software was developed in the Microsoft *Visual Basic* environment, as an extension of the management software. It shares a component responsible for archiving all the data of the electromagnetic register of telecommunications facilities (Figure 3.11).

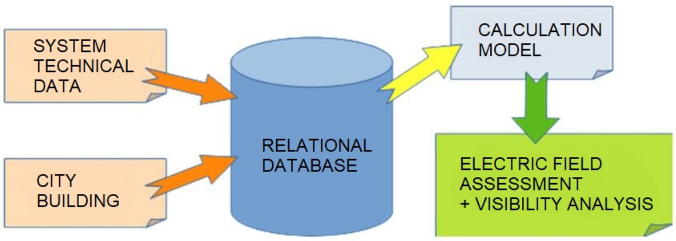

Figure 3.11: Scheme of the connections that are the basis of the *ValutaEdifici* software.

This application was created with the aim of estimating the electric field produced by the installations in a predominantly urban context, for which there is information available that describes the position, shape and height of the buildings (base, eave and ridge heights).

For this purpose, the solids representing the buildings have been converted into three-dimensional arrays of points with coordinates (x, y, z), significantly simplifying the computational component. The matrix was obtained by intersecting a two-dimensional grid of points with a 3 meters × 3 meters grid with the polygons describing the base of the buildings. The matrix was then extended in height for each building, from the base elevation to the eaves elevation increased by 1.5 meters, with a 1-meter interval (Figure 3.12).

Figure 3.12: Example of an evaluation point grid for the *ValutaEdifici* software.

The calculation model used is the same as in *Cemview*, but in this software, it is applied directly to all the points representing the buildings in the area under evaluation. The result of the assessment produces a CSV file that contains all the georeferenced points that exceed a predetermined threshold. This threshold can also be set to zero, meaning that the CSV file returned will contain the electric field values for all the points that make up the considered buildings. Additionally, for each building, the point with the highest value is highlighted. By loading the CSV file into a GIS software, it is possible to visualize the evaluation in a geographic context. During the calculation, the contribution of each individual installation considered in the assessment is tracked to highlight which installation has the greatest impact on the estimated overall field value (Figure 3.13).

This significantly facilitates ARPA's technical opinion release activity, which is a preventive activity before the installation of the installations. Recently, an optical visibility analysis between sources and evaluated points has been added to this software to determine where attenuation coefficients can be applied to the estimated values. Yet, this new optical visibility analysis feature of *ValutaEdifici* software was not utilized in this thesis work.

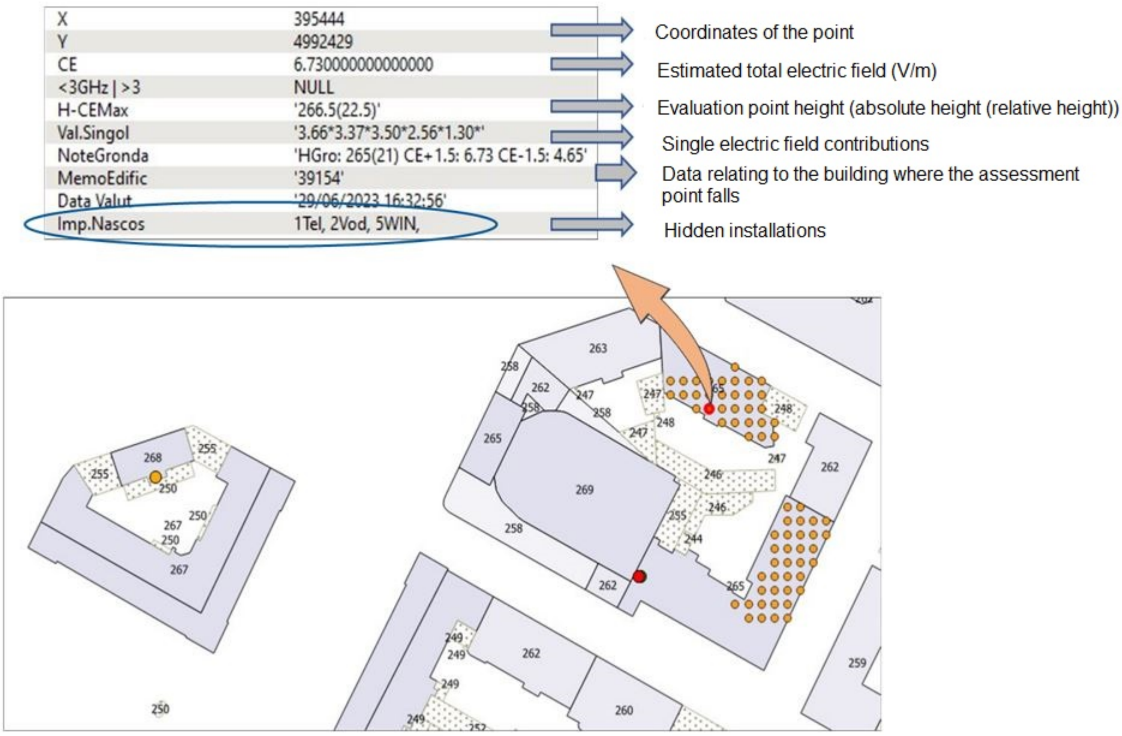

Figure 3.13: Contributions of each individual Base Station considered in the electric field estimation from *ValutaEdifici* software.

For the work of this thesis, the output data from the *Cemview* and *ValutaEdifici* software have been provided by Arpa Piemonte for the three areas of interest, specifically simulating the electric field:

1. within some selected representative buildings that could showcase typical cases of population exposure to the electric field generated by telecommunications installations (using the *ValutaEdifici* software);

2. inside all the buildings within the areas of interest, from which to derive the field distribution (using the *ValutaEdifici* software);

3. in the centroids of all the buildings within the areas of interest at various heights (using the *Cemview* software).

All the simulated electric field values provided by Arpa Piemonte were calculated according to the *free space* and *far-field* model. In the subsequent calculation of the population exposure indicator, this results in a cautious evaluation, as it doesn't consider the role that buildings may play in attenuating the electric field produced by RF sources.

Anyway, for these values, coefficients for various technologies were applied to authorized BS powers both within *CemView* and *ValutaEdifici*. These coefficients have the aim of decreasing in a plausible manner the power that is used to simulate the antennas and takes into account the temporal variability of emissions from installations over a 24-hour period and is defined for each signal, as well explained in Subsection 2.1.5.

Typical exposition buildings - shapefile

Taking into consideration the estimated electric field values provided, in the first case, only two or three buildings were selected for each area of interest that could be representative of exposure scenarios. For these individual buildings, the output files from the *ValutaEdifici* software were provided once loaded into the QGis software, which includes the shapefile (Figure 3.14) along with the corresponding dbf file containing tabular information.

Inside the "attribute table", there are as many rows as there are points that make up the three-dimensional matrix representing the individual building. Each point has multiple features, among which are included:

- building identification number;
- X and Y coordinates of the point (EPSG:32632);
- Z-coordinate of the point (a.s.l and a.g.l.) (unit of measurement: meters);
- total simulated electric field value at that point (unit of measurement: V/m);
- simulated electric field contribution for each individual BTS (unit of measurement: V/m);
- building's base height (a.s.l.), building's eave height (a.g.l. and a.s.l.) (unit of measurement: meters);
- number of above-ground building floors.

For the three areas of interest, the identification codes of the individual buildings considered were as follows: 151569 and 152182 for “Corso Belgio”; 100751, 235800 and 266983 for “Via Vigliani”; 31381_1027560, 32140 and 83814_1027555 for “Via Togliatti”.

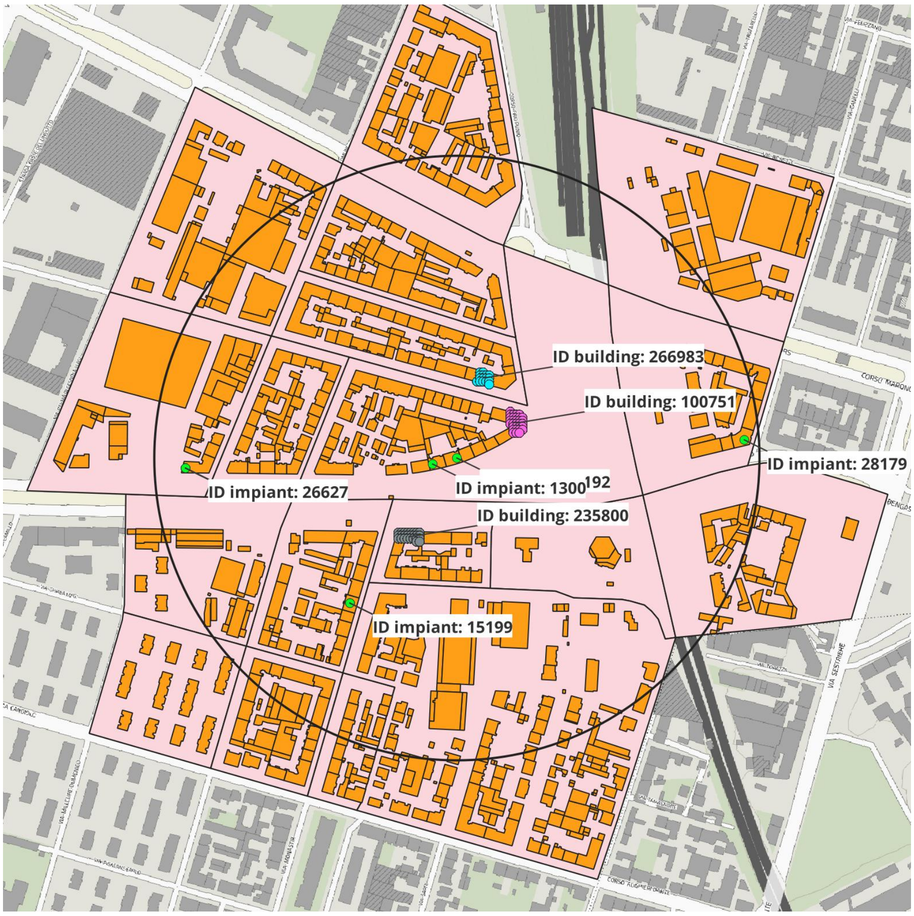

Figure 3.14: In grey, blue and pink: tridimensional evaluation point grid layer in “Via Vigliani” area of interest.

Tutti_punti buildings - csv

In the second case, simulated electric field values were provided for all points corresponding to the three-dimensional matrices inside all the buildings in the areas of interest. This output comes from the *ValutaEdifici* software and is in CSV format, named “Tutti_punti_@@_Alf.csv”, where @@ represents the ID of the base station considered as the center of the 300-meter radius area of interest. For the three areas of interest, the received files were: *Tutti_punti_12654_Alf.csv* for “Corso Belgio”, *Tutti_punti_1192_Alf.csv* for “Via Vigliani” and *Tutti_punti_1197_Alf.csv* for “Via Togliatti”.

In this CSV file, like in the *attribute table* for data on individual typical buildings, there are as many rows as there are points representing all the three-dimensional matrices used to depict all the buildings within the areas of interest. The features included are a subset of those available for individual buildings. In particular, the information regarding the number of above-ground floors and the elevation at the base and eave is missing. However, these details can be indirectly derived from the elevation information of the assessment point (z). It’s important to note the essential presence of the building’s identification number “MemoEdificio” (Figure 3.15).

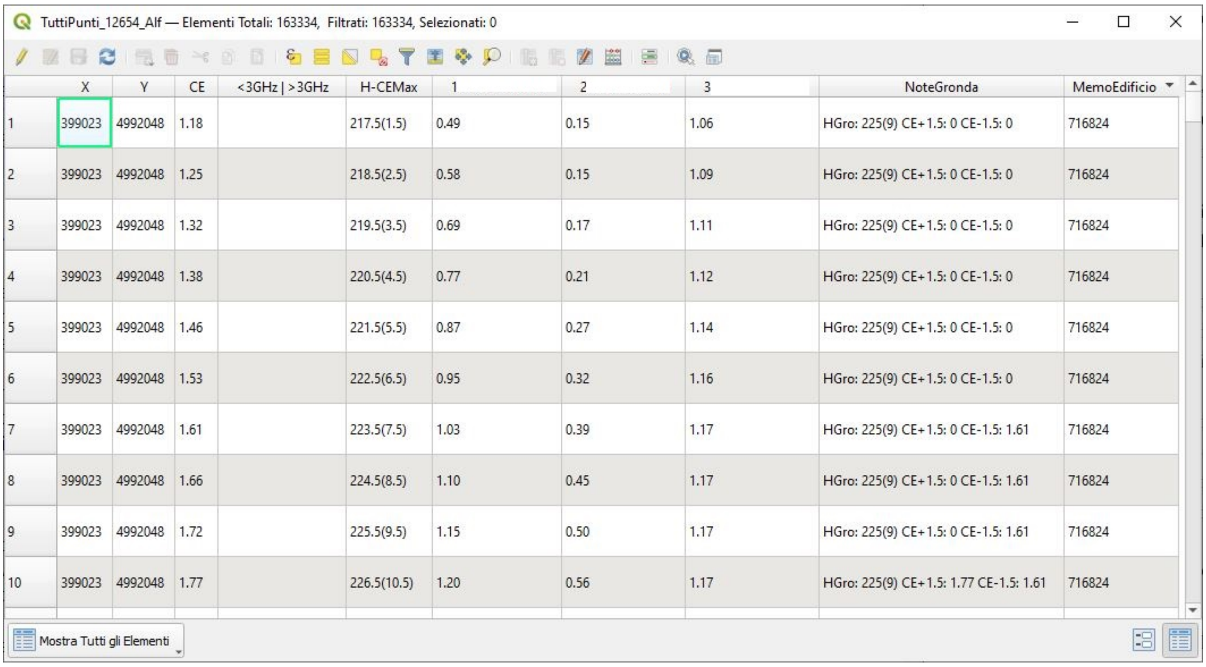

	X	Y	CE	<3GHz | >3GHz	H-CEMax	1	2	3	NoteGronda	MemoEdificio
1	399023	4992048	1.18		217.5(1.5)	0.49	0.15	1.06	HGro: 225(9) CE+1.5: 0 CE-1.5: 0	716824
2	399023	4992048	1.25		218.5(2.5)	0.58	0.15	1.09	HGro: 225(9) CE+1.5: 0 CE-1.5: 0	716824
3	399023	4992048	1.32		219.5(3.5)	0.69	0.17	1.11	HGro: 225(9) CE+1.5: 0 CE-1.5: 0	716824
4	399023	4992048	1.38		220.5(4.5)	0.77	0.21	1.12	HGro: 225(9) CE+1.5: 0 CE-1.5: 0	716824
5	399023	4992048	1.46		221.5(5.5)	0.87	0.27	1.14	HGro: 225(9) CE+1.5: 0 CE-1.5: 0	716824
6	399023	4992048	1.53		222.5(6.5)	0.95	0.32	1.16	HGro: 225(9) CE+1.5: 0 CE-1.5: 0	716824
7	399023	4992048	1.61		223.5(7.5)	1.03	0.39	1.17	HGro: 225(9) CE+1.5: 0 CE-1.5: 1.61	716824
8	399023	4992048	1.66		224.5(8.5)	1.10	0.45	1.17	HGro: 225(9) CE+1.5: 0 CE-1.5: 1.61	716824
9	399023	4992048	1.72		225.5(9.5)	1.15	0.50	1.17	HGro: 225(9) CE+1.5: 0 CE-1.5: 1.61	716824
10	399023	4992048	1.77		226.5(10.5)	1.20	0.56	1.17	HGro: 225(9) CE+1.5: 1.77 CE-1.5: 1.61	716824

Figure 3.15: *Attribute table* of a “Tutti_Punti” file. The column names containing the contributions of the individual systems have been obscured to omit information about the telephone operators.

Buildings’ centroids - csv

In the third case, simulated electric field values were provided for the centroids of all the buildings within each considered area of interest and at two different elevations. This was accomplished using the *Cemview* software. The term "centroid" refers to the center of gravity of the building with respect to the horizontal xy plane. These centroids were assigned dual assessment elevations, one at 5,0 m above ground level and the other at 7,5 m above ground level for each building. The reasons and purposes for choosing these two different assessment elevations for the centroids of the buildings will be explained and compared later on (Subsection 3.6.2).

For now, it is enough to know that the choice of an assessment elevation of 5,0 m a.g.l. results from the typical height of the floor of a second above-ground story in a residential building, which is approximately 3 meters, plus an additional 2 meters to consider the entire height of the human body. This elevation is also found in the literature ([40], [41], [42]). In the past, this choice was justified by referring to the most populated above-ground floor based on ISTAT data from the 1981 permanent population census. These data included information about the resident population distributed by floor in residential buildings, which is not present in the ISTAT data used for this work.

On the other hand, the choice of an assessment elevation of 7,5 m a.g.l. is based on considerations that will be explained later in Section 3.6.1. It suffices to know that it results from the typical height of the floor of a third above-ground story in a residential building, which is approximately 6 meters, plus an additional 1.5 meters to consider the hypothetical exposure of the population residing on that third floor. This elevation aligns with the nominal height relative to the reference floor level used in electromagnetic field measurements.

The two provided files are in CSV format, where each row corresponds to the centroid of a building. Therefore, there will be as many rows as there are buildings within the considered area of interest. The important features included are (Figure 3.16):

- *X (m), Y (m), H (m)*: the coordinates (x, y, z) of the points;
- *E Ris*: the electric field value (in V/m) calculated at those points;
- *CIT_AR*: the identification code for the buildings or centroid points.

Vigliani_val_centroidi_7-5 — Elementi Totali: 521, Filtrati: 521, Selezionati: 0

	X (m)	Y (m)	Quota	H (m)	E Ris	CIT_AR	QT_GRONDA	ALTEZZA_VO	NUM_PIANI
1	394007,9	4985558,6	234	7,5	2,2	71957	252	17,77	5
2	394035,7	4985542,5	234	7,5	2,11	71958	239	4,98	1
3	394047,6	4985526,6	234	7,5	2,13	71959	242	7,84	2
4	393977,2	4985558,1	234	7,5	2,38	71960	255	21,3	6
5	393981,6	4985583,9	234	7,5	2,25	71961	255	21,55	6
6	394047,5	4985595,1	233	7,5	1,82	71962	238	4,52	1
7	394066,7	4985590,5	232	7,5	1,87	71963	242	10,09	2
8	393918,4	4985602,7	234	7,5	2,64	71964	256	21,79	5+1
9	393959	4985662,3	232	7,5	1,98	71965	243	11,04	3
10	393881,7	4985594,2	235	7,5	2,78	71979	249	14,67	4

Mostra Tutti gli Elementi

Figure 3.16: *Attribute table* of estimated electric field values in the centroids of buildings in "Via Vigliani" area of interest (in this case Z coordinate = 7,5 m a.g.l.).

3.4 Issue: choosing the electric field value to associate with the indicator

Throughout the discussion, it has been highlighted that the indicator you want to calculate is based on the relationship between the resident population exposed to radiofrequency electromagnetic fields and the electric field values to which they are exposed. Due to its nature as an environmental indicator rather than an epidemiological study, this relationship must necessarily be qualitative (and not quantitative), and therefore simplified and justified at the same time.

On one hand, procedures for distributing resident population data relative to chosen territorial bases (whether individual buildings or entire census sections) are well-established and simplified (Subsection 3.2.1). On the other hand, the same cannot be said for the choice of the electric field value to associate with this distributed population. Moreover, concerning the population, the available data is limited and aggregated (only *resident* population, not accounting for residents or the movements of workers, lack of information about population per floor, etc.). Therefore, the procedures described in the Subsection 3.2.1 can be considered valid, even though the level of precision is not high.

The difficulty then lies in choosing the electric field value to associate with this population and concurrently finding criteria that can justify this choice. The selected electric field value must meet the criteria of *significance* and *representativeness* of population exposure. It can also be, at most, an overestimated value, that is, prudent, since one of the cornerstones of preventive assessments on exposure to electromagnetic fields and, more generally, the European Union's environmental policy is the *prudent avoidance principle* [18].

The *prudent avoidance principle* is a precautionary principle in risk management which states that reasonable efforts to minimise potential risks should be take when the actual magnitude of the risks is unknown.

In fact, the availability of electric field data is higher compared to that of the population. Since Arpa Piemonte possesses the radioelectric data of RF sources and the software for simulating the electric field generated by them, different simulation methods (described in Subsection 3.3.4) can yield electric field values as outputs with varying levels of detail (three-dimensional grid of points or point values at defined heights).

For this reason, and based on all the discussions so far, there is a need to search for a procedure that can identify and justify the choice of the representative value to be associated with each territorial basis, onto which the resident population will then be distributed. Therefore, two analysis methods were investigated and compared.

One approach is to consider the simulated electric field values on three-dimensional grids corresponding to the buildings (using *ValutaEdifici* software) and, through an analysis of descriptive statistics of these three-dimensional spatial distributions of electric field, attempt to derive a specific characteristic value for each building. This *volumetric approach* allows for a high level of detail in the electric field distribution. However, it becomes a disadvantage when dealing with the large amount of electric field data that needs to be managed when extending the indicator calculation to large territorial scales.

A second approach, with the aim of simplification and to enable easier scalability of the method, for example, at the municipal, provincial, or even regional scale, is to consider the simulated electric field value at a single point within the space occupied by each building (using *Cemview* software). Since there is only one point for each building, it must have three well-justified spatial coordinates. Horizontally, it is reasonable to consider the centroid as the most suitable location to represent the building and, consequently, the distribution of the resident population within it. However, the question arises regarding the choice of height above ground level (i.e., the vertical axis) to assign to the point where the electric field simulation is performed with electric field calculation software.

The goal of the following Section 3.5 and Section 3.6 is indeed to find justification for the choice of this height above the ground in the *volumetric approach* in relation to the *point-wise approach*, which is more suitable for large-scale applications of the indicator being pursued.

3.5 Volumetric approach to simulated electric field values

Regarding the *volumetric approach* to simulated electric field values, it was chosen to follow two complementary paths using the three-dimensional grid of points output from the *ValutaEdifici* software by Arpa Piemonte.

Firstly, the aim was to closely examine the horizontal and vertical distribution of the electric field in some representative buildings, which in turn represent typical exposure to these fields for the population (Subsection 3.5.1).

Secondly, the objective was to investigate the three-dimensional distribution of the electric field for all buildings within the areas of interest through data aggregation using key statistical indicators (Subsection 3.5.2).

3.5.1 Typical exposition buildings: 3D visualization and floors' pie charts

As mentioned, to gain a deeper understanding of the typical exposure scenarios of buildings to the electric field generated by base stations, only specific buildings within each area of interest were considered. These buildings were previously presented in the *Typical exposition buildings - shapefile* section in Subsection 3.3.4. It's worth noting that for the three areas of interest, the identifying codes of the individual buildings considered were:

- 151569 and 152182 for “Corso Belgio”;
- 100751, 235800 and 266983 for “Via Vigliani”;
- 31381_1027560, 32140 and 83814_1027555 for “Via Togliatti”.

It should be noted that information regarding these buildings was provided in shapefile format, and the electric field values were simulated using the *ValutaEdifici* software on a three-dimensional grid with a resolution of $3m \times 3m \times 1m$.

For these buildings that exemplify exposure scenarios, the vertical and horizontal distribution of the simulated electric field was studied. The vertical distribution was visualized through the three-dimensional representation of the grid, and the horizontal distribution involved grouping the data by each above-ground floor and visualizing it using pie charts of the simulated electric field values.

Vertical E.F. distribution: 3D visualization

To visualize the values of the three-dimensional grid of electric field, a *Python* script was employed.

The .dbf file shipped alongside the .shp file, containing tabular information of the grid, was transformed into a *Pandas dataframe*. Subsequently, *feature engineering* was performed to adapt the data for the intended purpose: from a *string-type* column containing information about height a.s.l. and a.g.l. of the evaluation point, two *float-type* columns were created by separating this information.

Furthermore, the values of X and Y for the grid points were recalculated by subtracting the corresponding minimum values from each of them. This is because these are geographic coordinates expressed in the EPSG:32832 reference system, which is in millions. To make the labels on the axes more informative in the three-dimensional visualization, this choice was made.

Throughout this process, the information about the simulated electric field intensity is encoded using the color of the individual points in the visualization. This can be done with either a continuous color scale (*matplotlib* colormap: magma_r) or a discrete color scale (*matplotlib* colormap: tab20).

In the first case of a continuous color scale, the assignment of colors to the various points is automatic. In the second case of a discrete color scale, it was necessary to digitize the electric field values into bins with a selectable width. For the buildings in “Corso Belgio” and “Via Vigliani”, a bin width of 0.5 V/m was used, while for the buildings in “Via Togliatti”, a double bin width of 1 V/m was used. This is justified by the fact that the latter buildings are the installation sites for multiple base stations, meaning that the antennas are located on the rooftops of the buildings. This leads to an extreme variability of the electric field in a limited space, the larger binwidth allows for a tidier, better display.

Thanks to the *matplotlib* library, it was possible to visualize this grid and make it animated by rotating it by 180° with respect to the vertical axis, which is the azimuth. The viewing angle is adjustable from the command line (for the generated images, an elevation angle of 45° was used). The result of the animation was saved in .gif format thanks to the use of the Python library *imageio*. For obvious reasons, only one representative frame for each building considered is presented here, both with a continuous and a discrete color scale (from Figure 3.17 to Figure 3.24).

What has been achieved is of great interest as it has allowed to appreciate the spatial tridimensional distribution of simulated electric field for some sample buildings. This is currently not possible with the *Cemview* and *ValutaEdifici* calculation software, which operate in two dimensions.

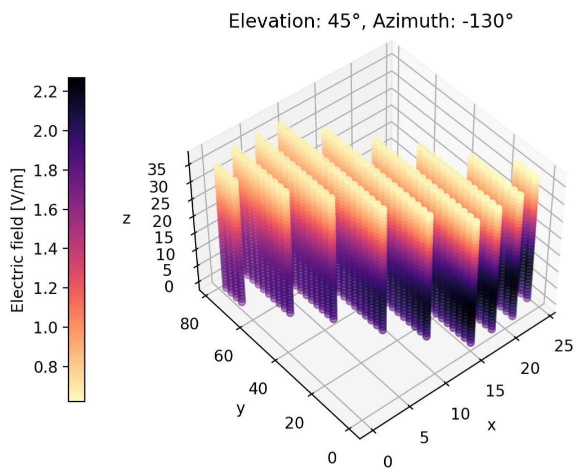

(a) Continuous electric field values.

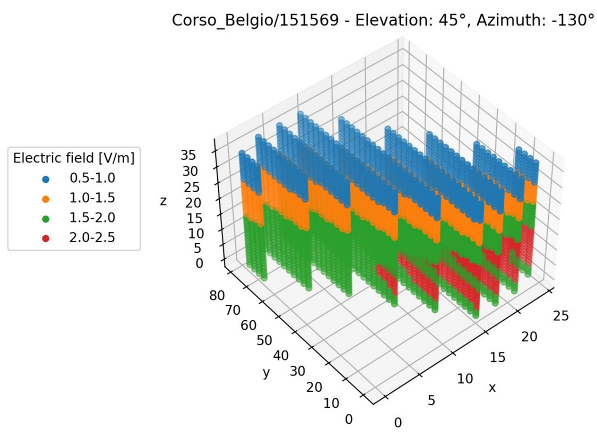

(b) Categorized electric field values.

Figure 3.17: 3D visualization of the E.F. values - building 151569, Corso Belgio.

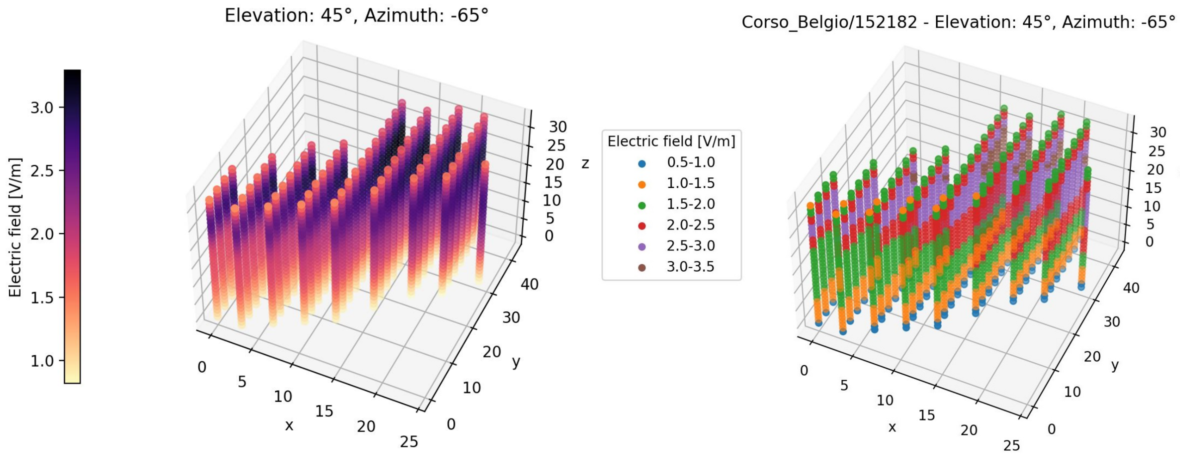

(a) Continuous electric field values. (b) Categorized electric field values.

Figure 3.18: 3D visualization of the E.F. values - building 152182, Corso Belgio.

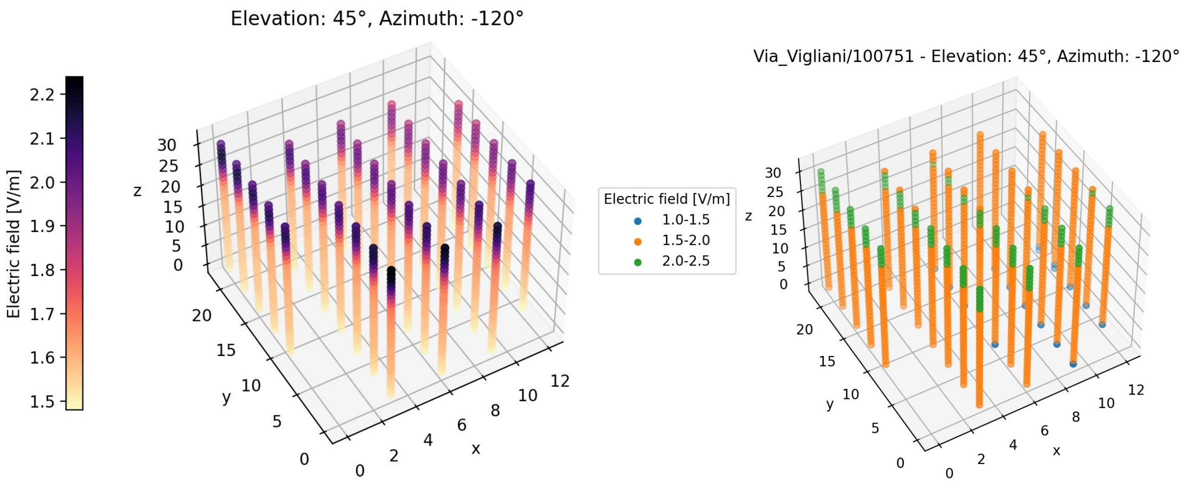

(a) Continuous electric field values. (b) Categorized electric field values.

Figure 3.19: 3D visualization of the E.F. values - building 100751, Via Vigliani.

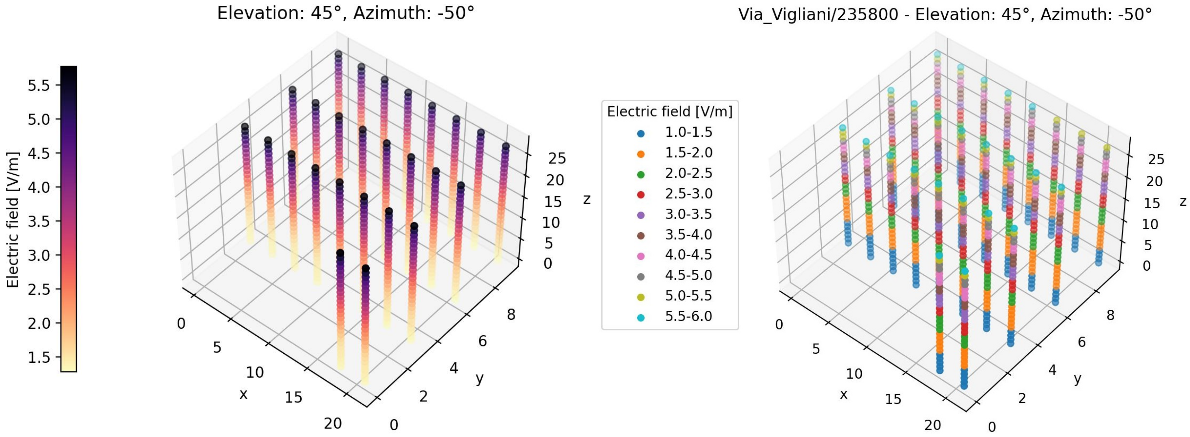

(a) Continuous electric field values.

(b) Categorized electric field values.

Figure 3.20: 3D visualization of the E.F. values - building 235800, Via Vigliani.

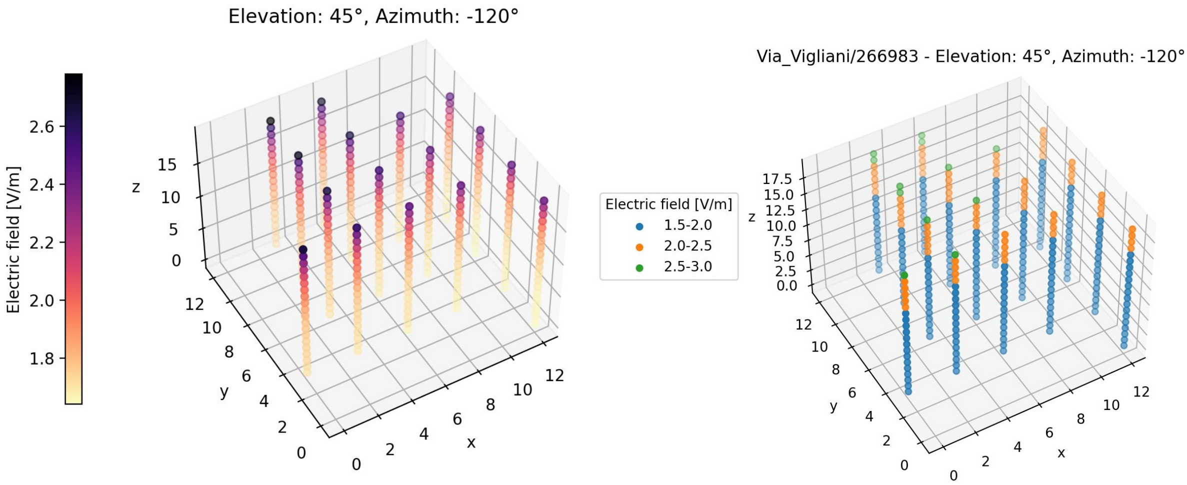

(a) Continuous electric field values.

(b) Categorized electric field values.

Figure 3.21: 3D visualization of the E.F. values - building 266983, Via Vigliani.

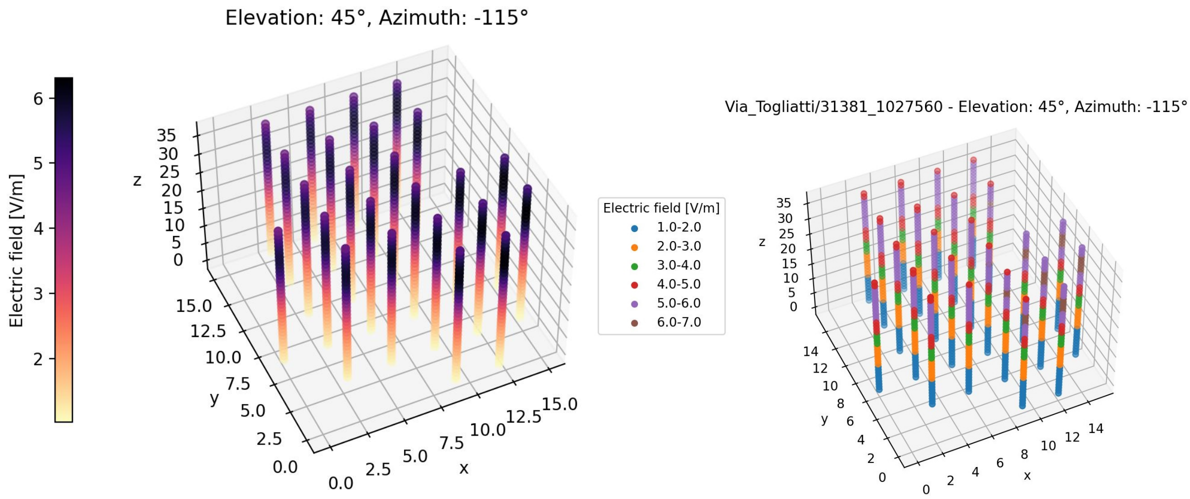

(a) Continuous electric field values.

(b) Categorized electric field values.

Figure 3.22: 3D visualization of the E.F. values - building 31381_1027560, Via Togliatti.

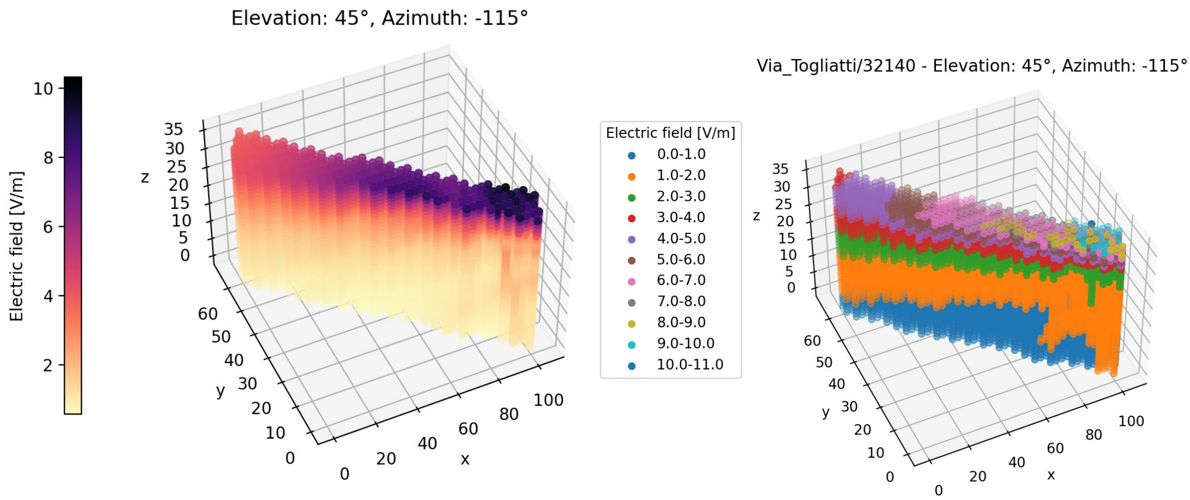

(a) Continuous electric field values.

(b) Categorized electric field values.

Figure 3.23: 3D visualization of the E.F. values - building 32140, Via Togliatti.

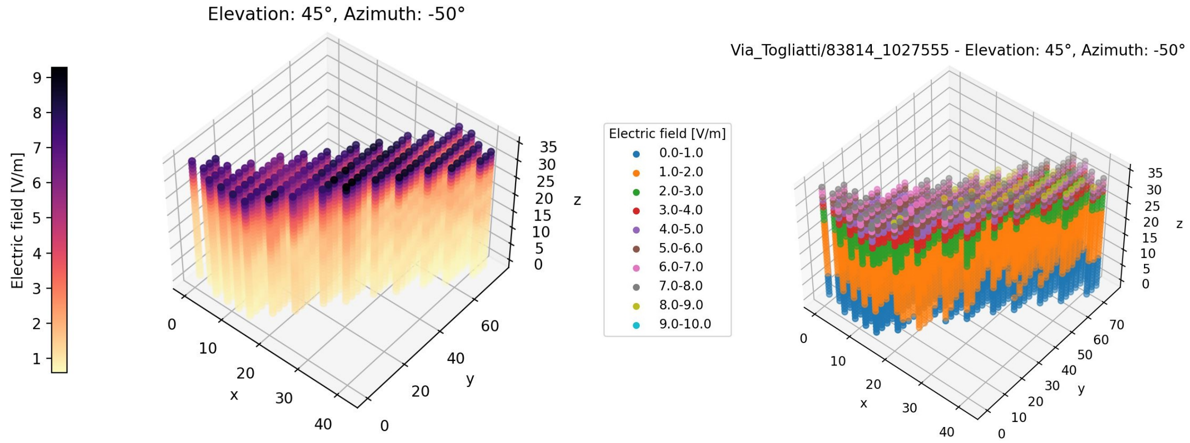

(a) Continuous electric field values. (b) Categorized electric field values.

Figure 3.24: 3D visualization of the E.F. values - building 83814_1027555, Via Togliatti.

Horizontal E.F. distribution: floors' pie charts

Also in this case, to deepen our understanding of the horizontal distribution of the simulated electric field in the selected buildings, a *Python* script was used.

As in the previous point, the .dbf file shipped with the .shp file was transformed into a *Pandas dataframe*, and the same *feature engineering* process was applied to obtain two *float-type* columns with the a.s.l. and a.g.l. heights of the simulation points. For each building, the mean and standard deviation of all simulated electric field values were calculated. The results are shown in Table 3.2.

	ID building	**Total electric field mean [V/m]**	**Total electric field std dev [V/m]**	**Type of exposition**
Corso Belgio	151569	1,49	0,46	Greater exposure on lower floors
	152182	2,04	0,57	Standard case
Via Togliatti	31381_1027560	3,54	1,71	Great vertical variability
	32140	2,2	1,71	BS installation, great vertical variability
	83814_1027555	2,1	1,71	BS installation, great vertical variability
Via Vigliani	100751	1,68	0,18	Standard case, less vertical variability
	235800	2,78	1,27	Standard case, great vertical variability
	266983	1,91	0,25	Standard case, less vertical variability

Table 3.2: Summary of the individual example buildings considered for each area of interest and their type of exposure.

The next step was to provide the option to group the simulated electric field data for each building, both for individual simulation slices (i.e., each 1 meter interval) and for above-ground floors. The latter refers to the aggregation of data belonging to three distinct intervals for all intermediate floors, while for the first above-ground floor and the top above-ground floor, only two simulation slices are aggregated since these start 1,5 m above the ground and end 1,5 m above the eave level.

For both the simulated electric field data aggregated per simulation slice and per floor, the mean, standard deviation and all major statistical indicators (counts, minimum value, maximum value, 25th, 50th, and 75th percentile) were calculated. For the sake of brevity, these are not shown here.

To make the analysis immediately understandable, which aims to examine the horizontal distribution of the simulated electric field, pie charts were chosen to represent these values grouped by above-ground floor. For brevity, only the pie charts related to the most significant exposure cases will be displayed (from Figure 3.25 to Figure 3.28).

Indeed, from a *qualitative* observation of Figures 3.17 - 3.24 and a more *quantitative* examination of the pie charts in Figures 3.25 - 3.28, it can be stated that typical exposure cases are quite diverse. They are briefly summarized in Table 3.2, and to make it clearer, they are:

- *Greater exposure on lower floors*: as the height above ground level (a.g.l.) increases, the simulated electric field decreases. This means that lower floors are exposed to higher electric field values (Figures 3.25 and 3.26);

- *Standard case (greater exposure on upper floors)*: as the height above ground level (a.g.l.) increases, the simulated electric field increases. This is the most common exposure scenario, where higher floors are exposed to higher electric field values (Figure 3.27);

- *Great vertical variability (BS installation)*: a particular case is certainly that of buildings housing base station installations (Figure 3.28). In this case, the horizontal and vertical variability of the simulated electric field, especially in the upper floors, are high due to their proximity to the base station.

From these results, an important consideration can be drawn: the potential exposure scenarios for buildings to the electric field are diverse and varied, moreover they differ significantly from each other. The reasons for these differences are so diverse and discretionary that it's not possible to identify them with *a priori* criteria and apply a solid reasoning based on them. For this reason, the issue addressed in Section 3.4 was approached from a more general perspective, as explained in the next Subsection 3.5.2.

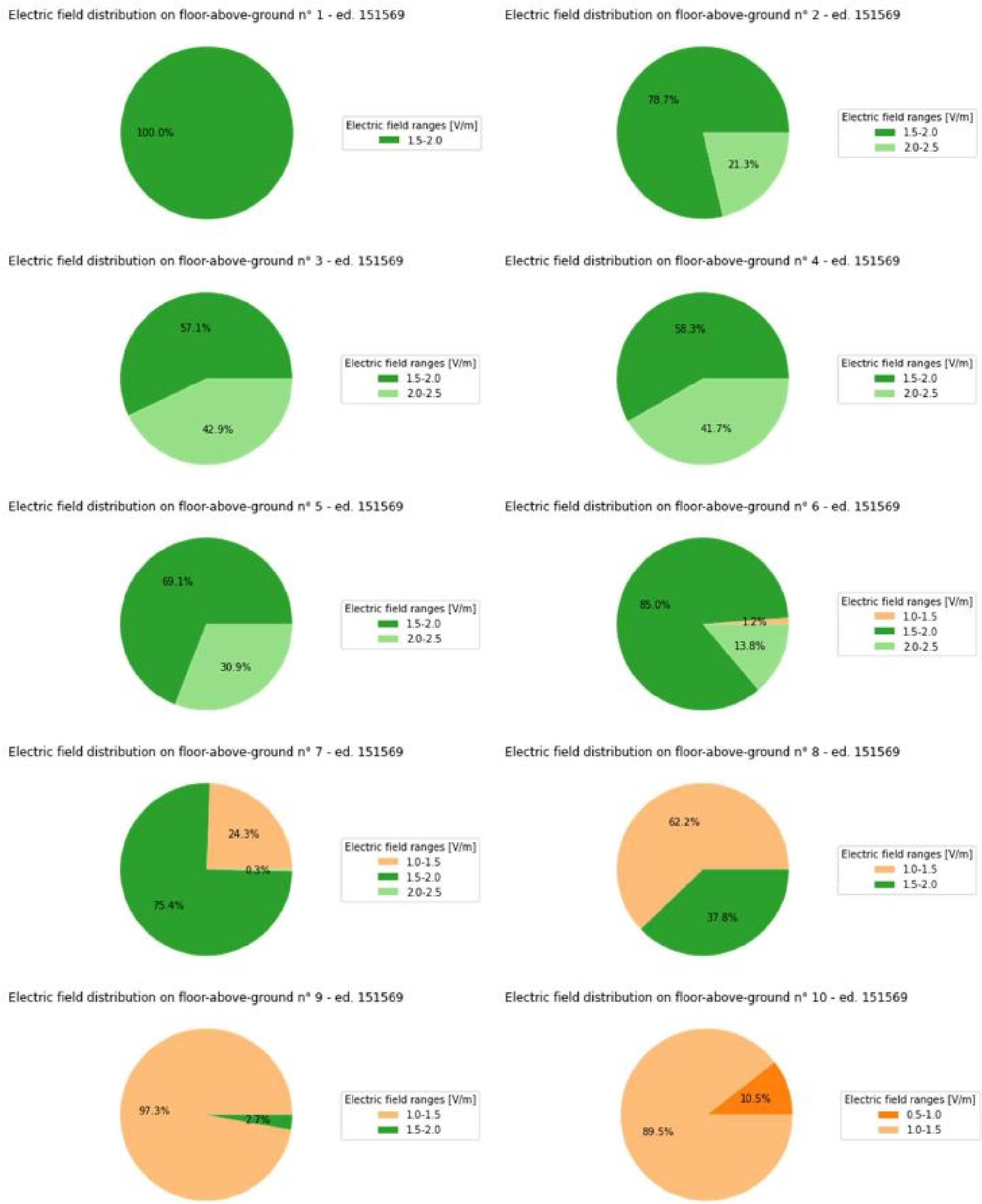

Figure 3.25: Pie charts of the horizontal distribution of the simulated electric field. Exposure case: *greater exposure on lower floors* (first part).

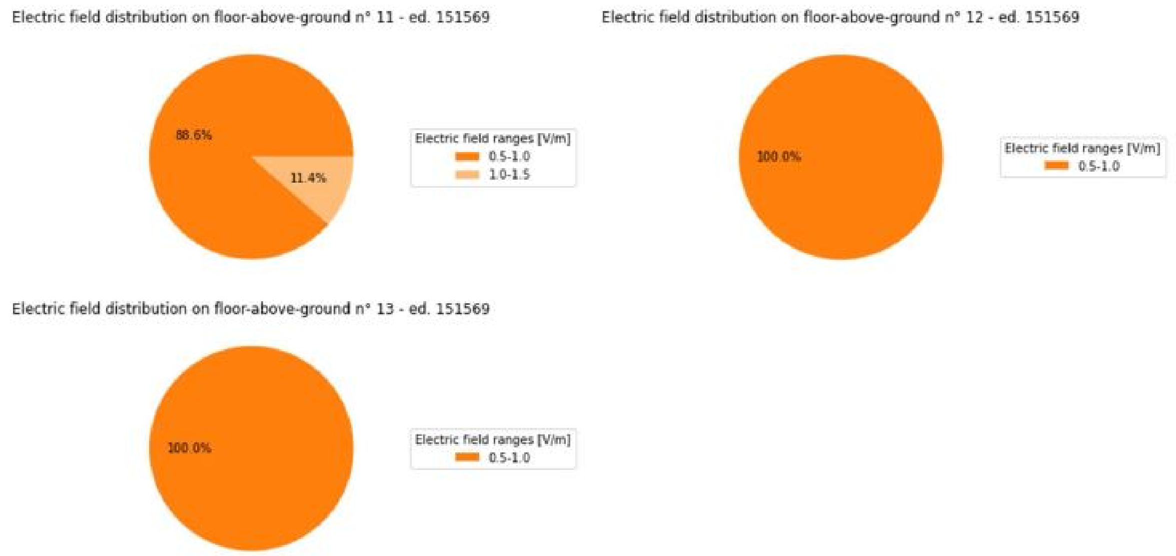

Figure 3.26: Pie charts of the horizontal distribution of the simulated electric field. Exposure case: *greater exposure on lower floors* (second part).

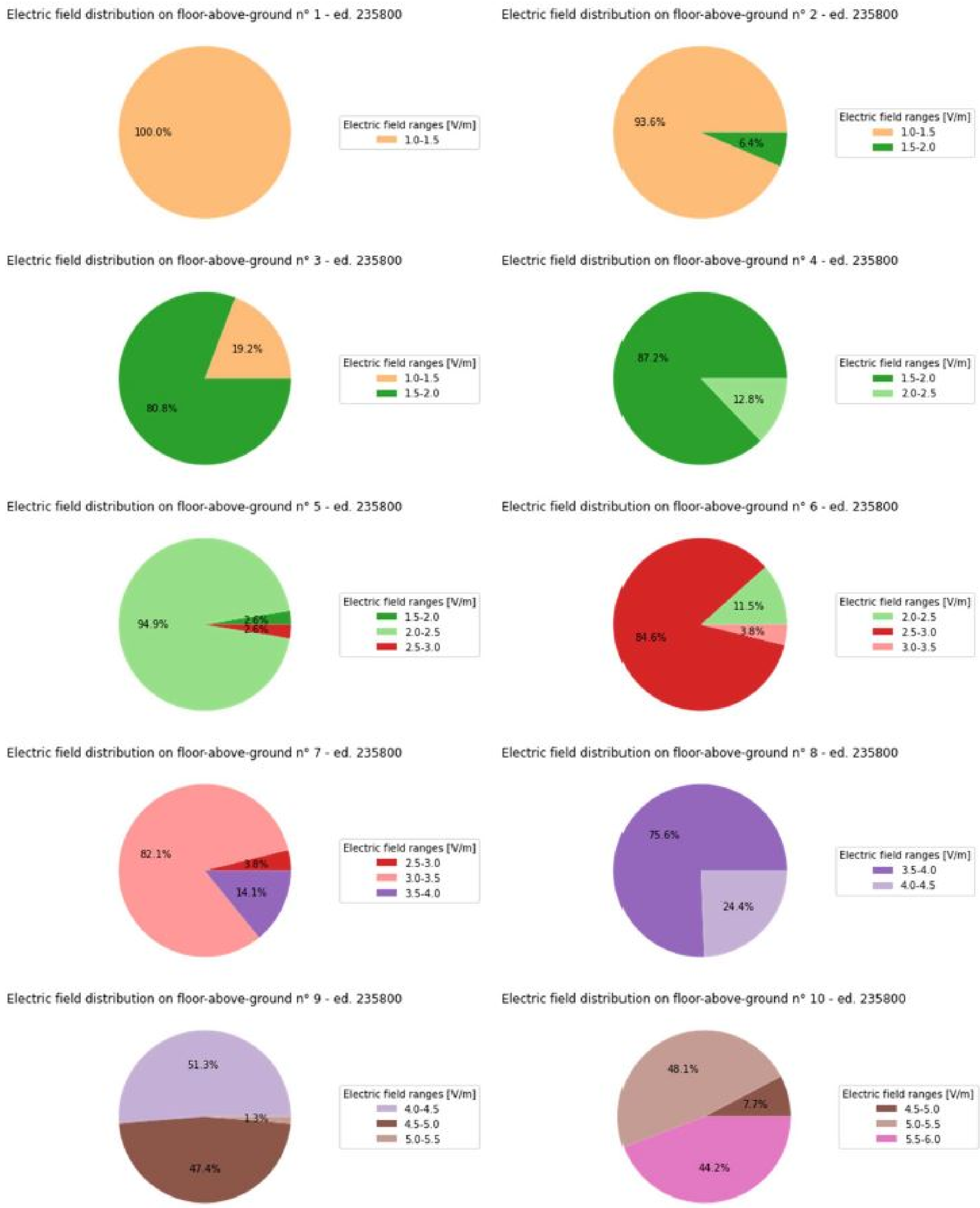

Figure 3.27: Pie charts of the horizontal distribution of the simulated electric field. Exposure case: *standard case (greater exposure on upper floors)*.

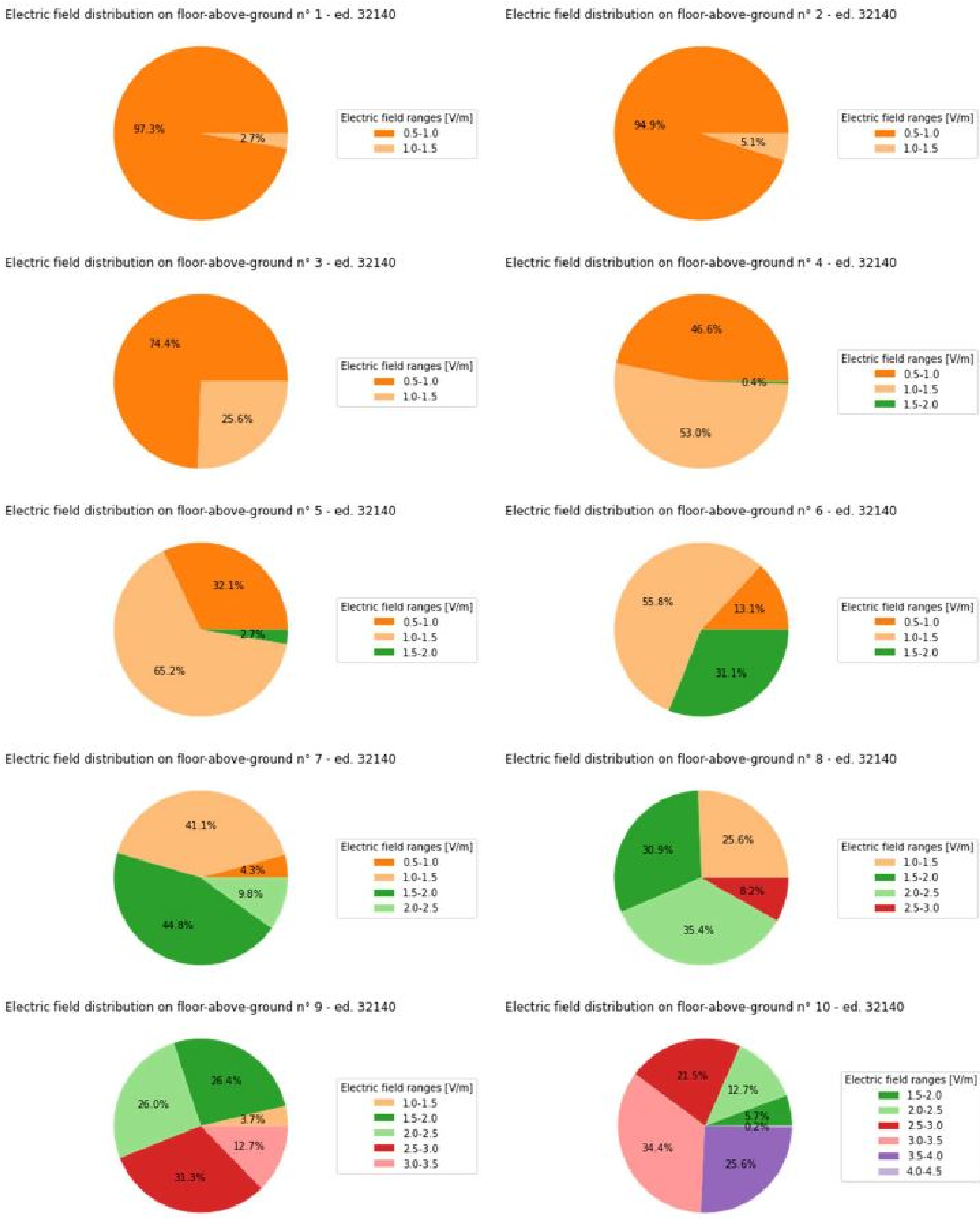

Figure 3.28: Pie charts of the horizontal distribution of the simulated electric field. Exposure case: *great vertical variability (BS installation)*.

3.5.2 Descriptive statistics of all buildings in the areas of interest

A more general perspective than subdividing the specific exposure cases was to consider the simulated electric field values in the three-dimensional grids corresponding to *all* the buildings in each area of interest, not just some of them. The data in question is available as the output of the *ValutaEdifici* software and had already been briefly introduced in the section "Tutti_punti buildings - csv" in Subsection 3.3.4. Please note that for the three areas of interest, the received files were:

- *Tutti_punti_12654_Alf.csv* for "Corso Belgio";
- *Tutti_punti_1192_Alf.csv* for "Via Vigliani";
- *Tutti_punti_1197_Alf.csv* for "Via Togliatti".

Indeed, having this larger dataset allows for a more comprehensive analysis. Therefore, histograms were created for each area of interest to visualize the distributions of key statistical indicators, including: mean, standard deviation, minimum value, 25th percentile, 50th percentile (median), 75th percentile, 95th percentile, maximum value and mode.

In this case, it is possible to have *distributions* of the statistical indicators because each value shown in the histograms to be presented is the result of aggregating all the simulated electric field values belonging to each individual building, which can be discriminated by its identification code. Therefore, the distribution of the standard deviations takes on significant importance as it describes the variability of electric field values within individual buildings in each area of interest.

These considerations were carried out using a *Python* script that converts the "Tutti_punti" file from CSV format to a *Pandas dataframe*. As previously seen, it obtains two *float-type* columns with the a.s.l. and a.g.l. heights of the simulation points.

Using the Pandas *groupby* function, it's possible to group all the points belonging to individual buildings based on their identification code (column "MemoEdificio"). For these subsets, the aforementioned values are calculated and stored, which include: mean, standard deviation, minimum value, 25th percentile, 50th percentile (median), 75th percentile, 95th percentile, maximum value and mode.

In particular, the mode was calculated using the *mode* function from the Python *statistics* library, rounding the simulated electric field values for each building to the first decimal place. This is because, by definition, the mode is the most frequently occurring value in a frequency distribution, and the *mode* function, in case there are multiple values vying to be the mode, selects the first of them based on their order of appearance in the data. Since these values originally had two decimal places and the electric field inside each building varies to some extent, there is a real possibility that, without rounding, the most frequent occurrence could be the result of a random choice. This justifies rounding the simulated electric field values to one decimal place and explains why the resulting mode histogram appears so different from the others (Figure 3.29D, Figure 3.30D and Figure 3.31D).

At this point, the calculated statistical indicators for all the buildings in the area of interest are collected in a *Pandas dataframe*, and this dataframe is used to generate the respective histograms of interest. For the purposes of this thesis, it was considered appropriate to use 50 bins. The histograms created in this way, one for each statistical indicator, are then automatically saved in a single PDF file.

The results of these analyses for the mean, standard deviation, median and mode are presented in Figure 3.29 for "Corso Belgio", Figure 3.30 for "Via Vigliani" and Figure 3.31 for "Via Togliatti". The results with other calculated statistical indicators are reported in Appendix A.

From the observation of these histograms, it is noticeable that for each of the three areas of interest, the distribution of means is very similar to that of medians (or 50th percentile), making the two statistical indicators comparable.

Simultaneously, the distribution of standard deviations (which are specific to each building within the area of interest) is consistently well concentrated on low values, typically below approximately 0,5 V/m. This means that, for the most part, the simulated electric field within each building has low variability. In fact, the cases where there is significant variability in the electric field are those where, as illustrated in Subsection 3.5.1, the building hosts the base station installation or is very close to it (*great vertical variability - BS installation* case). These cases can, therefore, be limited to a small number of buildings compared to all the buildings considered for each area of interest.

It is important to keep in mind that the purpose of this *volumetric approach* was to derive a representative value of the simulated electric field for each building, which could then be associated with the resident population for the calculation of the indicator.

In this regard, the considerations just presented can lead to assert that it is reasonable to consider the *mean simulated electric field value* for each building as representative when you have its three-dimensional grid of simulation points available. This is because the distribution of the mean values is very similar to the distribution of median values, so there would be no substantial differences in choosing the first statistical indicator over the second. Furthermore, thanks to the distribution of standard deviations, we can be confident in stating that these mean values in most cases deviate only slightly from the simulated values for the entire volume of the individual buildings.

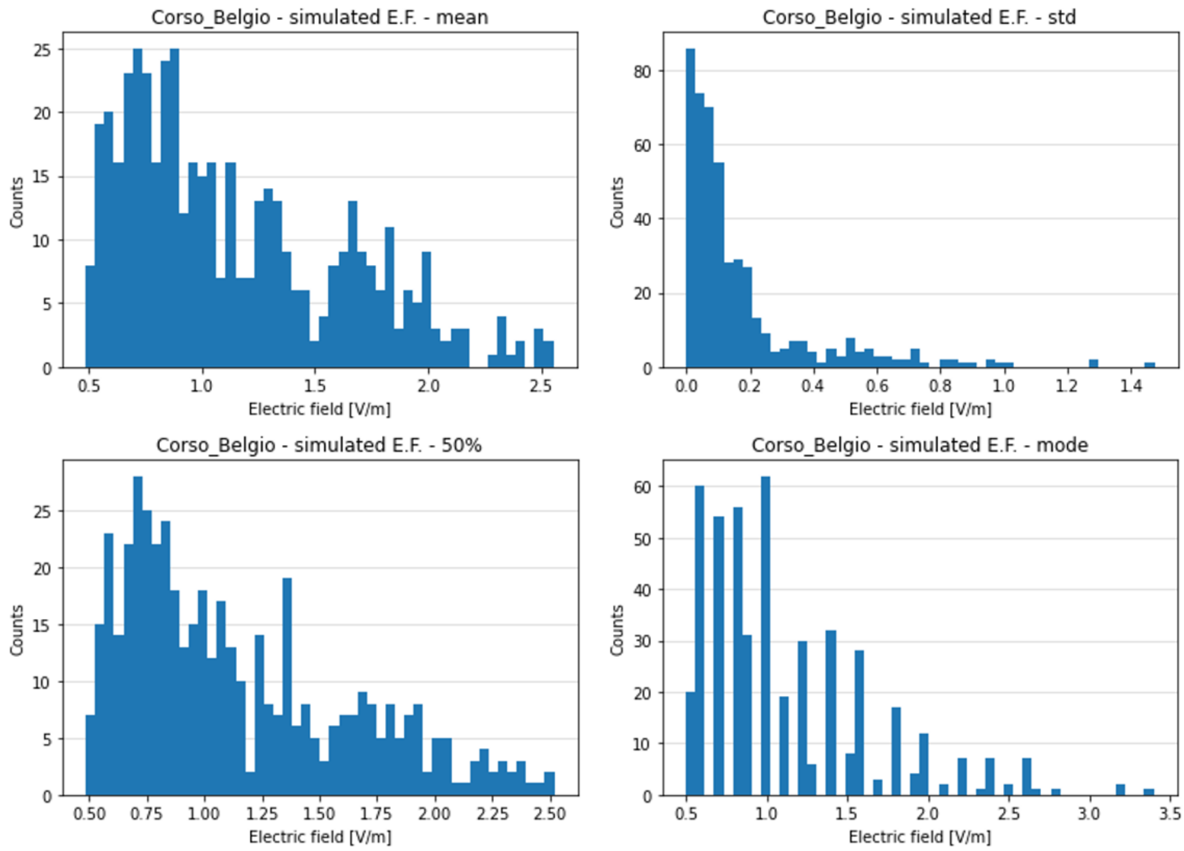

Figure 3.29: Histograms of the statistical indicators (A - mean, B - standard deviation, C - median, D - mode) of the simulated e.f. values in the three-dimensional grids of all the buildings, “Corso Belgio”.

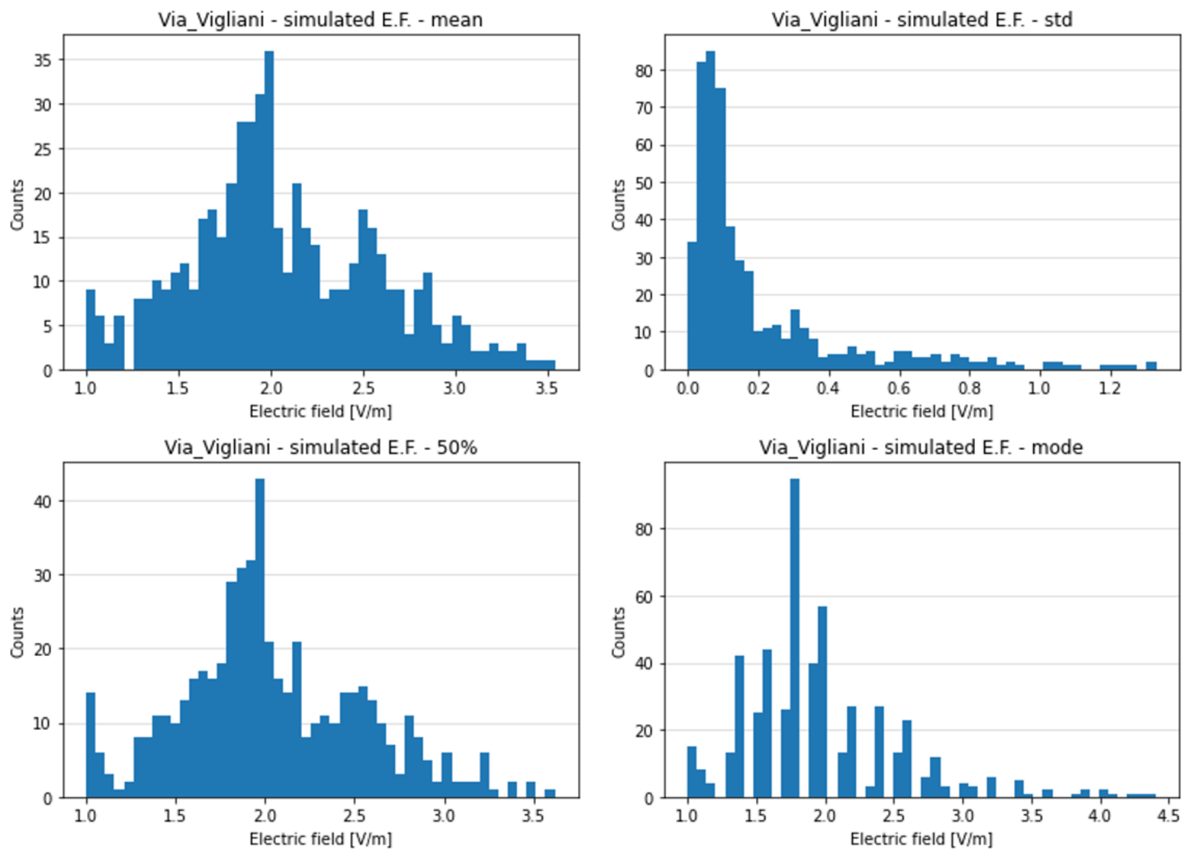

Figure 3.30: Histograms of the statistical indicators (A - mean, B - standard deviation, C - median, D - mode) of the simulated e.f. values in the three-dimensional grids of all the buildings, "Via Vigliani".

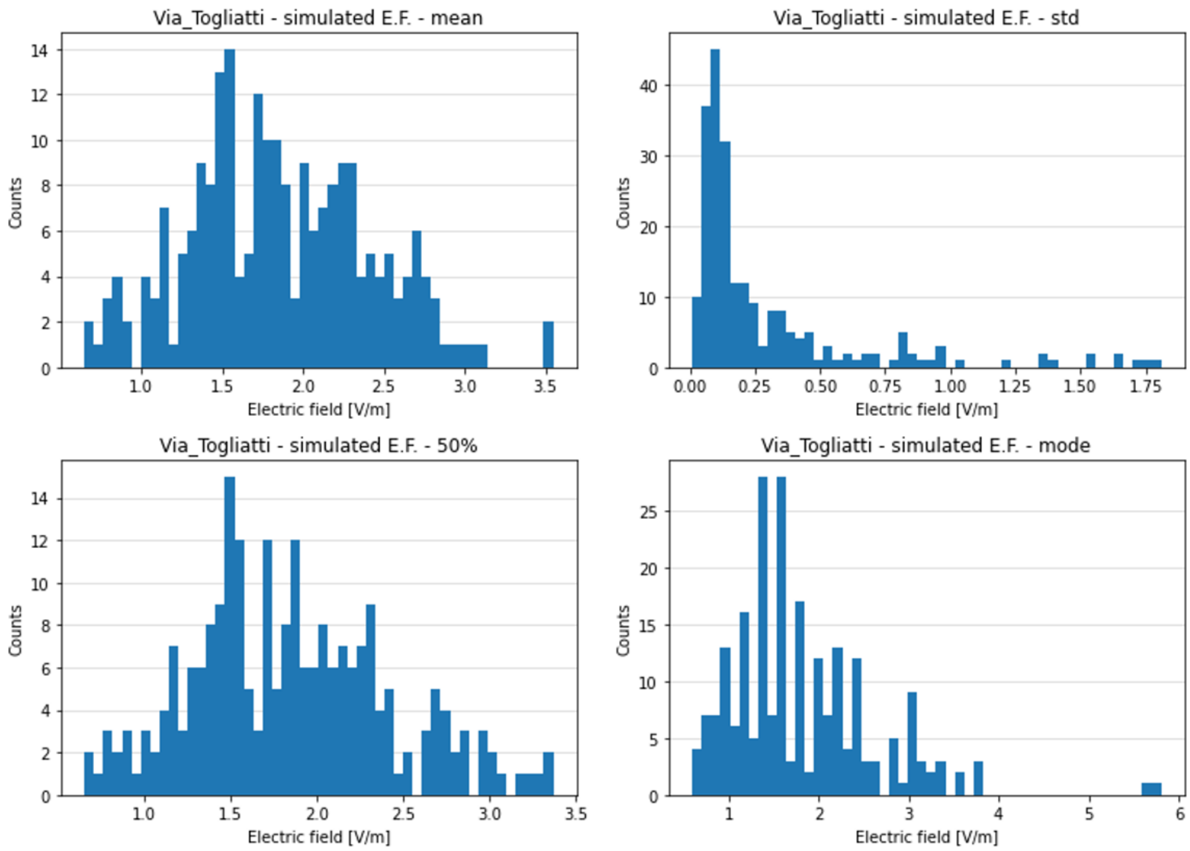

Figure 3.31: Histograms of the statistical indicators (A - mean, B - standard deviation, C - median, D - mode) of the simulated e.f. values in the three-dimensional grids of all the buildings, "Via Togliatti".

3.6 Point-wise approach to simulated electric field values

It was mentioned that the *point-wise approach* aims to achieve greater simplicity and scalability. To do this, for each building in the areas of interest, a single simulation point will be considered. This point will have its X and Y coordinates on the horizontal plane corresponding to the building's centroid. However, there remains uncertainty regarding the Z coordinate of this point, which is the height above ground at which to evaluate the simulated electric field using the *Cemview* software.

To clarify this uncertainty, we relied on studies already conducted by various Regional Agencies regarding the distribution of building heights in major urban centers. In addition, similar analyses were conducted for the cities of Bologna and Cesena to contribute to this understanding. From the results of these analyses for the Metropolitan City of Turin, two heights were derived as eligible for the role of above ground level (a.g.l.) standard evaluation heights for calculating the indicator using the *point-wise approach*. The studies conducted by other Agencies aim to extend this approach to supra-regional contexts.

An attempt was made to compare the distribution of simulated electric field values at the centroids at these two selected heights with the results from the previous subsection, i.e. the *volumetric approach* (Subsection 3.5.2).

3.6.1 Z coordinate of the evaluation points: frequencies of buildings' heights in major urban centres

The method chosen to address the choice of the Z coordinate for the simulation points of the electromagnetic field generated by the base stations in each area of interest was to refer to the studies mentioned in the paragraph "Arpa reports on frequencies of buildings' heights in major urban centers" in Subsection 3.3.1. These studies, conducted by various Regional Agencies, concern the most common building heights in major Italian cities, including the metropolitan city of Turin.

For convenience, the results already presented in Subsection 3.3.1 are reported below:

- *Arpa Piemonte - Metropolitan City of Turin*: from the inspection of the weighted heights distribution (h/A), it was deduced that the most frequent eave height is that of the 2nd/3rd L.A.G.. Taking into account the building volumes, the result varies slightly, settling at the 3rd/4th L.A.G.;

- *Arpa Valle d'Aosta - Aosta*: the conducted studies highlight that the most frequent level is the 2nd/3rd L.A.G.;

- *Arpa Trento - Trento*: the prevailing height of the buildings is at the 3rd/4th L.A.G.;

- *Arpa Veneto - Belluno, Padova, Rovigo, Treviso, Venezia, Verona, Vicenza*: for all the Veneto provincial capitals, it has been found that the most frequent level is the 2nd L.A.G..

With the aim of extending the discussion to a *supraregional scale* and contributing original insights as Arpae Emilia-Romagna, similar analyses were conducted in some cities in the Emilia-Romagna region. The focus was particularly on the cities of Bologna and Cesena, for which data in CSV format are readily available (described in the paragraph "Bologna and Cesena buildings data - CSV" in Subsection 3.3.1).

For each of these cities, an *R* script was employed to conduct analyses similar to the processing conducted by Arpa Piemonte for the city of Turin. CSV files containing information on buildings were read, opening a dialog to select a file from the computer using the *dlgOpen* function from the *svDialogs* library.

For the Municipality of Bologna, the original file contains 66,124 elements. Filters were applied to these and buildings meeting the following criteria were eliminated:

- use with a stay of less than four hours a day, that is: "", "Baracca", "Cabina ENEL", "Campanile", "Cimitero", "Collegamento in quota", "Edificio diroccato", "Mura storiche", "Portico", "Serra", "Silos", "Tettoia/ pensilina";

- base height a.s.l. of 0 meters (since the Municipality of Bologna does not border the sea);

- eave height a.s.l. lower than the first not null base height a.s.l. (equal to 20,5 m a.s.l.);

- eave height a.g.l. equal to 0 meters (it would mean having zero height);

- eave height a.g.l. higher than 40 meters (to exclude the presence of possible bell towers, etc.);

- building area less than 50 square meters (to exclude service buildings or buildings not having habitable characteristics).

The number of buildings remaining post filtering for the Municipality of Bologna is 37549 elements.

For the Municipality of Cesena, the original file contains 62616 elements. Similarly to Bologna, filters were applied and buildings with the following characteristics were therefore eliminated:

- use with a stay of less than four hours a day, that is: "", "CAMPANILE", "CIMITERO", "SERRA FISSA" in the column "TIPO_EDIL" and "IN DISUSO-DIRUTO" in the column "STATO";

- base height a.s.l. of 0 meters and at the same time eave height a.g.l. equal to 0 metres. This is because Cesena is located on the coast, and there may be buildings with a 0 m a.s.l. base height but a non-zero height. Therefore, a more complex condition is required;

- eave height a.g.l. equal to 0 meter;

- eave height a.g.l. higher than 40 meters (to exclude the presence of possible bell towers, etc.);

- building area less than 50 square meters (to exclude service buildings or buildings not having habitable characteristics).

The number of remaining buildings after filtering for the Municipality of Cesena is 32,492 elements.

It's worth noting that the two municipalities in question have significantly different populations (Bologna with approximately 390,000 inhabitants and Cesena with approximately 96,000 inhabitants). Nevertheless, the initial number of buildings and the number after filtering are very similar. This behavior is likely due to how the municipal GIS offices partition the buildings: a single building unit in Cesena is divided into multiple elements compared to how it's done in Bologna.

Once a clean dataset of the buildings was obtained, distributions of various parameters for the two municipalities were compared. Firstly, the percentage distribution of eave heights a.g.l., divided into 3-meter height classes, as this is assumed to be the standard height of a floor above ground (Figures 3.32). It can be observed that the *mode* of the percentage distributions of eave heights a.g.l. falls into the 6-9 meter bin for both municipalities.

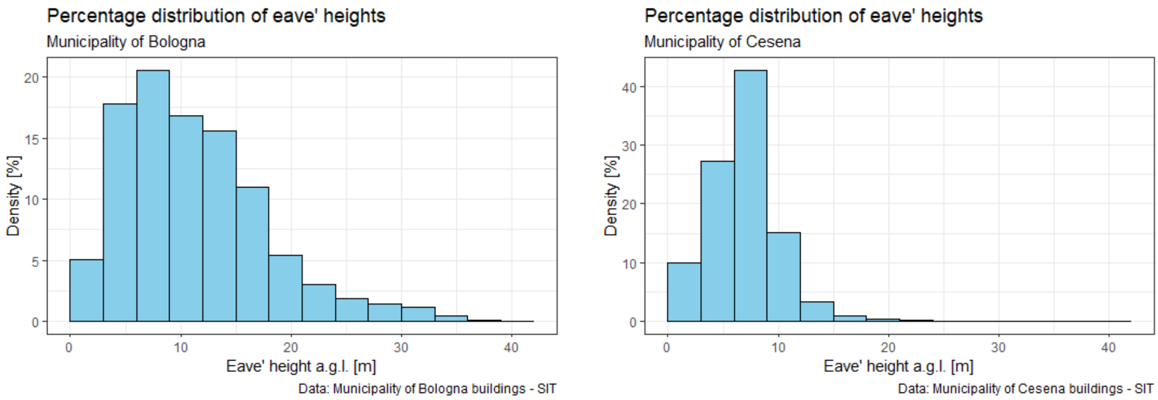

Figure 3.32: Comparison between percentage distributions of eave' heights for the Municipality of Bologna (left side) and of Cesena (right side) (height classes of 3 meters).

For completeness, a boxplot of the eave heights a.g.l. for all post-filtered buildings was also plotted (Figure 3.33), as well as a breakdown by usage.

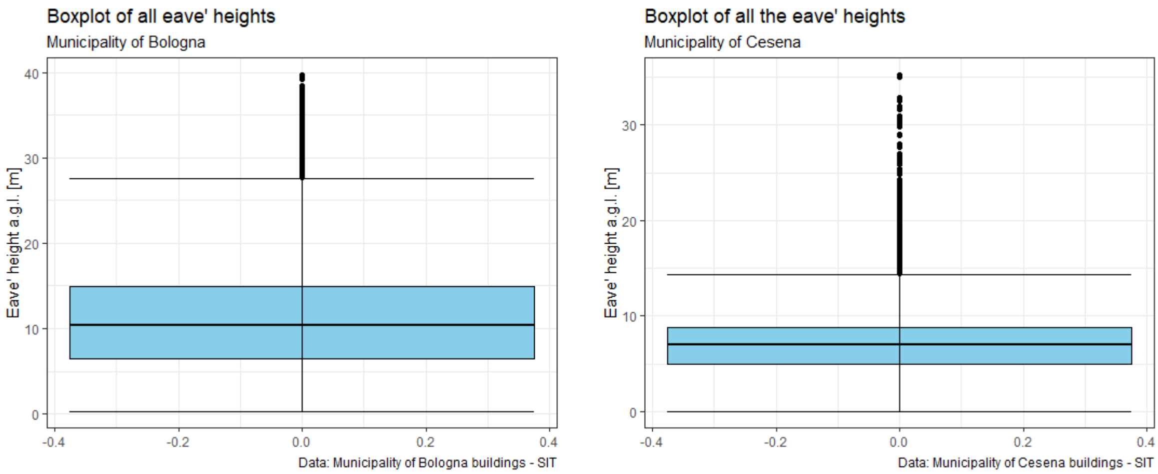

Figure 3.33: Comparison between boxplots of all eave' heights a.g.l. for the Municipality of Bologna (left side) and of Cesena (right side).

For Bologna (Figure 3.33-left), the arithmetic mean of above-ground eave heights is 11,3 m a.g.l., while the geometric mean is 9,5 m a.g.l..

For Cesena (Figure 3.33-right), the arithmetic mean of above-ground eave heights is 7,1 m a.g.l. and the geometric mean is 6,4 m a.g.l..

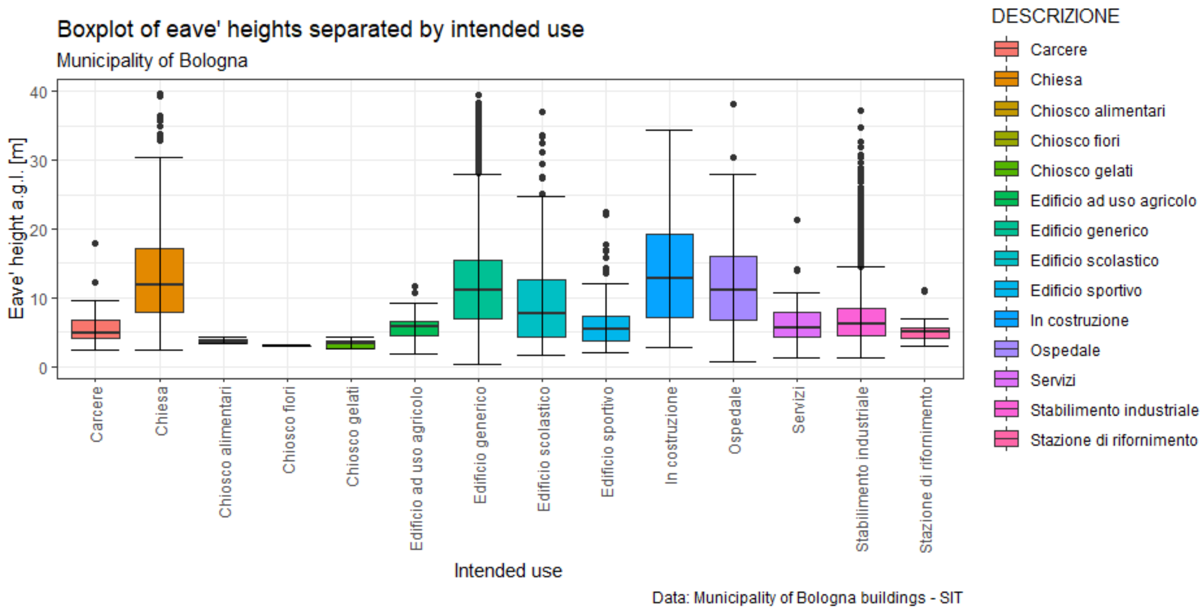

Figure 3.34: Boxplots of Bologna eave' heights divided by intended use.

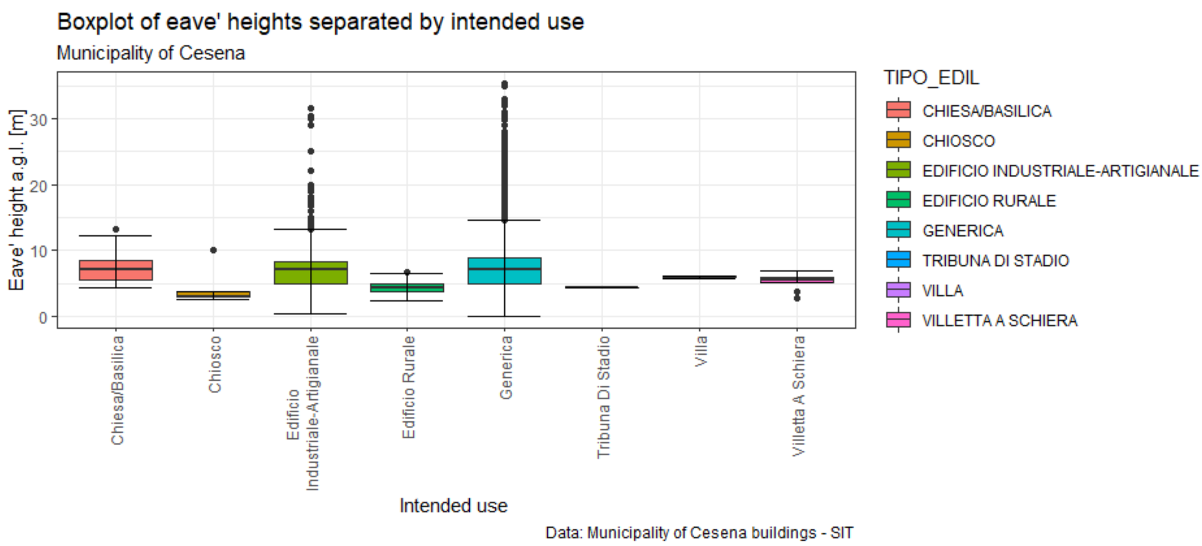

Figure 3.35: Boxplots of Cesena eave' heights divided by intended use.

From the boxplots divided by usage for Bologna (Figure 3.34) and Cesena (Figure 3.35), it can be observed that churches, hospitals, and industrial buildings tend to be quite tall, sometimes even taller than generic residential buildings.

A comparison was also made between the percentage distributions of the areas of the two municipalities buildings, using area classes of 50 square meters up to approximately the 95th percentile of the area distribution (Figure 3.36).

Just like for the city of Turin, the trends here are strongly decreasing, with the most frequent area class corresponding to the first bin for both municipalities ($50 \div 100m^2$). It is noted that, as expected for a regional capital, the distribution of areas for Bologna extends to slightly higher values than Cesena.

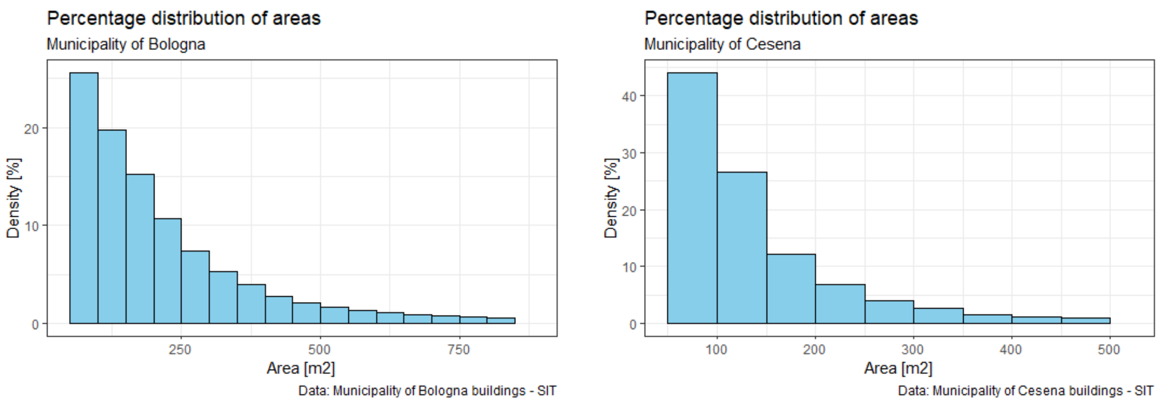

Figure 3.36: Comparison between percentage distributions of areas for the Municipality of Bologna (left side) and of Cesena (right side).

At this point, for the buildings in the two municipalities, the weighted eave heights a.g.l. with respect to the area was calculated and divided into classes of $0.05m^{-1}$ width (Figure 3.37). Again, both distributions show a similarly rapidly decreasing trend, with the mode corresponding to the $0 - 0.05m^{-1}$ bin. Consequently, as for Turin, considerations were made to deduce the most likely above-ground floor level for the municipalities of Bologna and Cesena, taking into account the most probable values from the distributions of areas and weighted eaves heights a.g.l..

In this regard, both for the Municipality of Bologna and for the Municipality of Cesena:

$$\tilde{h} = \tilde{A} \cdot (\widetilde{h/A}) = 100\ m^2 \cdot 0.05\ m^{-1} = 5\ m \tag{3.4}$$

This height corresponds to the most frequent *eave height a.g.l.* through this analysis.

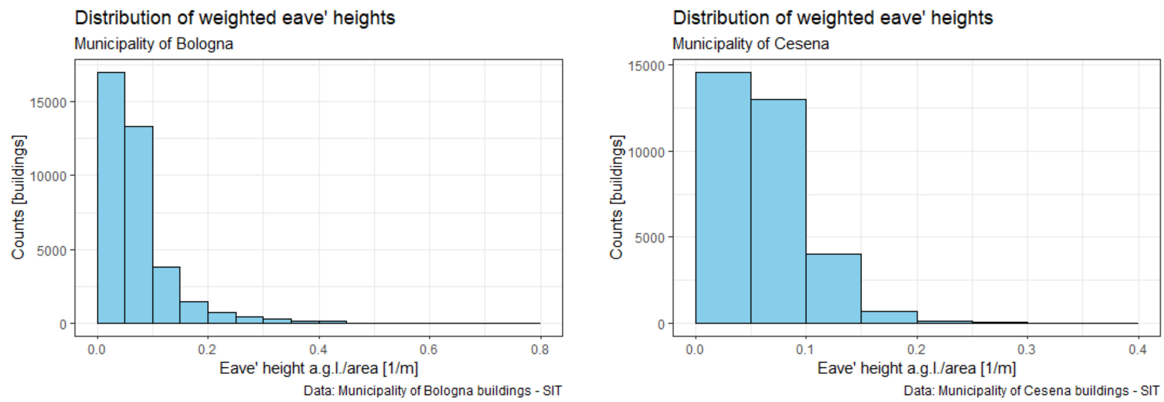

Figure 3.37: Comparison between distributions of weighted eave' heights a.g.l. for the Municipality of Bologna (left side) and of Cesena (right side).

An eave at 5 meters above the ground, in turn, corresponds to the 2nd/3rd L.A.G..

Finally, for both municipalities, the percentage distributions of the volumes at the eaves were visualized by modeling the volumes as rectangular prisms, i.e., the volume was calculated for each building as the product of the eave heights a.g.l. and its area. These distributions display volume classes of 500 m^3 up to a volume value approximately corresponding to the 95th percentile of the volume distribution (Figure 3.38).

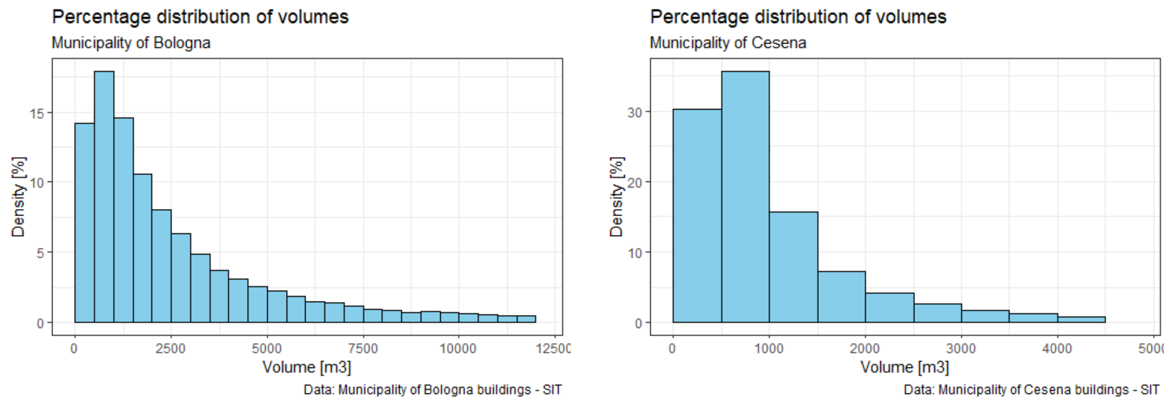

Figure 3.38: Comparison between percentage distributions of volumes for the Municipality of Bologna (left side) and of Cesena (right side).

The trend of the eave volume distributions for the Municipalities of Bologna and Cesena (Figure 3.38) is similar and it is initially increasing, reaches a most frequent value and then begins to decrease. For both municipalities, the mode corresponds to the second bin ($500 \div 1000\ m^3$).

Similar to the previous step, considerations were made regarding the values with higher probability in the distributions of areas and eave volumes so that it was possible to infer the most probable above-ground floor height through this additional method.

In this regard, both for the Municipality of Bologna and for the Municipality of Cesena:

$$\tilde{h} = \frac{\tilde{V}}{\tilde{A}} = \frac{1000\ m^3}{100\ m^2} \approx 10m \tag{3.5}$$

This height corresponds to the most frequent eave height a.g.l. through this analysis. An eave at 10 meters above the ground, in turn, corresponds to the 4th L.A.G..

During all these considerations, the criterion for determining the most probable values has been to use the upper bounds of the binwidth intervals in the formulas. This is done to somewhat account for the tails of the distributions towards higher values.

It should be noted that the subject of this thesis is certainly the calculation of the "levels of radiofrequency electromagnetic field exposure for the population" indicator, particularly in the city of Turin. For this reason, with respect to the search for a significant height above ground for point evaluations of the electric field, the results presented for Turin metropolitan city were considered valid, i.e., a height that could correspond to the 2nd/3rd L.A.G. (result of considerations on weighted heights) or the 3rd/4th L.A.G. (result of considerations on volumes).

With the goal of *scalability* and considering all the results from other Agencies (Arpa Valle d'Aosta, Appa Trento, Arpa Veneto, Arpa Emilia-Romagna), among the options of choosing the 2nd, 3rd, or 4th L.A.G., it was decided to consider two specific heights as suitable: 5,0 m a.g.l. and 7,5 m a.g.l. compared to the base of each individual building, corresponding to the 2nd and 3rd L.A.G..

The first value of 5,0 m a.g.l., as explained earlier, corresponds to the height of the first floor above ground (3 meters) increased by 2 meters to encompass the entire extent of a hypothetical resident standing at the 2nd L.A.G..

The second value of 7,5m a.g.l. corresponds to the height of the first two floors above ground (3+3 meters) increased by 1,5 meters, this time to be comparable to the height at which radiofrequency electromagnetic field measurements are legally required to be taken at the 3rd L.A.G..

3.6.2 Simulated electric field values in the buildings' centroids at two eligible heights

Once the two suitable heights a.g.l. to be associated with the assessment points for each building in the areas of interest were selected, simulated electric field values were collected at these centroids and for these heights. These data have already been briefly presented in the "Buildings' centroids - csv" paragraph of Subsection 3.3.4. There is one file for each height, and they are the result of simulations performed by Arpa Piemonte using the *Cemview* software.

It is important to note that, for each building in the area of interest, the point evaluation approach considers two centroids at two different heights, i.e., two evaluation points that are candidates to represent the exposure of the entire building. On this occasion, the goal is to discern which of the two heights can be chosen as the final height to assign to the evaluation points on which the indicator calculation will be based.

To do this, with the help of a *Python* script, the CSV files containing the simulated electric field values at centroids with heights of 5,0 m a.g.l. and 7,5 m a.g.l. are read and transformed into *Pandas dataframes*. Furthermore, to find a connection point between the *volumetric approach* and the *point-wise approach*, the corresponding "Tutti_punti" files were also loaded and the necessary operations were performed to make the data usable.

By filtering the values in the column that contains the identification code of the building associated with the simulated electric field value (i.e., the "CIT_AR" column), we ensure that only those simulated electric field values at the centroids of the buildings with a volumetric counterpart, i.e., the values of the electric field simulated on the three-dimensional grid, are considered.

From these filtered values of simulated electric field at two heights in the centroids, the first step is to visualize their distribution for each area of interest using the Python library *matplotlib*, with an appropriate number of bins (50 in this case). These distributions show the number of buildings as a function of the simulated electric field values at the centroids for the two considered heights and they are shown in Figure 3.39 for "Corso Belgio", Figure 3.40 for "Via Vigliani" and Figure 3.41 for "Via Togliatti".

What can be observed is that for all three areas of interest, there is no substantial difference between the distributions of centroids at 5,0 m a.g.l. (left side of Figures 3.39 -

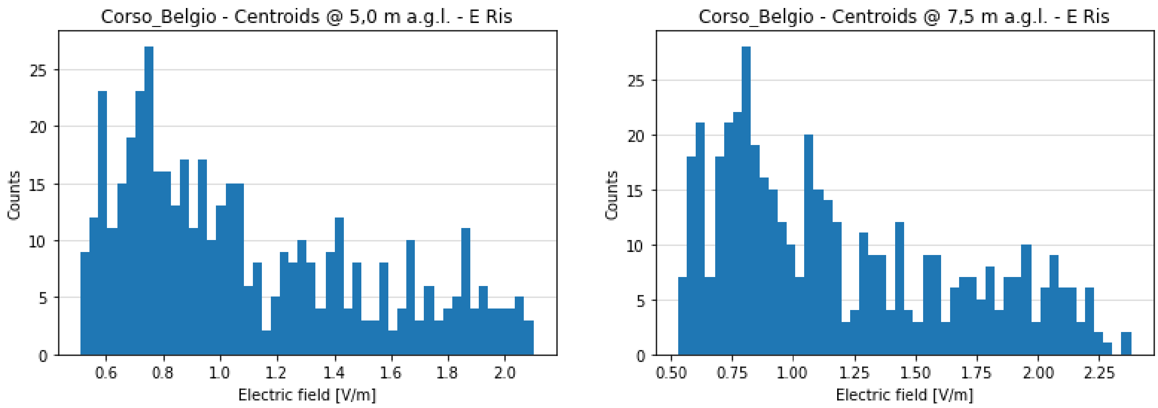

Figure 3.39: Comparison between distributions of electric field values simulated in centroids at heights of 5,0 m (left side) and 7,5 m (right side) a.g.l. for "Corso Belgio" area of interest.

3.41) and the distributions of centroids at 7,5 m a.g.l. (right side of Figures 3.39 - 3.41). The most frequent simulated electric field values, meaning those with the highest counts, fall into the same approximate ranges for both evaluation heights, and the shapes of the distributions resemble each other. Specifically, the most frequent simulated electric field values in the centroids are within:

- $0.6 - 0.9\ V/m$ for "Corso Belgio";
- $1.7 - 2.2\ V/m$ for "Via Vigliani";
- $1.6 - 1.9\ V/m$ for "Via Togliatti".

This leads to the conclusion that the choice of either of the two suitable evaluation heights for the centroids (5,0 m a.g.l. or 7,5 m a.g.l.) is effectively equivalent.

At this point, in order to reasonably assert the thesis that the simulated electric field values at building centroids (whether they are at a height of 5,0 m a.g.l. or 7,5 m a.g.l.) can be considered as representative point values of building exposure, a comparison was made with the results obtained through the *volumetric approach* (Subsection 3.5.2). This comparison was carried out by overlaying the distribution of simulated electric field values at the centroids with the distributions of the statistical indicators obtained from the corresponding three-dimensional grids of evaluation points (mean, minimum value, 25th percentile, 50th percentile (median), 75th percentile, 95th percentile, maximum

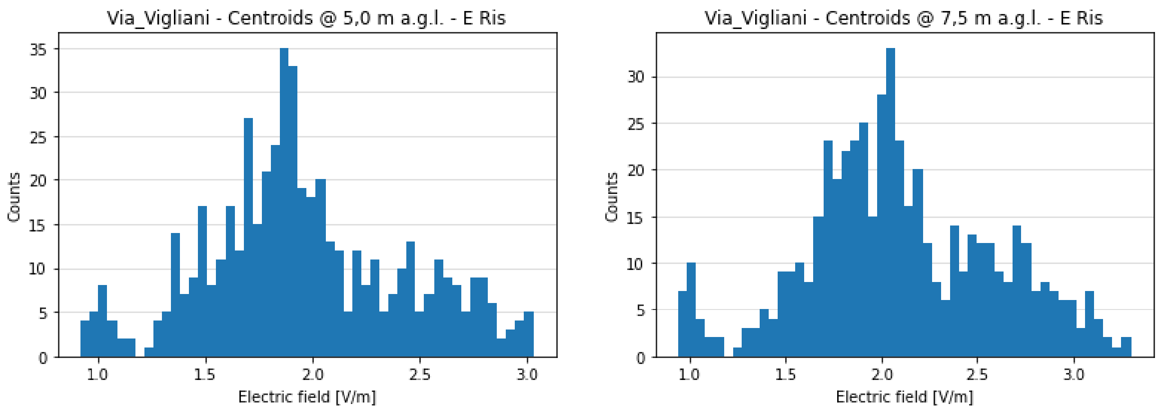

Figure 3.40: Comparison between distributions of electric field values simulated in centroids at heights of 5,0 m (left side) and 7,5 m (right side) a.g.l. for "Via Vigliani" area of interest.

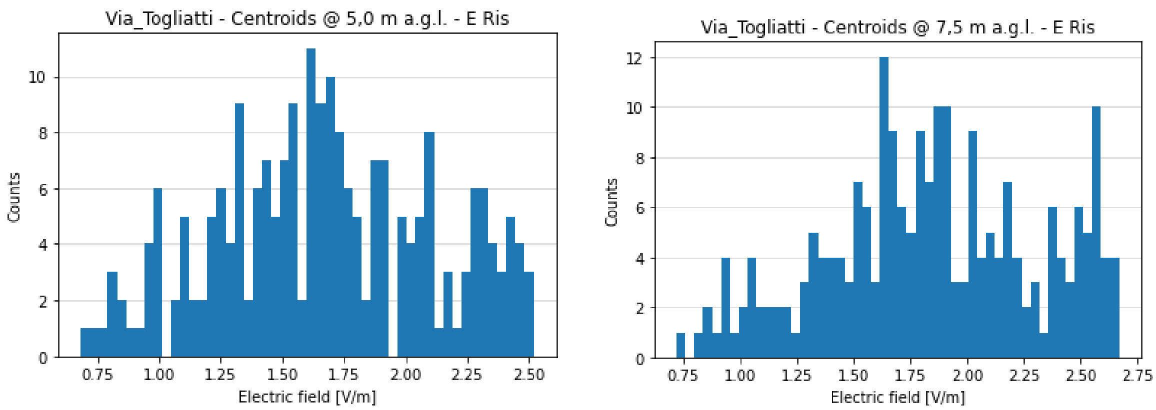

Figure 3.41: Comparison between distributions of electric field values simulated in centroids at heights of 5,0 m (left side) and 7,5 m (right side) a.g.l. for "Via Togliatti" area of interest.

value and mode). This was done for each of the two heights assigned to the evaluation centroids.

Regarding the comparisons with the means, which is the statistically representative indicator of the three-dimensional grid of evaluation points, the results can be seen in Figure 3.42 for "Corso Belgio", Figure 3.43 for "Via Vigliani" and Figure 3.44 for "Via Togliatti". The comparisons with the other statistical indicators are reported in Appendix B.

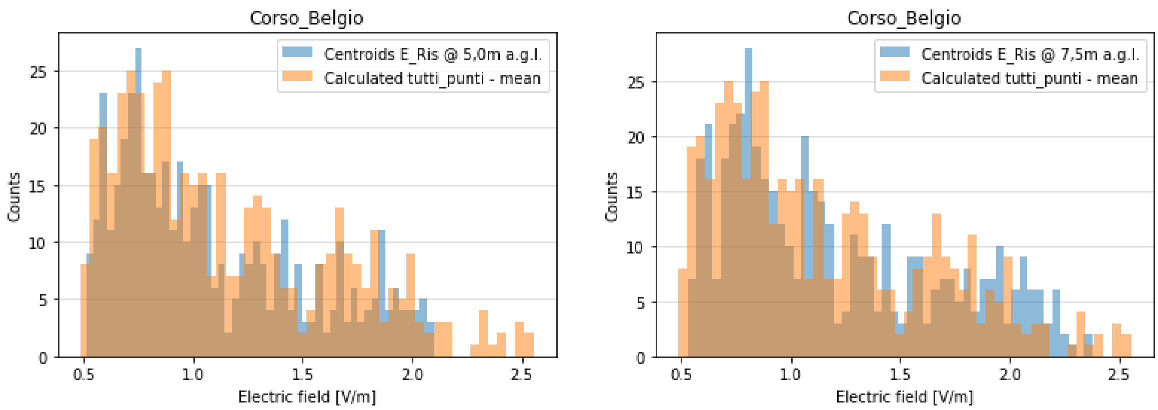

Figure 3.42: Comparison between the distribution of the simulated electric field values in the centroids (light blue) at 5,0 m a.g.l. (left side) and at 7,5 m a.g.l. (right side) and the *means*' distribution obtained from the *volumetric approach* (orange), "Corso Belgio".

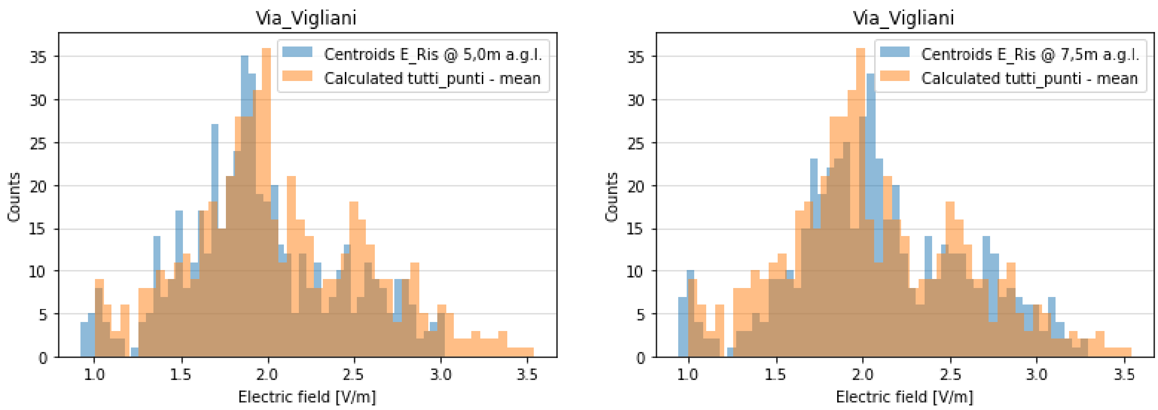

Figure 3.43: Comparison between the distribution of the simulated electric field values in the centroids (light blue) at 5,0 m a.g.l. (left side) and at 7,5 m a.g.l. (right side) and the *means*' distribution obtained from the *volumetric approach* (orange), "Via Vigliani".

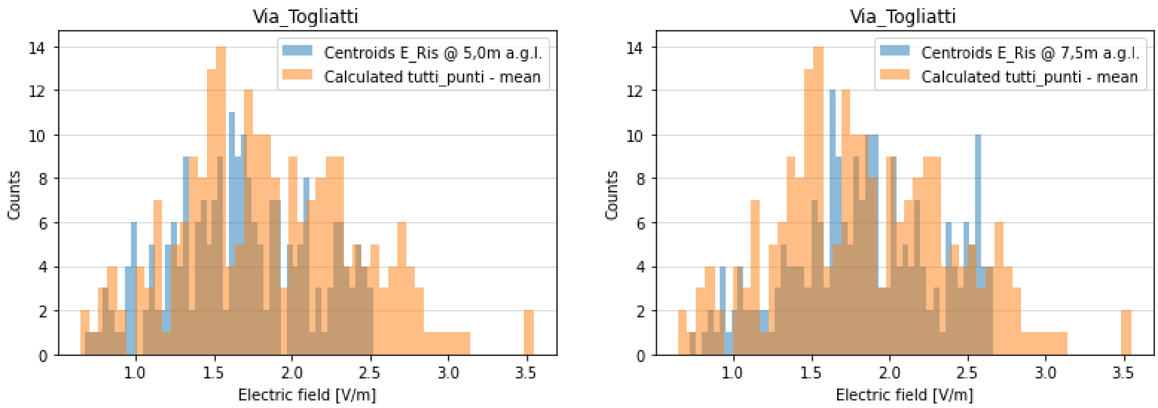

Figure 3.44: Comparison between the distribution of the simulated electric field values in the centroids (light blue) at 5,0 m a.g.l. (left side) and at 7,5 m a.g.l. (right side) and the *means*' distribution obtained from the *volumetric approach* (orange), "Via Togliatti".

In this case, it's evident that a comparison with the standard deviation distribution from the *volumetric approach* is not possible. This is because the *point-wise approach* provides only a single value of simulated electric field per building and there is no associated dispersion. However, this level of simplification is suitable for the purpose of calculating the indicator.

For the interpretation of the comparisons in Figures 3.42 - 3.44, the assumption is made that the results obtained in Subsection 3.5.2 are valid. This means that when the three-dimensional grid of simulated electric field points for each building (*volumetric approach*) is available, it is reasonable to consider the mean of these values as a *representative* exposure value for each building.

With this assumption, it can be observed that the distribution of simulated electric field values at the centroids at 5,0 m a.g.l. and 7,5 m a.g.l. (shown in light blue in Figures 3.42 - 3.44) is comparable to the distributions of the mean simulated electric field values using the three-dimensional grid (shown in orange in Figures 3.42 - 3.44).

In particular, in each comparison, the most frequently occurring simulated electric field values in both distributions fall within the same intervals mentioned earlier, which are $0,6-0,9\ V/m$ for "Corso Belgio", $1,7-2,2\ V/m$ for "Via Vigliani" and $1,6-1,9\ V/m$ for "Via Togliatti". The overlap between the two types of graphs is so evident that it is considered redundant to burden the procedure with any further tests of the similarity of the two distributions.

As a result, in the context of assessing exposure to electromagnetic fields generated by radiofrequencies, the *representativeness* of the mean of the simulated electric field values on the three-dimensional grid in the *volumetric approach* can also be transferred to the value of the electric field simulated at the centroid point in the *point-wise approach*. It is worth noting that from the comparison of the electric field values at the centroid points at the two different heights (Figures 3.39 - 3.41), it has been concluded that both heights (5,0 m a.g.l. or 7,5 m a.g.l.) can be valid choices.

3.7 Justification of the choice of a representative electric field value per building

In Section 3.4, the issue of choosing a simulated electric field value that could be representative and significant for building exposure and, consequently, for the resident population to the electric fields generated by radio frequency sources was highlighted.

The issue was addressed through two approaches: the *volumetric* and the *point-wise* approach. From the considerations made for the volumetric approach, it was concluded that there are many and varied possible exposure scenarios (Subsection 3.5.1). However, some of these scenarios are infrequent and dictated by local conditions, such as the proximity of base stations, which are still limited in number compared to the quantity of buildings in the area. For this reason, it is advisable to determine which of these exposure scenarios is the most common and typical.

From the volumetric analyses conducted on a larger sample of buildings, specifically in the entire areas of interest (Subsection 3.5.2), it was observed that the simulated electric field values within the majority of these buildings exhibit very low variability (i.e., standard deviation) with respect to the mean value, typically below approximately 0,5 V/m.

This leads to the conclusion that, for the majority of buildings within the area, the mean values of the simulated electric field in the three-dimensional grid per building are a good representative of the exposure.

However, since this study also aims to be *simplified*, *efficient* and *scalable*, the *point-wise approach* was employed. We have considered the centroids of the buildings as the points for assessing the electric field, but had doubts about which height to associate with them. In Subsection 3.6.1, it is explained how the two candidate heights (5,0 m a.g.l. and 7,5 m a.g.l.) were derived from considerations regarding the most frequent values of area and weighted height for the city of Turin, also averaging the findings of all similar studies conducted by other ARPA/APPA. These heights ideally correspond to the 2nd L.A.G. and the 3rd L.A.G., respectively.

At this point, the distributions of simulated electric field values were compared using the *point-wise approach* at the two chosen heights and the values selected as representative of exposure, which are the distributions of the means calculated on the three-dimensional grid of each building (Subsection 3.6.2). From this comparison, an extremely close resemblance between the distributions is observed, particularly the intervals of the most frequent simulated electric field values are the same for both approaches. This allows to attribute a representative meaning to the values of the simulated electric field at the centroids of the buildings.

Another consideration that emerged in Subsection 3.6.2 is that there is actually no appreciable difference between choosing the 2nd L.A.G. or the 3rd L.A.G. (corresponding to selecting a height of 5,0 m a.g.l. or 7,5 m a.g.l.) as the preferable above-ground floor in the *point-wise approach*.

If the perspective of the "*Programma ricerca CEM*" is considered, where the calculation of the indicator, the objective of the present work, should be feasible by all Regional Agencies capable of obtaining the necessary data, taking into account all the reflections referred to thus far, the *point-wise approach evaluated at a height of 5,0 m a.g.l.* (equivalently, the 2nd L.A.G.) can be choosen as the suitable method to represent the exposure of each buildings and, consequently, the population to electromagnetic fields generated by RF sources.

This solution for calculating the "levels of radiofrequency electromagnetic field exposure for the population" indicator not only finds confirmation in previous studies [40], [41], [42] when complete ISTAT population data with detailed information on the resident population by floor are available, but also finds justification in this thesis work when the ISTAT data is less detailed. This allows for continuity in the studies conducted in the past and simultaneously supports future ones.

3.8 Indicator results: levels of radiofrequency electromagnetic field exposure for the population

From the previous Section 3.7, the simulated electric field value to be considered in the steps for calculating the environmental status indicator "levels of radio frequency electromagnetic field exposure for the population", as described in Subsection 3.2.1, has finally been determined.

At this point, having all the necessary data and having thoroughly examined and justified all the criteria involved, we can proceed to calculate the indicator for each of the three areas of interest: "Corso Belgio", "Via Vigliani" and "Via Togliatti". It should be noted that for these three cases, the *detailed procedure* for assigning the resident population to the buildings was used, as they are areas of interest with a small radius (300 meters).

Operationally, the software *QGIS* was used for spatial data manipulation. Once an "attribute table" was obtained, containing all the necessary information, a *Python* script was used to visualize population distributions according to exposure classes to the electric field simulated using the *point-wise approach* (evaluated with the *ValutaEdifici* software). This script was also used to derive characteristic electric field values to which the resident population is exposed (50th and 95th percentiles).

Firstly, the building layer of the city of Turin, as described in the section "Turin building data - shapefile" in Subsection 3.3.1, was taken into consideration. It's worth noting that the tabular information in this layer contains the following columns: "CIT_AR", "QT_SUOLO", "ALTEZZA_VO", "QT_GRONDA", "NUM_PIANI".

From this layer, the goal is to perform the calculation mentioned in the *detailed procedure* for assigning the resident population to each building $P_{E(i)}$, considering it to be directly proportional to the volume of the building itself (Equation 3.1).

The volume of each individual building, denoted as $V_{E(i)}$, is obtained using the built-in *Field Calculator* tool in QGIS. First, the column corresponding to the area ("AREA") is calculated using the expression *$area*. Then, the volume ("VOLUME") is calculated by multiplying the area by the height using the expression "AREA"·"ALTEZZA_VO".

For the total resident population of the entire territorial unit P_{tot}, data from ISTAT were required, which included the census sections layer and the population data stored in an .xlsx file, as described in Subsection 3.3.2. Using the vector data management tools, an *attribute join based on spatial location* was performed to add information about the census section number to each building's attribute data (that is column "SEZ2011", obtained from the census sections layer). Subsequently, a tabular join between the building "attribute table" and the population data in the .xlsx file was carried out using the *join* function. The joining process was based on the "SEZ2011" column and the target field was the total resident population data for each census section, which is stored in the "POPOLAZ_P1" column.

The next step is to associate the total volume of all buildings within the territorial unit in which each building is located, denoted as V_{tot}. QGIS provides a processing tool called *statistics by categories* that can be used for this purpose. The input layer for this tool is the buildings layer and the field for which the statistics want to be calculated is the volume ("VOLUME"). The categories used for the calculation are the census sections ("SEZ2011"). The result of this operation is a "Statistics by category" table, which includes various columns, one of which is "SUM", representing the total sum of volumes for all buildings falling within the same census section, denoted as V_{tot}. This column is then added to the attribute information of the buildings layer using the *join* function with the key field "SEZ2011".

With all the necessary information obtained for each building (i.e., each row of the table), the estimated resident population within each building can be calculated using Equation 3.1. This can be done using the QGis *Field Calculator*. A new column, denoted as "PE(i)", will be created with the expression involving columns: "POPOLAZ_P1" · "VOLUME" / "VOL_TOT_SE".

Finally, the .csv file containing the values of simulated electric field at the centroids of buildings at a height of 5,0 m a.g.l. is loaded. These data were presented in the "Buildings' centroids - csv" paragraph of Subsection 3.3.4. Using a *join* operation, the "attribute table" of the building layer is updated to include the simulated electric field value for each building at its centroid at the chosen height, represented in the column "CE_5,0E Ri". This is achieved by matching the building's identification code (in the column "CIT_AR") with the appropriate field in the .csv file.

This results in an "attribute table" for the building layer that contains everything needed for calculating the indicator according to the criteria and reasoning developed up to this point. Each row in the table corresponds to a building and it includes both the resident population calculated using the *detailed procedure* of assignment and the simulated electric field value at the centroid at a height of 5,0 m a.g.l..

At this point, a *Python* script is used to read this "attribute table", which is the .dbf file of the shapefile and transform it into a *Pandas dataframe*. Since it was noticed that there are census sections for which ISTAT did not provide resident population data, some *data cleaning* is required to remove the buildings belonging to these sections, which have been assigned a *NaN* value for resident population. For the three areas of interest under examination, this anomaly was only present for one census section of "Corso Belgio", resulting in a total of 18 sections for this area of interest instead of 19.

Finally, the cumulative population for each interval of associated simulated electric field values was determined, grouping resident population assigned to different buildings in the same area of interest. The width of these electric field intervals was chosen to be 0,5 V/m. Using the *matplotlib* library, the desired result was displayed, which is the "levels of radiofrequency electromagnetic field exposure for the population" indicator. On the x-axis, there are the simulated electric field classes, and on the y-axis, there is the number of resident populations exposed to these simulated electric field classes. This indicator also provided information regarding the percentiles.

Here are the results for the three areas of interest considered:

- for the area of interest "Corso Belgio" (Figure 3.45a), considering the values of simulated electric field at the centroids at a height of 5,0 m a.g.l., the resident population is exposed to a range of simulated electric field values between 0,5 V/m and 2,5 V/m (Figure 3.45b). Additionally, half (50th percentile) of the population is exposed to less than 1,22 V/m, while the majority of them is exposed to less than 2,04 V/m (95th percentile);

- for the area of interest "Via Vigliani" (Figure 3.46a), considering the values of simulated electric field at the centroids at a height of 5,0 m a.g.l., the resident population is exposed to a range of simulated electric field values between 0,5 V/m and 3,5 V/m (Figure 3.46b). Additionally, half (50th percentile) of the population is exposed to less than 1,83 V/m, while the majority of them is exposed to less than 2,82 V/m (95th percentile);

- for the area of interest "Via Togliatti" (Figure 3.47a), considering the values of simulated electric field at the centroids at a height of 5,0 m a.g.l., the resident population is exposed to a range of simulated electric field values between 0,5 V/m and 2,5 V/m (Figure 3.47b). Additionally, half (50th percentile) of the population is exposed to less than 1,43 V/m, while the majority of them is exposed to less than 2,3 V/m (95th percentile).

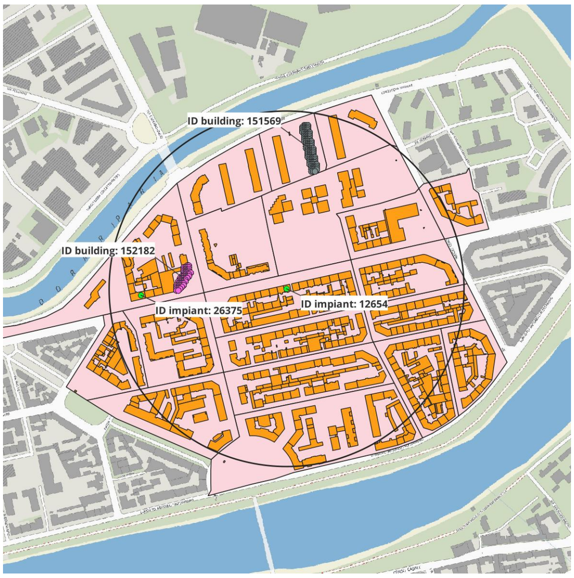

(a) "Corso Belgio" area of interest.

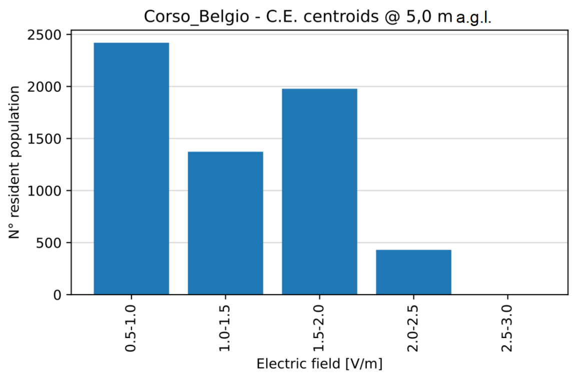

(b) "Corso Belgio" indicator.

Figure 3.45: Indicator *levels of radiofrequency electromagnetic field exposure for the population* for "Corso Belgio" area of interest, with electric field classes of 0,5 V/m.

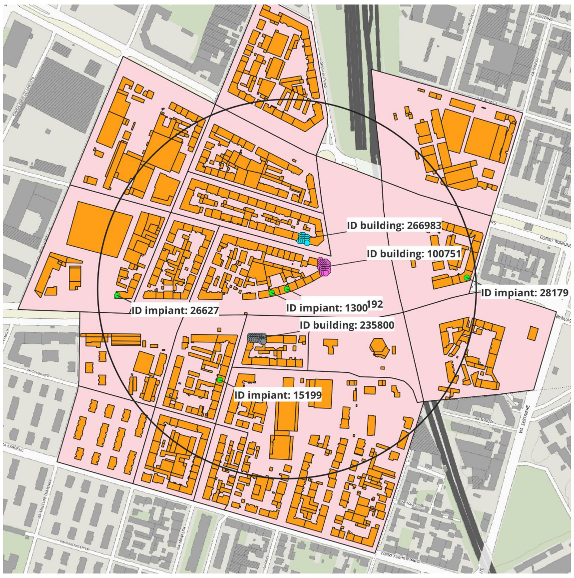

(a) “Via Vigliani” area of interest.

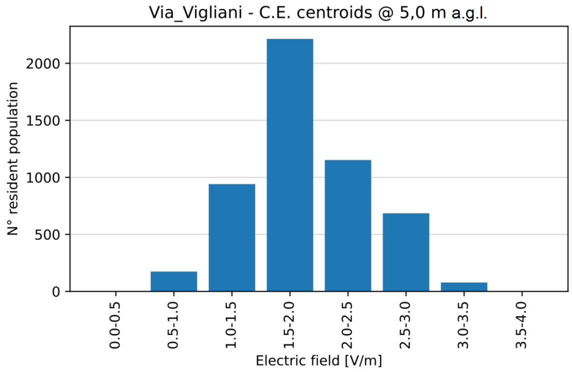

(b) “Via Vigliani” indicator.

Figure 3.46: Indicator *levels of radiofrequency electromagnetic field exposure for the population* for “Via Vigliani” area of interest, with electric field classes of 0,5 V/m.

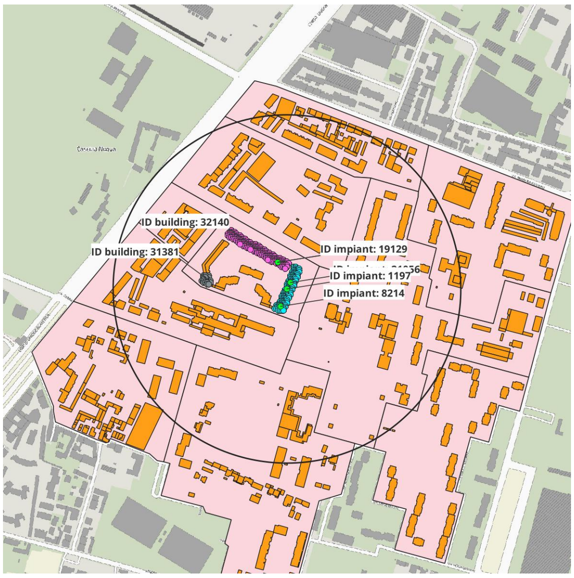

(a) “Via Togliatti” area of interest.

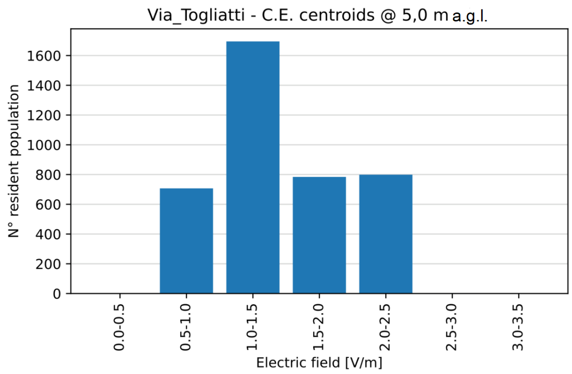

(b) “Via Togliatti” indicator.

Figure 3.47: Indicator *levels of radiofrequency electromagnetic field exposure for the population* for “Via Togliatti” area of interest, with electric field classes of 0,5 V/m.

Chapter 4

Experimental validation

The results obtained so far have considered electric field values to associate with the resident population simulated at the centroids of buildings at a height of 5,0m a.g.l. using the software *Cemview* or on a three-dimensional grid of evaluation points corresponding to the building using the *ValutaEdifici* software. As has already been said, these software tools utilize a *free space* and *far-field* electromagnetic field model for their calculations. Additionally, these values were adjusted, at most, by the power reduction coefficients declared by telecommunications providers and assessed by Arpa Piemonte during the authorization process for the installation or modification of base stations (as indicated in Subsection 3.3.4).

However, these values represent the maximum electric field values that could theoretically be reached. They are based on the maximum authorized power of the antennas, which is rarely actually reached. This is because the power requested by TLC operators during the authorization phase is always higher than the cell's requirements to avoid saturation and ensure its functionality even in cases of high traffic demand. In practice, the actual power levels used are always lower than those authorized.

Furthermore, these simulations involve many simplifications. They neglect ground, infrastructure and vegetation reflections (Section 1.4), and typically do not consider the attenuation factors characteristic of building structures for points inside buildings (Subsection 1.1.5).

All of this being said, it is foreseeable that the results obtained from the indicator calculations are likely to be overestimated, which can, to some extent, be accepted by invoking the *prudent avoidance principle*. However, the need for validating the underlying model of the indicator by comparing it with actual measurements of electric field values measured "in air", under real population exposure conditions, is evident. It is desirable that this validation could lead to the justification of the indicator model and simultaneously confirm the necessity, or lack thereof, of correction factors for it.

For this purpose, additional data were collected (including short-time measurements and the frequency distribution of the *relative percentage offsets* Δ_P (%) between the average of the mean powers exerted and the ones authorized, which will be described in detail in the following Section 4.1).

These data were useful, firstly, for making considerations regarding the *offset* between the values provided by the indicator from simulations and measurements taken indoors and outdoors under real conditions, also considering to what extent building walls attenuation and differences between power exerted and power authorized of base stations could affect the indicator values. Secondly, these data were used to calculate the "levels of radiofrequency electromagnetic field exposure for the population" indicator for a much larger area of interest (i.e. *area of validation*).

In the following sections the new data analyzed for this occasion, the two topics addressed using them and the resulting considerations that were made are going to be presented.

4.1 Test area and data for validating the indicator with measurements

To perform the desired validation, it was necessary to obtain new data provided by Arpa Piemonte, which have structures similar to those of the data presented in Section 3.3.

First of all, it was decided to expand the study to a much larger area of interest located in the center of the city of Turin (hereinafter referred to as "Torino centro"). This area has a circular shape, its center has coordinates in the WGS84/UTM 32N coordinate system (X=396262, Y=4991818) and a radius of 1500 meters. For the evaluations of simulated electric field, all contributions from all base stations falling within a slightly larger *area of influence*, with the same center and a radius of 1900 meters, were considered (Figure 4.1).

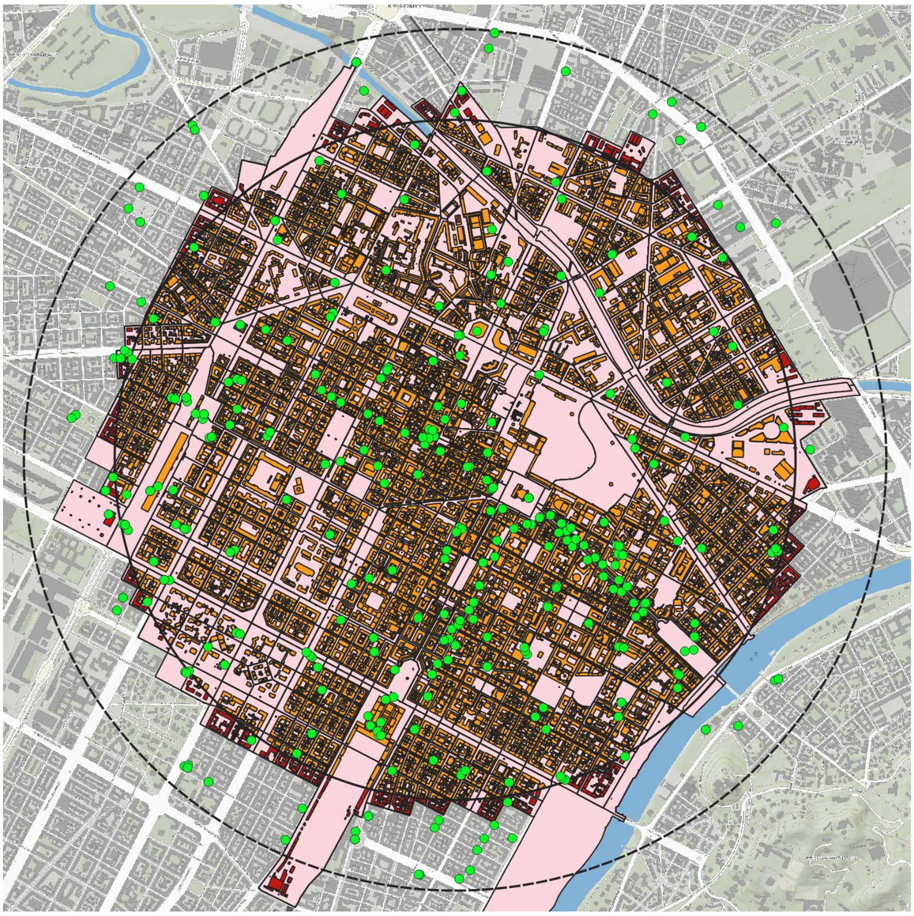

Figure 4.1: General overview of “Torino centro” area of interest. The green dots are the base stations considered, the dashed circular line is the *area of influence* of the inner area of interest (solid black line).

Population data for the territorial units and the corresponding census sections for this new area of interest are available in the same way as indicated in Subsection 3.3.2. Arpa Piemonte provided the following new files:

- the shapefile of buildings in Turin that fall within the “Torino centro” area of interest;
- the CSV output file from the *Cemview* software, containing simulated electric field values at a height of 5,0 m a.g.l. for all buildings within the “Torino centro” area of interest;
- the shapefile of short-time wideband measurements (6 minutes, also referred to

as "instantaneous" measurements) conducted both *indoors* and *outdoors* starting from 01/01/2022 within the "Torino centro" area of interest;

- the shapefile of *outdoor-only* instantaneous measurements conducted starting from 01/01/2022 within the "Torino centro" area of interest;

- the frequency distribution of the calculated *relative percentage offsets* Δ_P (%) between the average of the mean powers exerted and the ones authorized for each base station included in the *area of influence*, taking into consideration the sample hours 10 a.m.-3 p.m. of a sample weekdays (from Monday 11/09/2023 to Friday 15/09/2023).

The provided shapefiles for instantaneous measurements are a subset of the open dataset available on the "Portale CEM - campi elettromagnetici in Piemonte" of Arpa Piemonte (see a brief reference in Subsection 3.3.3) [53].

In particular, the "attribute table" of the shapefiles containing instantaneous measurements, whether total or outdoor-only, includes various features. The most useful ones include the description of the location where the measurements were taken, the above-ground level floor, the date of the measurement and the measured electric field value. As a result, the "attribute table" will have one row for each considered instantaneous measurement. The set of *outdoor* and *indoor* measurements includes 187 measurements, while the *outdoor-only* measurements, conducted exclusively on balconies and/or terraces, amount to 98 measurements.

Please note that the field with the information about the above-ground level floor has been sparsely populated compared to the total number of measurements. Often, this information is included within the description (a *string-type* column), and more commonly, it is omitted. Therefore, it is not easily possible to make more precise quantitative assessments of their height above ground level. However, when this information is available, it has been observed qualitatively that the majority of measurements were taken at higher floors, ranging from the 5th L.A.G. to as high as the 11th L.A.G.. This qualitative information must be considered in the subsequent comparison with the simulated electric field values at a height of 5,0 m a.g.l..

Furthermore, as was the case for the "Corso Belgio" area of interest, in this case as well, the ISTAT population data is not always complete. Among the 707 census sections included in the "Torino centro" area of interest, only 623 of them have associated resident populations. To a lesser extent, the same situation occurs for the census sections where the considered instantaneous measurements are located. Out of 17 census sections with instantaneous measurements (both *indoor* and *outdoor*), only 16 have information about the resident population, and out of these, only 14 include *outdoor* measurements.

As previously mentioned, Arpa Piemonte also provided a graph showing the frequency distribution of the *relative percentage offsets* Δ_P (%) between the average of the mean powers exerted and the ones authorized on an hourly basis for each base station considered within the *area of influence*.

The Δ_P values shown in the graph to be presented later (Section 4.2) have been calculated using the following formula:

$$\Delta_P(\%) = \left(\frac{\mu_{mean\ Power\ exerted} - \mu_{Power\ authorized}}{\mu_{Power\ authorized}} \cdot 100 \right)_{\forall\ hourconsidered} \tag{4.1}$$

The values derived from Equation 4.1 are reported in percentage, where they can range from -100% to +100%. A negative percentage indicates that the average of the mean powers exerted is lower than the average authorized powers, which is desirable and common. Conversely, a positive percentage implies that for some hours considered, mean powers higher than the authorized ones were used. This can happen in cases of cell overcrowding, for example.

The power values were obtained from the power meters available through the specific national database managed by ISPRA, along with the databases of individual mobile network operators where the required data were not present in the first mentioned database. Access to these databases is granted to ISPRA at the national level and to the regional ARPA agencies at the regional level. The data include technologies for which a coefficient value α_{24h} was declared during the authorization phase.

For the provided graph, Arpa Piemonte chose to perform the calculations based on Equation 4.1 for a five-day sample workweek period (from Monday 11/09/2023 to Friday 15/09/2023) only for the midday hours, specifically from 10 a.m. to 3 p.m..

The choice of the sample hours is suggested by recent literature [56], which indicates that during peak hours (from 10 a.m. to 3 p.m.) on working days, the 6-minute average tends to overestimate the 24-hour average. Moreover, this time period corresponds to when Arpa technicians usually conduct instant measurements since it aligns with their working hours and simultaneously, it is a time when private individuals or public facilities are generally more available for indoor measurements in residential or long-duration environments exceeding four daily hours.

The choice of the sample week was constrained by the availability of data on the ISPRA portal. This portal maintains a historical record of only 30 days from the current date. It stores all recorded data regarding hourly power output and authorized one for all cells that use the α_{24h} coefficients of the base stations throughout Italy, among other information. It is therefore left to the reader's imagination the immense amount of storage required to keep this information beyond 30 days, which is why it's impossible to have longer historical records.

For these calculations, Arpa Piemonte excluded all cells for which they were aware that requests for modifications or installations had been submitted after 11/09/2023.

In the following Section 4.2, considerations will be made regarding the comparison between values calculated from the instant measurements present in the shapefiles and this distribution of *relative percentage power offsets*.

However, the correspondence of the base stations considered between the two parts is not guaranteed, as one includes instant measurements from the beginning of 2022 onwards, while the other considers only five weekdays in September 2023. These are therefore two potentially quite different time periods. In any case, given the available knowledge [56] and contingent limitations (such as the unavailability of data older than 30 days), the considerations to be made in this regard can be considered a valuable indication for future studies.

4.2 Comparison between simulated and measured indicator values

Regarding the new data acquired, which also include measurements conducted in real exposure situations, the first objective was to investigate a possible *offset* between the results obtained from the indicator using simulated values and those obtained using the same method of the indicator but with the actual measured electric field values in real conditions. This was done both by considering all measurements (both *indoor* and *out-*

door) and by considering *outdoor-only* measurements to explore any potential influence on the measured values due to the attenuation caused by building walls. Below, further considerations will be addressed regarding the differences between the exerted base stations powers and those authorized with respect to the *offset* between instantaneous measurements and simulated values of electric field.

To account for all of this, only the census sections where instant measurements and population data were present were considered (Figure 4.2). As mentioned in Section 4.1, there are 16 sections when considering all measurements and 14 when considering *outdoor-only* measurements.

The "levels of radiofrequency electromagnetic field exposure for the population" in-

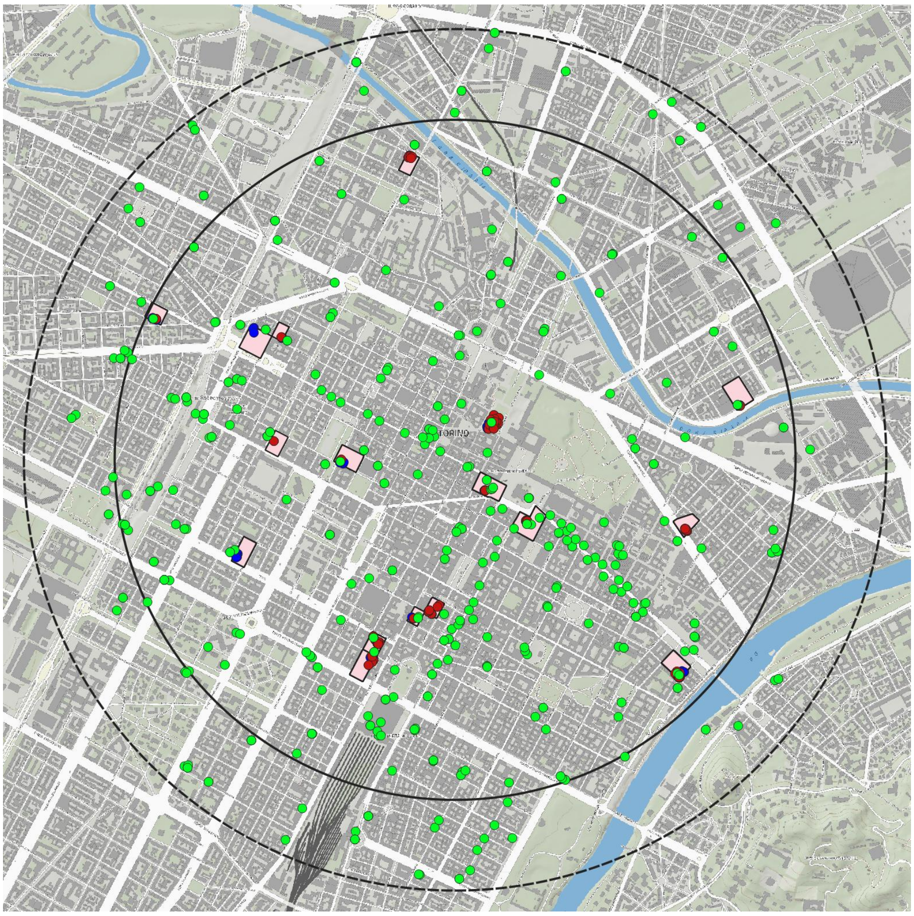

Figure 4.2: "Torino centro" area of interest census sections with measurements (in light pink). In red: *outdoor* measurements; in blue: *outdoor* and *indoor* measurements.

dicator was then calculated using the *general procedure* for population assignment to the census section (Subsection 3.2.1), given the radius of the area of interest (1500 meters). This translates into the direct assignment of the resident population to the entire territorial unit, without considering individual buildings. In turn, it was necessary to assign not to the buildings but to the census section a value of electric field. The process involved first assigning, for each territorial unit considered, the average of the simulated electric field values at 5,0 m a.g.l. for all buildings' centroid points, and then the average of the measured electric field values in that section (differentiating between total measurements before and outdoor measurements after).

The calculation of the average of these electric field values was performed by adding the necessary lines of code in the *Python* script already described in Section 3.8. Therefore, it was not necessary to add columns related to area, volume and population per building in QGis, which are instead useful for the *detailed procedure* of resident population assignment.

To quantify the *offset* between the indicator with simulated values and the one with measured values, a simple calculation of the difference was performed for each census section considered. This calculation involved finding the difference between the average of the simulated electric field values at the centroids of the buildings and the average of the measured electric field values (Equation 4.2):

$$\Delta_{EF} = (\mu_{EF\ centroids} - \mu_{EF\ selected\ measurements})_{\forall\ census\ section\ w/\ selected\ measurements} \tag{4.2}$$

The form of Equation 4.2 signifies that if the offset Δ_{EF} is positive, it indicates that associating the resident population with the simulated electric field values at the buildings centroids at 5,0 m a.g.l. is an overestimate compared to associating the values actually measured in real conditions. Conversely, if Δ_{EF} is negative, it's an underestimate.

Lastly, as many offsets Δ_{EF} are obtained as there are considered census sections; its average $\mu_{\Delta_{EF}}$ is provided, on which further reflections can be developed.

Indicator calculation with all measurements (indoor and outdoor)

In the case of the 16 census sections corresponding to both *indoor* and *outdoor* measurements, the results obtained for the calculation of the indicator by assigning the average simulated electric field values at 5,0 m a.g.l. (Figure 4.3a) and the average of the electric

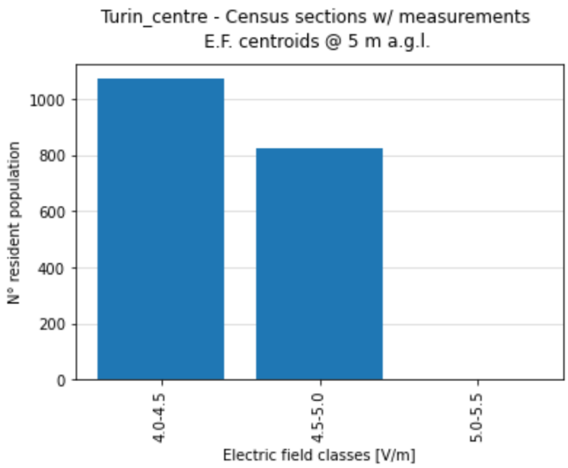

(a) Using *simulated* electric field values at the centroid points at 5,0 m a.g.l..

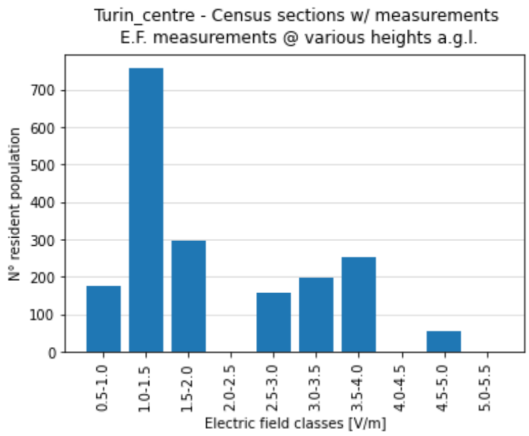

(b) Using *measured* electric field values (both *outdoor* and *indoor*) at various heights.

Figure 4.3: Indicator *levels of radiofrequency electromagnetic field exposure for the population* for "Torino centro" area of interest, with electric field classes of 0,5 V/m.

field values measured considering all measurements (Figure 4.3b) are shown. Again, the width of the electric field classes was chosen to be 0,5 V/m.

From the comparative observation of the *simulated indicator* and the *measured indicator* results, it can be observed that:

- for the first one, there are only two electric field classes concentrated in the medium-high range (4-5 V/m). The variability (*range*) of the averages of the electric field values simulated at 5,0 m a.g.l. is 0,79 V/m (rounded to 1 V/m for the displayed electric field classes);

- for the second one, there are seven populated electric field classes covering many ranges (from 0,5 V/m to 5,0 V/m). The variability (*range*) of the averages of the electric field values measured at various heights a.g.l. is 4,27 V/m (rounded to 4,5 V/m for the displayed electric field classes).

From the calculation of the *offset* Δ_{EF} for each of the 16 considered census sections and the corresponding average offset $\mu_{\Delta_{EF}}$, it is found that this value is +2.44 V/m (Table 4.1, first column). This means that based on the evidence gathered from cases with measurements conducted both *indoors* and *outdoors*, on average, the *simulated indicator* will overestimate the *measured indicator* by approximately 2,5 V/m.

The causes of this overestimation could be attributed, as indicated in the introduction of Chapter 4, to the difference between authorized and actually exerted power levels or to the attenuation caused by building walls in real exposure situations. To understand the extent to which the latter factor may contribute to the overestimation observed in the indicator, it was decided to conduct the same analyses of this paragraph by excluding *indoor* measurements and considering only the instantaneous *outdoor* electric field measurements.

Indicator calculation with outdoor-only measurements

In the case of the 14 census sections corresponding to *outdoor-only* measurements, the results for the indicator calculation are shown by assigning the average values of the electric field simulated at 5,0 m a.g.l. (Figure 4.4a) and the average values of the electric field measured with *outdoor-only* measurements (Figure 4.4b). Here as well, the width of the electric field classes was chosen to be 0,5 V/m.

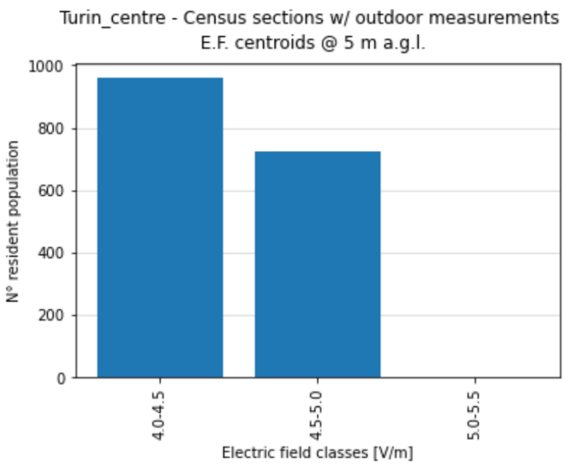

(a) Using *simulated* electric field values at the centroid points at 5,0 m a.g.l..

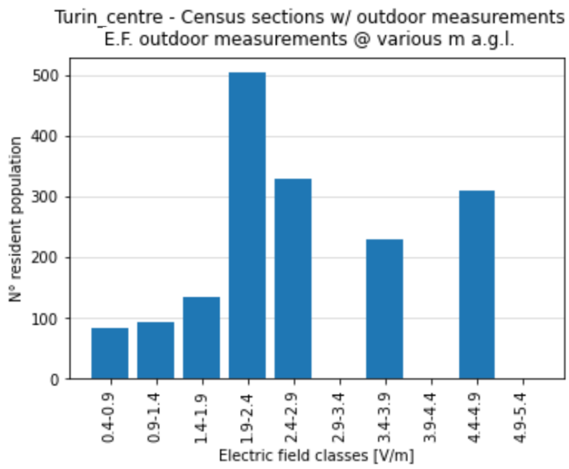

(b) Using *measured* electric field values (only outdoor) at various heights.

Figure 4.4: Indicator *levels of radiofrequency electromagnetic field exposure for the population* for "Torino centro" area of interest, with electric field classes of 0,5 V/m.

From the comparative observation of the *simulated indicator* and the *measured indicator* results, it can be observed that:

- for the first one, exactly as in the previous case, there are only two electric field classes concentrated in the medium-high range (4-5 V/m). The variability (*range*) of the averages of the electric field values simulated at 5,0 m a.g.l. is 0,79 V/m (rounded to 1 V/m for the displayed electric field classes);

- for the second one, there are seven populated electric field classes covering many ranges (from 0,4 V/m to 4,9 V/m). The variability (*range*) of the averages of the electric field values measured at various heights a.g.l. is 4,47 V/m (rounded to 4,5 V/m for the displayed electric field classes).

	SEZ2011	Δ_{EF} **w/ all measurements [V/m]**	Δ_{EF} **w/ outdoor measurements [V/m]**
1	12720000208	+3,79	+3,79
2	12720000234	+3,25	+2,35
3	12720000137	+2,17	+2,17
4	12720000146	-0,32	-0,32
5	12720000123	+3,14	+2,33
6	12720000045	+3,23	+2,30
7	12720003132	+3,16	-0,32
8	12720000300	+0,87	—
9	12720000441	+2,64	+0,61
10	12720000053	+4,11	+4,31
11	12720000170	+0,88	+0,53
12	12720000459	+2,90	+2,20
13	12720000688	+0,53	-0,21
14	12720000080	+3,29	+2,97
15	12720000178	+2,93	—
16	12720001022	+2,43	+1,93
	$\mu_{\Delta_{EF}}$ **[V/m]:**	**+2,44**	**+1,76**

Table 4.1: Electric field *offsets* considering census sections with all measurements (*indoor* and *outdoor*) and with *outdoor-only* measurements. Mean electric field offsets for both conditions considered.

From the calculation of the *offset* Δ_{EF} for each of the 14 census sections considered and the corresponding average offset $\mu_{\Delta_{EF}}$, it is found to be approximately +1.76 V/m (Table 4.1, second column). This means that based on the evidence gathered for the case of *outdoor-only* measurements, on average, the *simulated indicator* will overestimate the *measured indicator* by approximately 1,8 V/m.

As expected, the *simulated indicator* has a slightly lower overestimation when compared to the *measured indicator* with *outdoor-only* measurements ($\mu_{\Delta_{EF}} \approx\ 1,8\ V/m$) compared to the comparison with the *measured indicator* including not only *outdoor* but also *indoor* measurements ($\mu_{\Delta_{EF}} \approx\ 2,5\ V/m$).

It can be stated that the attenuation of building walls seems to contribute on average by about 0,7 V/m to the overestimation of the "levels of radiofrequency electromagnetic field exposure for the population" indicator as calculated in this work. However, it should be remembered that this assumption is subject to the availability of instant measurement data, which were taken at various heights above the ground (not only at 5,0 m a.g.l.), as they were carried out for environmental monitoring purposes during the daily work of Arpa Piemonte technicians, without the ultimate goal of validating this work. Nevertheless, it is believed that these considerations may have general validity.

There remains a need to seek a possible explanation for the remaining average *offset* $\mu_{\Delta_{EF}} \approx\ 1,8\ V/m$ between the *simulated indicator* and the *measured indicator* with *outdoor-only* measurements.

If the possible factors that can influence the outdoor environment are considered, it is therefore hypothesized that the main cause of this average *offset* in electric field values $\mu_{\Delta_{EF}}$ may be the difference between the powers actually used "in air" by the base stations and the authorized powers in the preliminary phase. Other factors such as the visibility of the installation, reflections, pointing directions, or antenna tilt can certainly have an impact, but they are considered secondary to the issue of the base stations powers.

As was explained in Section 4.1, Arpa Piemonte has provided a graph of the frequency distribution of the calculated *relative percentage offsets* Δ_P (%) between the average of the mean powers exerted and the ones authorized for each base station included in the *area of influence*, taking into consideration the sample hours 10 a.m.-3 p.m. of a sample weekdays (from Monday 11/09/2023 to Friday 15/09/2023). The *relative percentage offsets* Δ_P (%) are calculated according to Equation 4.1 and the graph that was provided is presented in Figure 4.5.

From Figure 4.5, it can be observed that the mode of the frequencies, which is the

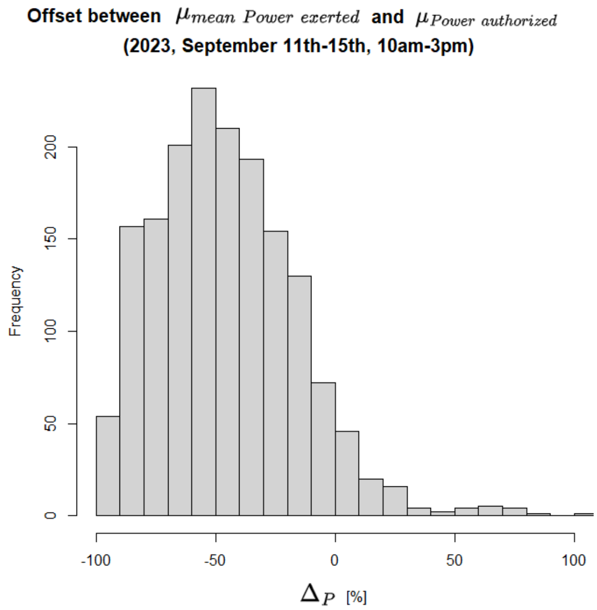

Figure 4.5: Frequency distribution of the calculated *relative percentage offsets* Δ_P between $\mu_{mean\ Power\ exerted}$ and $\mu_{Power\ authorized}$. Sample weekdays: 2023, September 11th-15th; sample hours: 10 a.m.-3 p.m..

most common value of the *relative percentage offsets* Δ_P (%), is in the bin between -50% and -60%. In general, the frequency distribution is primarily distributed over negative values of Δ_P, as expected. The interpretation of this graph suggests that, generally, the average powers exerted are around half of the authorized ones.

Now, it is necessary to compare these analyses performed on the powers exerted and authorized respectively with the values of the electric field measured and simulated. A reference to the calculations made in the 14 census sections corresponding to *outdoor-only* measurements is made, where the average values of the electric field measured with *outdoor-only* measurements and the average values of the electric field simulated at 5.0 m a.g.l. were calculated. From this, it was concluded that the average offset $\mu_{\Delta_{EF}}$ between the *simulated indicator* and the *measured indicator* is approximately 1,8 V/m.

With these average electric field values (measured and simulated), the *relative percentage offsets* of the squares of the electric field means, denoted by Δ_{EF^2} (%), were calculated. The formula used follows the form of Equation 4.1 (*relative percentage offsets* Δ_P), considering the quadratic relationship between power and electric field of an electromagnetic wave (Equation 1.12). The formula is as follows:

$$\Delta_{EF^2}(\%) = \left(\frac{\mu^2_{EF\ outdoor\ measurements} - \mu^2_{EF\ centroids}}{\mu^2_{EF\ centroids}} \cdot 100\right)_{\forall\ census\ section\ w/\ outdoor\ measurements} \tag{4.3}$$

Thanks to Equation 4.3, the *relative percentage offsets* of the squares of the electric field means, Δ_{EF^2}, were calculated for each of the 14 census sections considered. The average, $\mu_{Delta_{EF^2}}$, was then calculated, resulting in -53% (Table 4.2).

	SEZ2011	Δ_{EF^2} **w/ outdoor measurements** [%]
1	12720000208	-96
2	12720000234	-73
3	12720000137	-71
4	12720000146	-89
5	12720000123	+27
6	12720000045	-82
7	12720003132	-70
8	12720000441	+27
9	12720000053	-45
10	12720000170	-99
11	12720000459	-25
12	12720000688	-77
13	12720000080	+4
14	12720001022	-73
	$\mu_{\Delta_{EF^2}}$ **[%]:**	**-53**

Table 4.2: *Relative percentage offsets* of the squares of the electric field means considering census sections with *outdoor-only* measurements Δ_{EF^2} and the mean of these *offsets* $\mu_{\Delta_{EF^2}}$.

From the reasoning conducted so far, it can be observed that the mode of the *relative percentage offsets* of the averages of the mean powers exerted and authorized ones, *mode*(Δ_P) (between -50% and -60%), is comparable to the average of the *relative percentage offsets* of the squares of the measured and simulated electric field means, $\mu_{\Delta_{EF^2}}$ (equal to -53%).

This could confirm the hypothesis regarding the significant influence of the powers actually used in real exposure conditions compared to authorized ones in the calculation of the indicator. It is important to note that by itself, this cannot be considered a definitive result, given the various degrees of uncertainty, but it can still be an interesting indication that can lead to very useful general considerations.

4.3 Indicator results on validation area of interest

The second objective to achieve with the data acquired for validating the model underlying the indicator was to calculate the “levels of radiofrequency electromagnetic field exposure for the population” indicator for the entire *validation area* “Torino centro”.

Since it is a large-radius area of interest (1500 meters), in this case as well, the *general procedure* for population assignment to the census sections was used (as described in Subsection 3.2.1). It is important to note that for “Torino centro”, there are 623 census sections with information on the resident population out of a total of 707. For each of these sections, the value of the electric field associated with the resident population was the average of the electric field values simulated at the centroids of all the buildings within each territorial unit, at a height of 5,0 m a.g.l..

The *Python* code used was very similar to that in Section 4.2. The results obtained from the calculation of the indicator, with the characteristics just described, were pre-

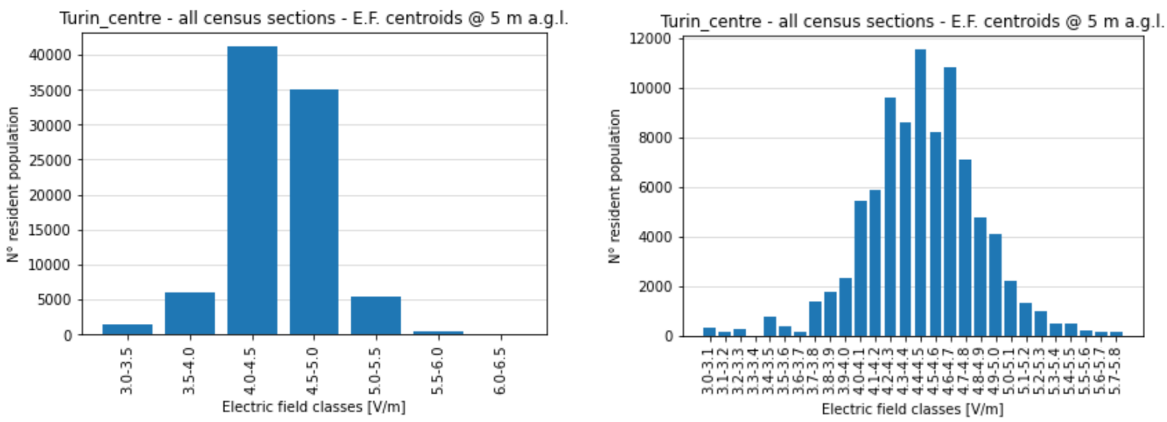

(a) With electric field classes of 0,5 V/m. (b) With electric field classes of 0,1 V/m.

Figure 4.6: Indicator *levels of radiofrequency electromagnetic field exposure for the population* for “Torino centro” area of interest, using simulated electric field values in the centroids at 5,0 m a.g.l..

sented using two different electric field classes binwidths: in Figure 4.6a, the width is 0,5 V/m, while in Figure 4.6b, the width is 0,1 V/m. The choice to display the results using these two different electric field classes binwidths was made because the first allows for a direct comparison with the results obtained so far, while the second allows for an appreciation of the detailed shape of the indicator distribution.

For the "Torino centro" area (Figure 4.6a), the calculation of the indicator for all census sections with available resident population data revealed that half (50th percentile) of the resident population is exposed to less than 4,46 V/m, while the majority of the population is exposed to less than 5,05 V/m (95th percentile). There are six populated field strength classes with a width of 0,5 V/m, ranging from values of 3,0 V/m to 6,0 V/m, with a variability (*range*) of 2,86 V/m (approximately 2,9 V/m). It is reassuring to note that the simulated electric field values to which the resident population is exposed are always below the *attention value* of 6 V/m.

From Figure 4.6b, it's evident that the shape of the indicator's distribution calculated for this very extensive *validation area* resembles a Gaussian distribution, with an average value of approximately $\mu \approx 4,5\ V/m$. It is known that, in general, those characteristics or phenomena that result from a large number of small, independent factors (e.g., a measurement process or a calculation process) tend to follow a normal distribution. When measuring the same subject repeatedly, the instrument generally does not produce the exact same value each time due to measurement errors, which result from the accumulation of a large number of small independent factors influencing the process.

It is well known that the values produced by radiofrequency electromagnetic field simulations are also influenced by various independent factors as well (power attenuation, gain in a given direction, pointing direction, etc.). Therefore, finding that these values are distributed according to a Gaussian distribution is what one would expect. The mean of n independent variables tends to follow a normal distribution as n increases, regardless of the original distributions (*Central Limit Theorem*).

In the case of a Gaussian distribution, it is well known that the mean, mode and median are the same. It is then demonstrated that the distribution of the indicator in Figure 4.6b is a Gaussian distribution because the following position indices were calculated as a confirming test and the results were:

- mean $\approx 4,47\ V/m$ (average value);

- mode $\approx 4,42\ V/m$ (most frequently occurring value);
- median $\approx 4,46\ V/m$ (middle value).

These results confirm that the distribution is indeed Gaussian, as the mean, mode, and median all coincide at approximately 4,45 V/m.

Through a short *Python* script using the libraries *seaborn* and *fitter*, further proof of the normality of this distribution was sought. First, the results obtained from the indicator for the *validation area* "Torino centro" were visualized again with minimal bin width (Figure 4.7a). Secondly, using an instance of Fitter() applied to the indicator data, four probability distributions were tested: gamma, lognormal, beta and normal.

The results can be seen in Figure 4.7b, while the summary table of the method is presented in Table 4.3.

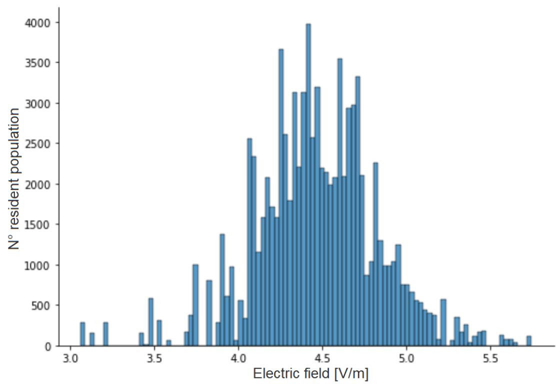

(a) Indicator results on the *validation area* using *seaborn* library.

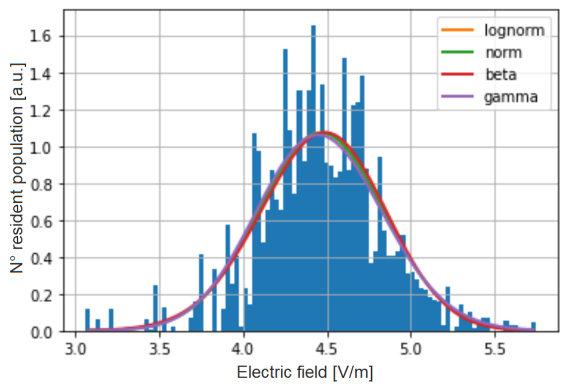

(b) Examined distributions to fit to the indicator data using *fitter* library. The number of resident population is in arbitrary units.

Figure 4.7: Attempts to identify the best probability distribution that best fits the indicator data on the *validation area* "Torino centro".

	sumsquare_error	**aic**	**bic**	**kl_div**	**ls_statistic**	**ks_pvalue**
lognorm	3,693765	428,185172	-904364,879111	inf	0,042442	1,200594 e-140
norm	3,697695	425,085117	-904281,025822	inf	0,042699	2,354881 e-142
beta	3,714220	427,649393	-903858,796717	inf	0,043320	1,626686 e-146
gamma	3,768988	426,900310	-902558,953730	inf	0,045363	1,262963 e-160

Table 4.3: Results from the *fitter* instance for the indicator data on the *validation area* "Torino centro".

The probability distribution that best fits the indicator data for the "Torino centro" *validation area* is the one that minimizes the error, in this case, the *sum of squares error*. It is noticeable that both the *lognormal* and the *normal* probability distributions are both excellent candidates because they have the smallest error among the considered distributions. Thanks to the *fitted_param* method of the *fitter* library, it was possible to obtain the parameters of the various distributions used by Fitter on the data, particularly for the *normal* distribution, the parameters are as follows:

- mean $\mu \approx 4,47\ V/m$;
- standard deviation $\sigma \approx 0,37\ V/m$.

These results are reassuring in asserting that the indicator's results in the "Torino centro" *validation area* follow a Gaussian distribution. This implies that the factors influencing the values produced by the electromagnetic field simulations are independent of each other.

Furthermore, it is worth noting that the most probable values of this distribution (Figure 4.6a) coincide with the most probable values of the distributions obtained in the previous sections regarding the studies with instantaneous measurements (Figure 4.3a and Figure 4.4a). Therefore, it is reasonable to claim that the 16 (or 14) census sections where instant measurement data is available can be considered a representative sample of the most likely real exposure scenarios for the population. This, in turn, could lead to the assertion that the considerations developed for the census sections with available instant measurements (Section 4.2) can be extended to the entire *validation area*.

Chapter 5

Discussion of the results

During the discussion, it seemed clear the need to set further objectives: firstly, that of being able to motivate the choice of which estimated electric field value and at which altitude to use as the chosen value for each considered building and secondly, that of investigate any correction factors that could be applied to the indicator to make it more compliant with the real exposure of the population.

The first objective was possible by combining considerations of the frequency of the building heights of some of the major urban centers with a descriptive statistical analysis of the distribution of the estimated electric field within the volume of the considered buildings. For the second objective, reasoning was carried out by comparing the simulated electric field values with the measured ones (where available).

In order to achieve the set objectives, it was chosen to focus attention on three *areas of interest* in the urban area of the metropolitan city of Turin, namely "Corso Belgio", "Via Vigliani" and "Via Togliatti".

In these areas, data were collected regarding various aspects: on the population through the *ISTAT* (Istituto Nazionale di Statistica) 2021 Permanent Population Census referring to the 2011 census sections; on the buildings of the metropolitan city of Turin (with indication of the buildings' geometries, the number of levels above ground, the ground levels and the eave heights) and on the total electric field values generated by the BTS systems present in the vicinity of the *areas of interest* evaluated both in a tridimensional grid in correspondence with the buildings and in the their centroids at two eligible heights corresponding to the second and third floor above ground. These simulated electric field values were calculated through some softwares produced by ARPA Piemonte, which are used within the free and open-source *QGis* software [47]).

The collected data were manipulated through the use of QGIS and *Python* scripts, thus following a procedure illustrated in the"RTI_CTN_AGF 2/2005" guidelines [40] it was possible to calculate the environmental indicator of population exposure to RF electromagnetic fields for each area of interest and consequently estimate how much of the resident population is exposed to which classes of simulated electric field generated by base stations.

In order to find a justification for the choice of the simulated electric field values to associate to the resident population, it was necessary to compare the results of two different approaches to the same problem.

The first approach (*volumetric*), using *Python* scripts, focuses on the analysis of the electric field data estimated in the buildings' volume thanks to a three-dimensional grid of evaluation points with a $3m \cdot 3m \cdot 1m$ grid. The vertical and horizontal simulated electric field variability of some buildings characteristic of typical exposure situations was studied through their 3D visualization and usage of pie charts per floor. Considering all the buildings present in the *areas of interest*, the distributions of the main statistical indicators were calculated.

The second approach (*point-wise*) is to consider the simulated electric field value at a single point within the space occupied by each building. Horizontally, it is reasonable to consider the centroid as the most suitable location to represent the building and, consequently, the distribution of the resident population within it. However, the question arises regarding the choice of height above ground level (i.e., the vertical axis) to assign to the point where the electric field simulation is performed with electric field calculation software.

Thus, studies already carried out of the salient and most frequent characteristics of the buildings in the metropolitan city of Turin were taken into consideration, as well as those of some major urban centers, like Novara, Aosta, Trento, Belluno, Padua, Rovigo, Treviso, Venice, Verona and Vicenza. The same studies were carried out, through an *R* script, for the cities of Bologna and Cesena, since the necessary data was available thanks to the municipal SIT (*Sistemi Informativi Territoriali*).

From this, two eligible heights were chosen at which to evaluate the simulated electric field in the centroids, corresponding to the second and third level above ground. For each *area of interest*, their distributions were compared to the ones of the statistical indicators computed in the *volumetric* approach in order to find a justification for the choice of the centroids' height.

This study aims to obtain a *simplified*, *efficient* and *scalable* method to compute the indicator on a municipal, provincial or even ideally regional scale. Thus, the *point-wise approach* evaluated at a height of 5,0 m a.g.l. (equivalently, the 2nd L.A.G.) was chosen as the optimal simulated electric field value to assign to the resident population under consideration thus representing their exposure to electromagnetic fields generated by RF sources.

Once this choice was made, it was possible to calculate the values of the indicator object of this study for the selected three *areas of interest*.

Finally, an attempt was made to experimentally validate the model underlying the indicator by using the available database of electric field measurements carried out in a new *validation area*, in particular in the period 2021-2023. At the same time, comparisons were carried out between the indicator calculated with *simulated* electric field values and *measured* ones to investigate the foreseeable deviations of the theoretical results from the real situation, for which possible causes have been suggested, such as the attenuation of the buildings' walls or the difference between authorized powers and the powers exerted by the base stations.

Conclusions

This thesis investigated how to derive a meaningful indicator of the electromagnetic fields to which an individual of the population is exposed in a urban environment characterized by buildings of various sizes and cellular telephone systems (BTS – *Base Transceiver Stations*). The study turned out to be very complex and the work was carried out with the collaboration of different ARPAs and on areas of different municipalities.

The author's contribution to the work was the extraction of the above-mentioned indicator which is always necessary for the periodic reports of the environment status that ARPAs must prepare. By means of this contribution two secondary goals have also been achieved.

Firstly, to be able to motivate the choice of which estimated electric field value and at which altitude to use as the chosen value for each considered building; this was possible by combining considerations of the frequency of the building heights of some of the major urban centers with a descriptive statistical analysis of the distribution of the estimated electric field within the volume of the considered buildings.

Secondly, to investigate any correction factors that could be applied to the indicator to make it more compliant with the real exposure of the population; this was possible by comparing the simulated electric field values with the experimental data and also the authorised powers with the average exerted powers.

In more detail, BTS electric field values (estimated and measured) and BTS powers (authorized and exerted) from some areas of Turin, population data and building height data were analyzed. Python scripts, R scripts, QGIS and other ARPA in-house softwares were used for this purpose.

Regarding future developments, the following considerations can be made: this study may serve for eventual studies on correction factors and data dissemination on the various geoportals of the ARPA system.

Appendix A

Further statistical indicators of the volumetric approach

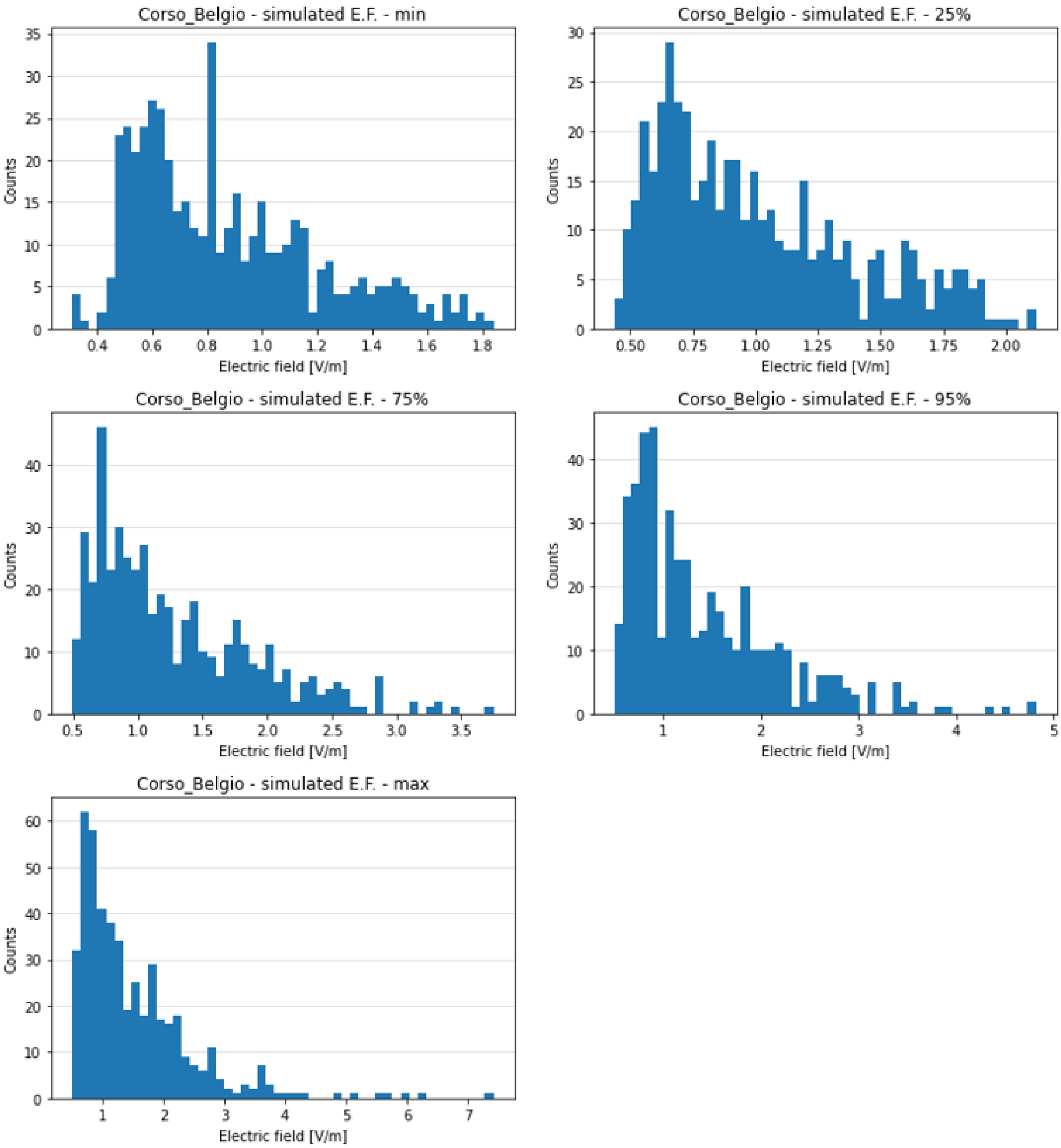

Figure A.1: Histograms of the statistical indicators (A - minimum value, B - 25th percentile, C - 75th percentile, D - 95th percentile, E - maximum value) of the simulated E.F. values in the three-dimensional grids of all the buildings, “Corso Belgio” area of interest.

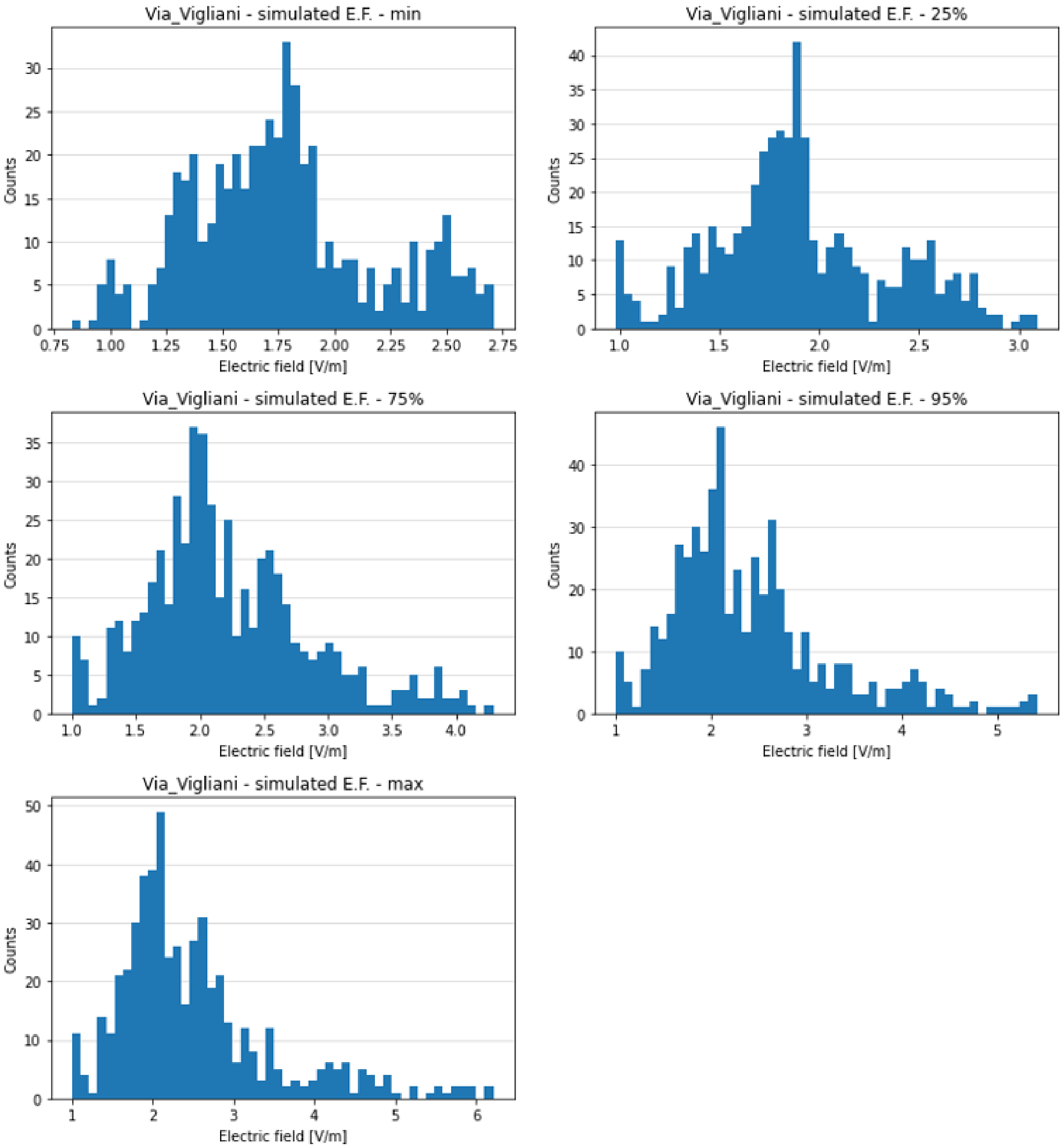

Figure A.2: Histograms of the statistical indicators (A - minimum value, B - 25th percentile, C - 75th percentile, D - 95th percentile, E - maximum value) of the simulated E.F. values in the three-dimensional grids of all the buildings, “Via Vigliani” area of interest.

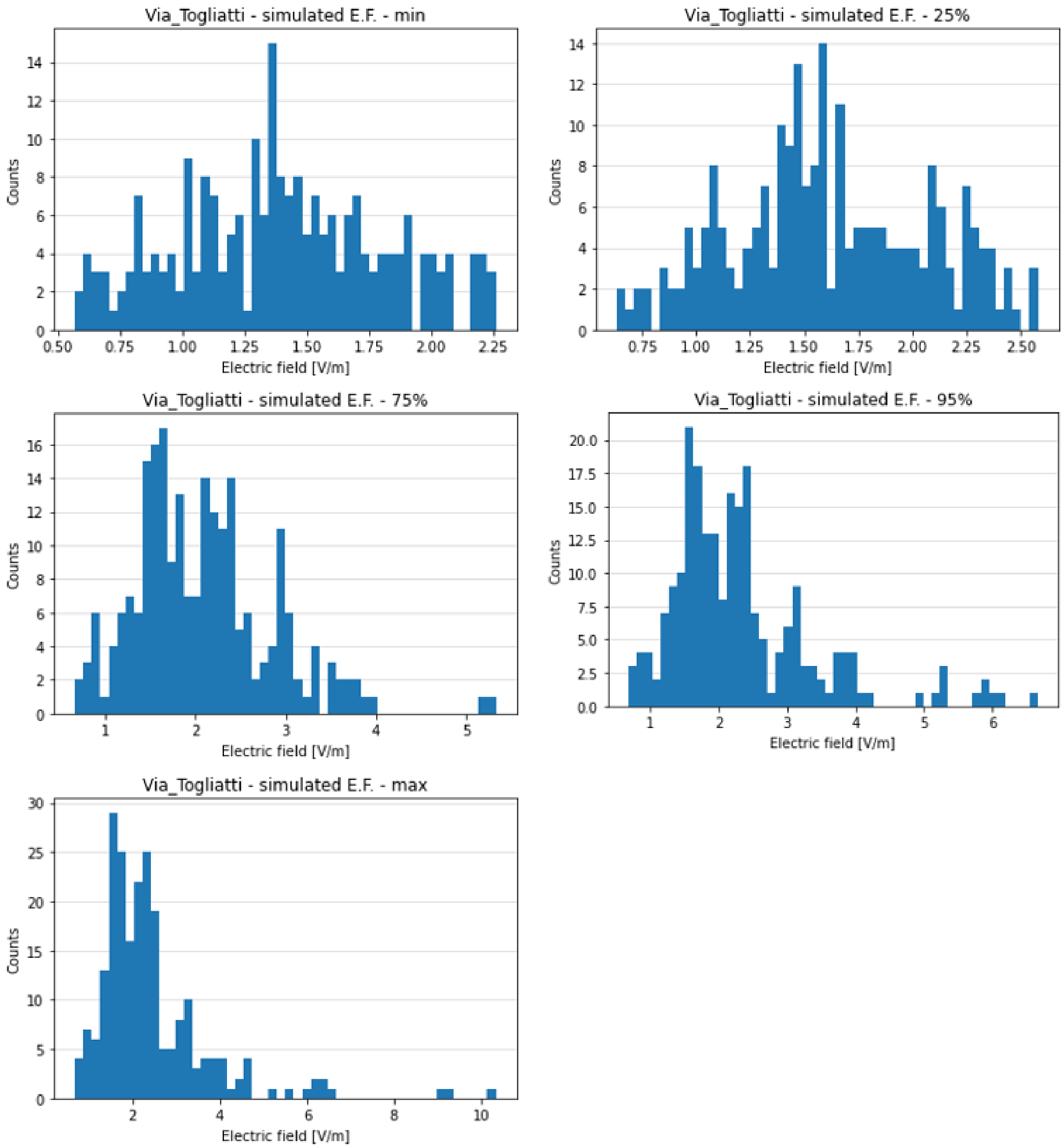

Figure A.3: Histograms of the statistical indicators (A - minimum value, B - 25th percentile, C - 75th percentile, D - 95th percentile, E - maximum value) of the simulated E.F. values in the three-dimensional grids of all the buildings, “Via Togliatti” area of interest.

Appendix B

Comparison between point-wise and volumetric approach: further statistical indicators

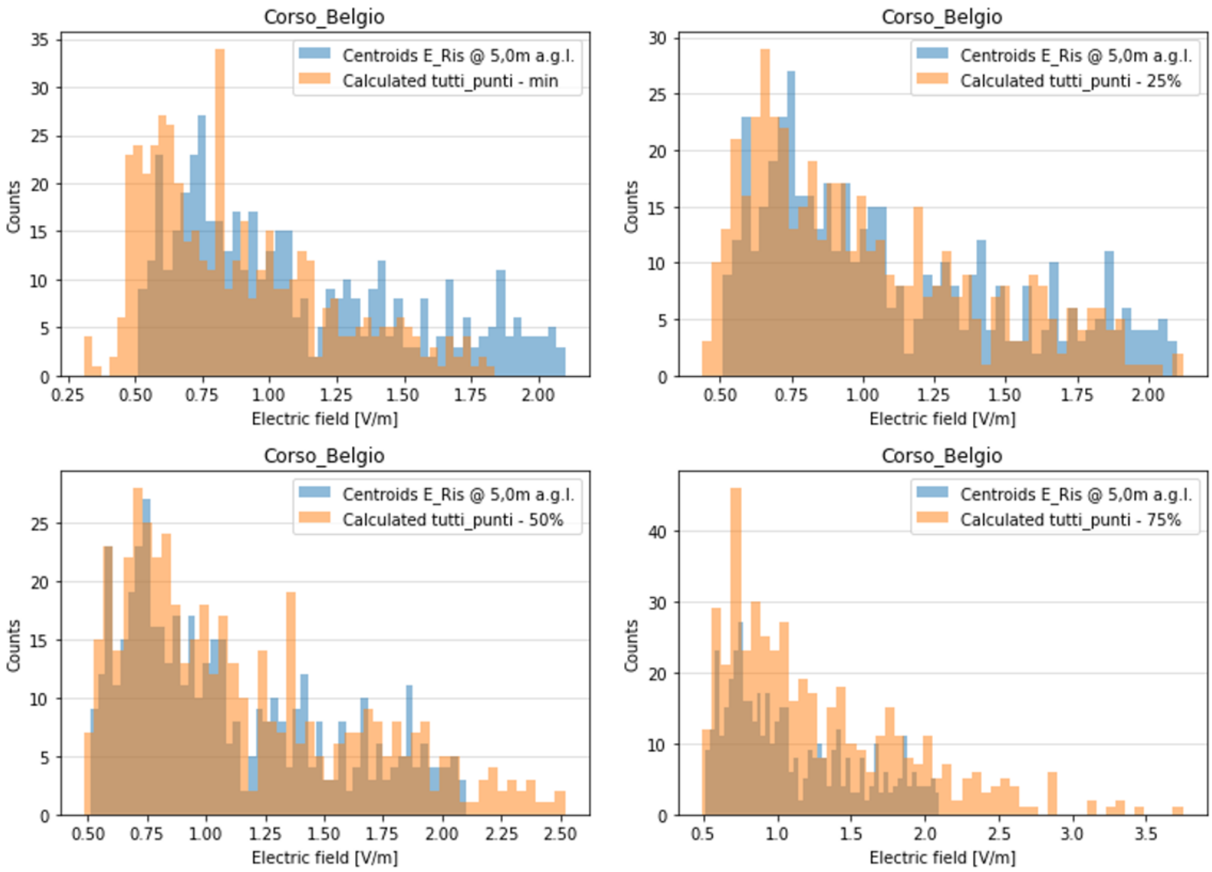

Figure B.1: “Corso Belgio” area of interest. Comparison between the distribution of the simulated electric field values at the centroid points at a height of 5,0 m a.g.l. (light blue) with the distributions of the following statistical indicators obtained from the three-dimensional grids (orange): A - minimum value, B - 25th percentile, C - 50th percentile, D - 75th percentile.

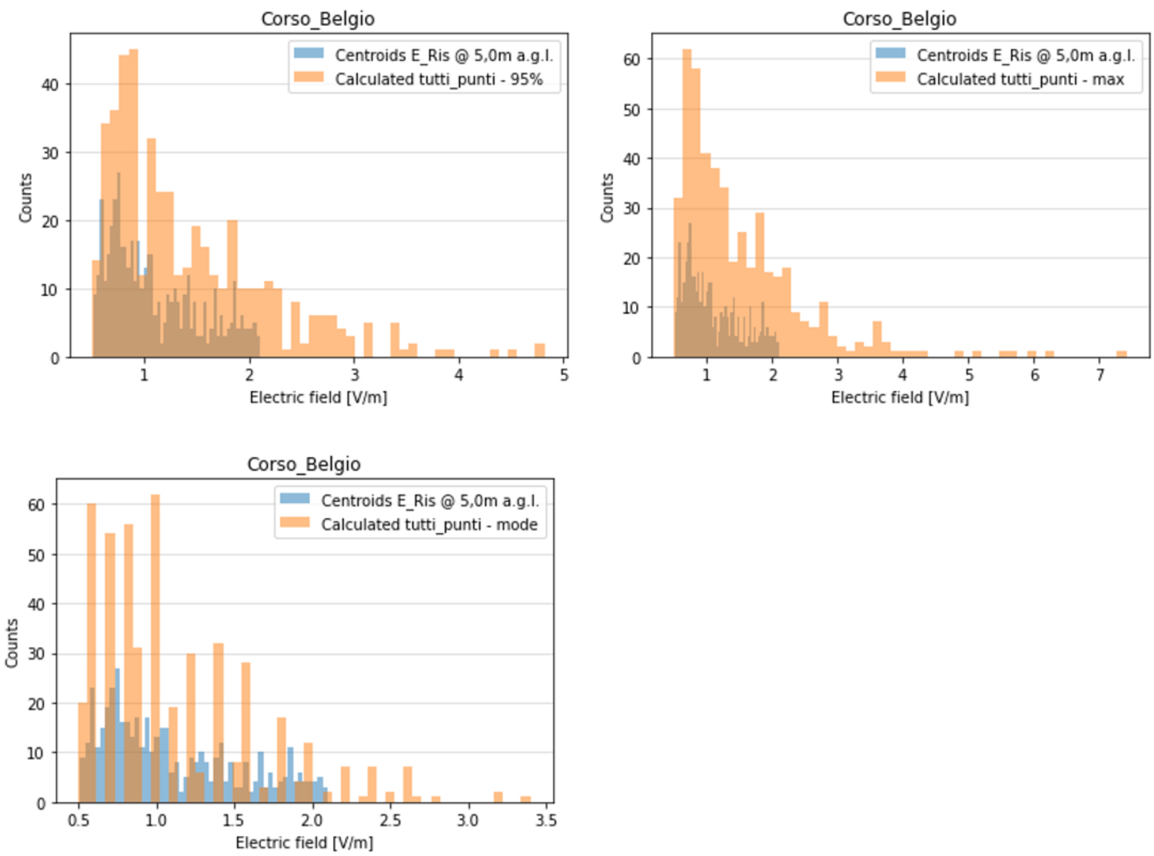

Figure B.2: "Corso Belgio" area of interest. Comparison between the distribution of the simulated electric field values at the centroid points at a height of 5,0 m a.g.l. (light blue) with the distributions of the following statistical indicators obtained from the three-dimensional grids (orange): A - 95th percentile, B - maximum value, C - mode.

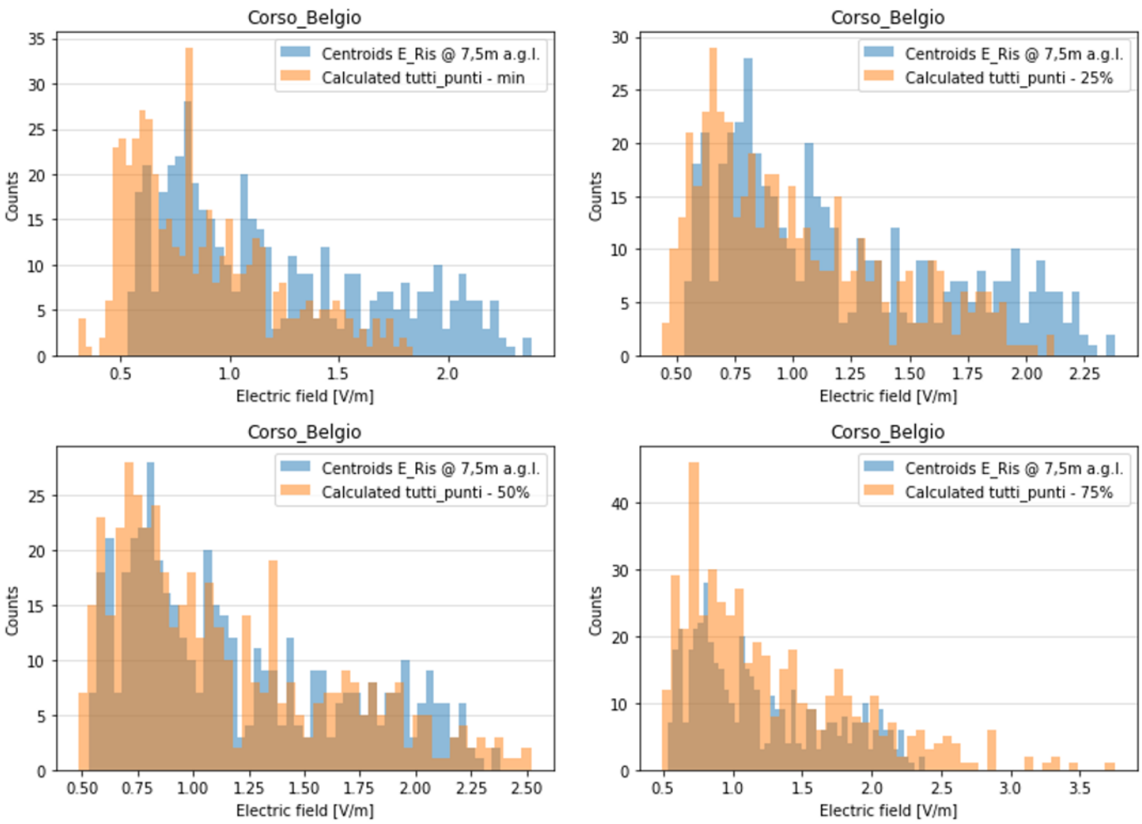

Figure B.3: “Corso Belgio” area of interest. Comparison between the distribution of the simulated electric field values at the centroid points at a height of 7,5 m a.g.l. (light blue) with the distributions of the following statistical indicators obtained from the three-dimensional grids (orange): A - minimum value, B - 25th percentile, C - 50th percentile, D - 75th percentile.

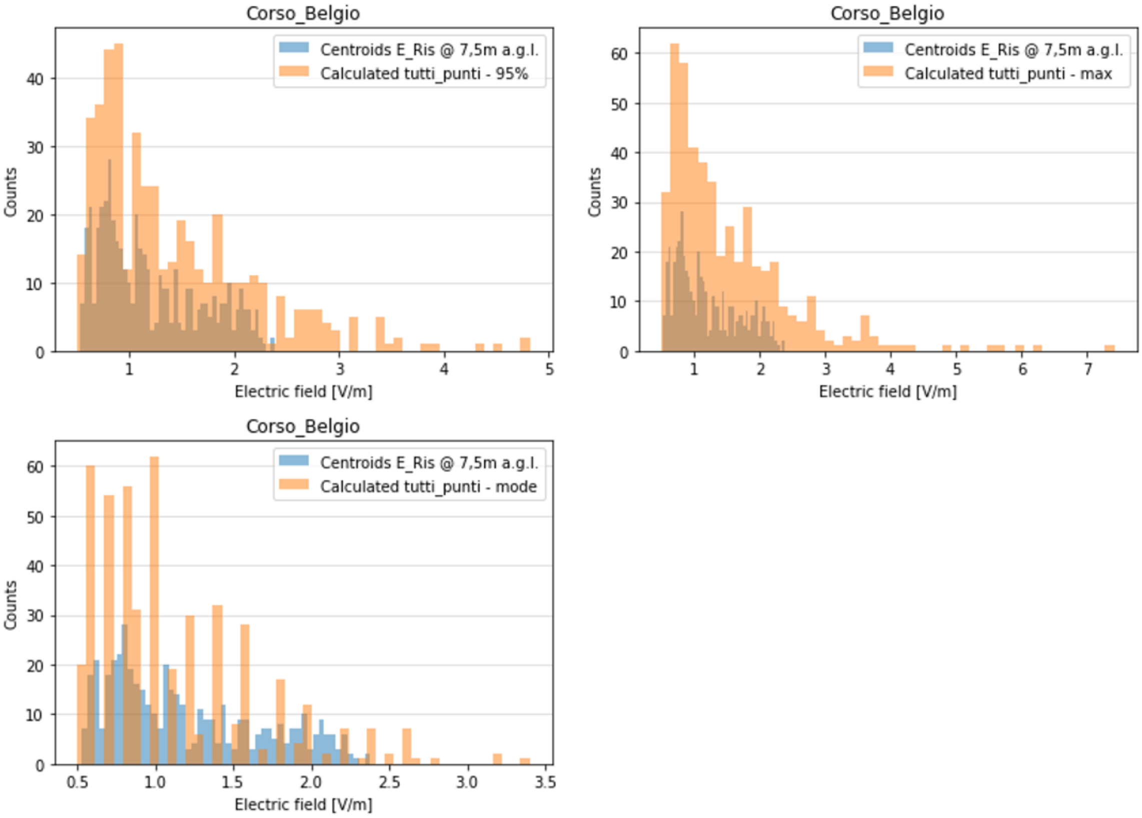

Figure B.4: "Corso Belgio" area of interest. Comparison between the distribution of the simulated electric field values at the centroid points at a height of 7,5 m a.g.l. (light blue) with the distributions of the following statistical indicators obtained from the three-dimensional grids (orange): A - 95th percentile, B - maximum value, C - mode.

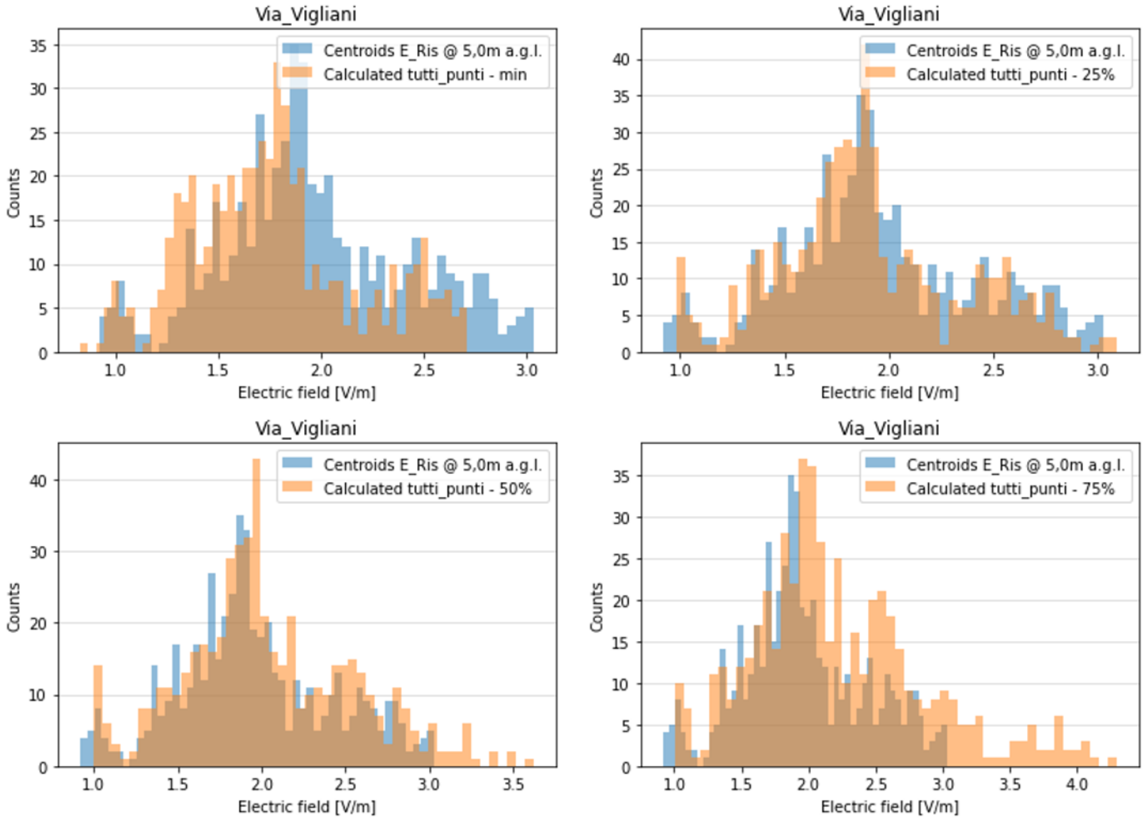

Figure B.5: "Via Vigliani" area of interest. Comparison between the distribution of the simulated electric field values at the centroid points at a height of 5,0 m a.g.l. (light blue) with the distributions of the following statistical indicators obtained from the three-dimensional grids (orange): A - minimum value, B - 25th percentile, C - 50th percentile, D - 75th percentile.

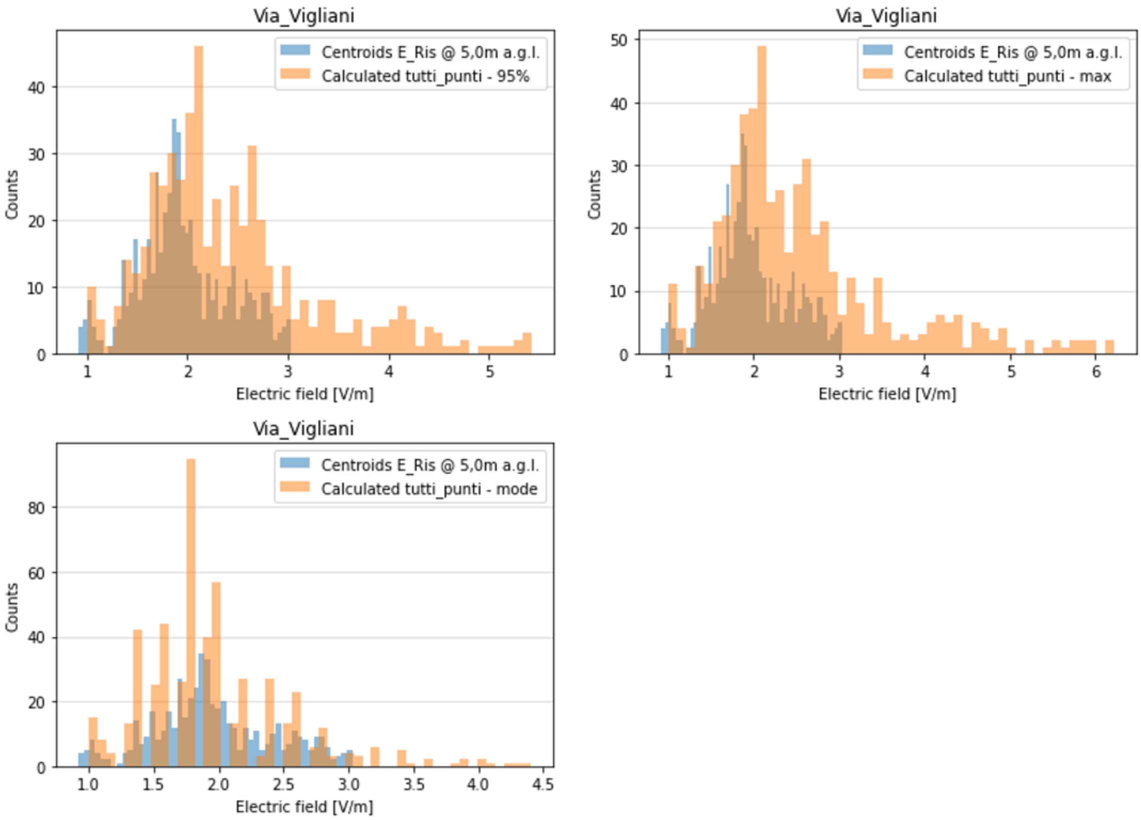

Figure B.6: "Via Vigliani" area of interest. Comparison between the distribution of the simulated electric field values at the centroid points at a height of 5,0 m a.g.l. (light blue) with the distributions of the following statistical indicators obtained from the three-dimensional grids (orange): A - 95th percentile, B - maximum value, C - mode.

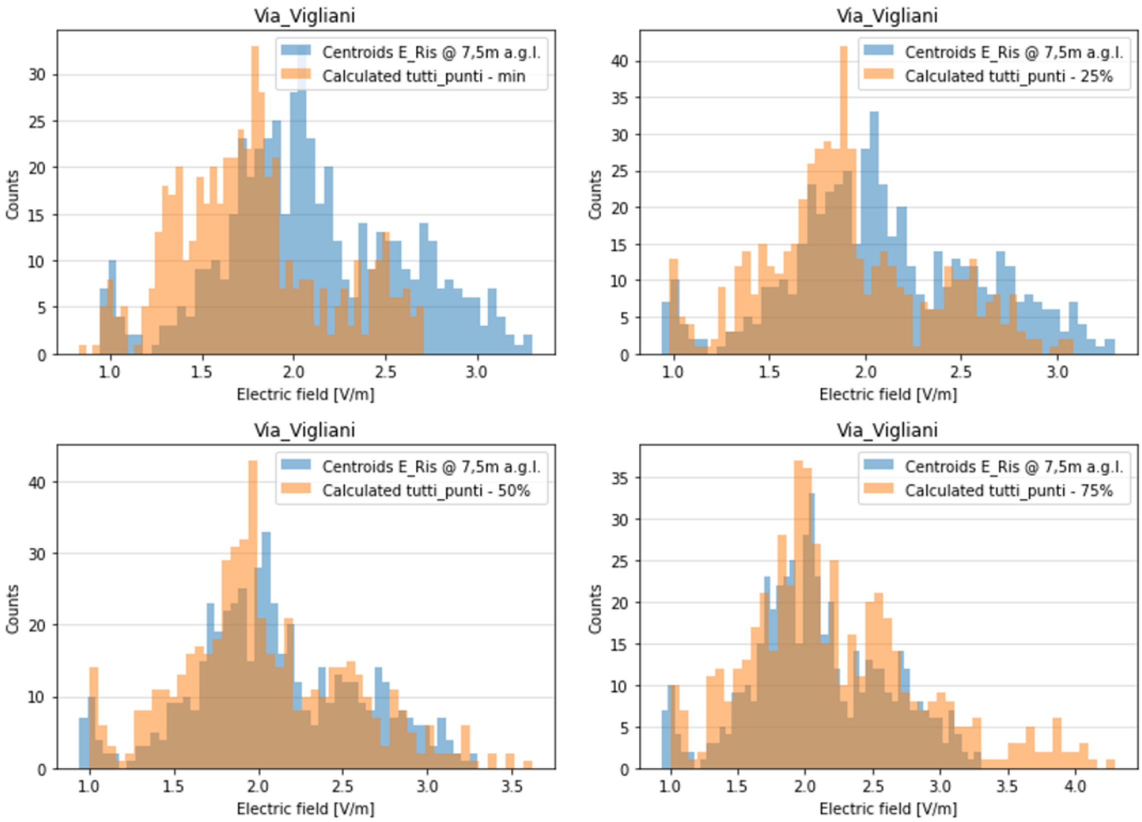

Figure B.7: "Via Vigliani" area of interest. Comparison between the distribution of the simulated electric field values at the centroid points at a height of 7,5 m a.g.l. (light blue) with the distributions of the following statistical indicators obtained from the three-dimensional grids (orange): A - minimum value, B - 25th percentile, C - 50th percentile, D - 75th percentile.

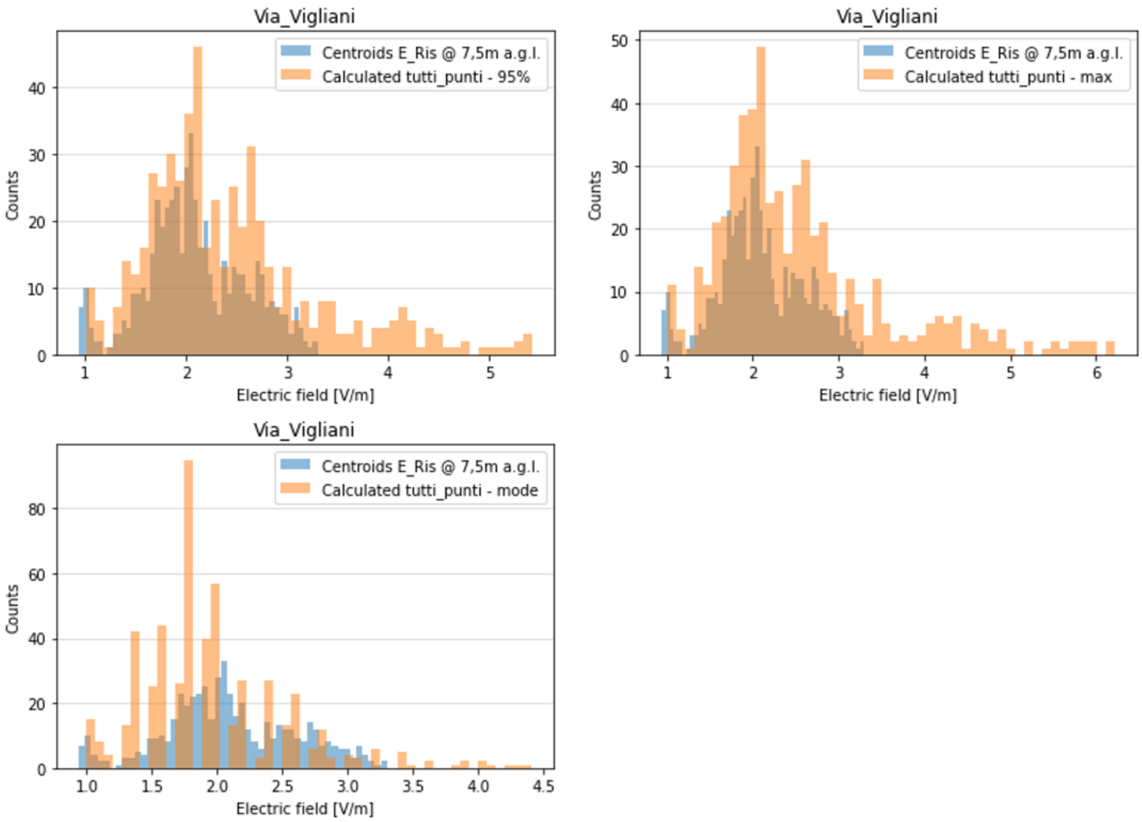

Figure B.8: “Via Vigliani” area of interest. Comparison between the distribution of the simulated electric field values at the centroid points at a height of 7,5 m a.g.l. (light blue) with the distributions of the following statistical indicators obtained from the three-dimensional grids (orange): A - 95th percentile, B - maximum value, C - mode.

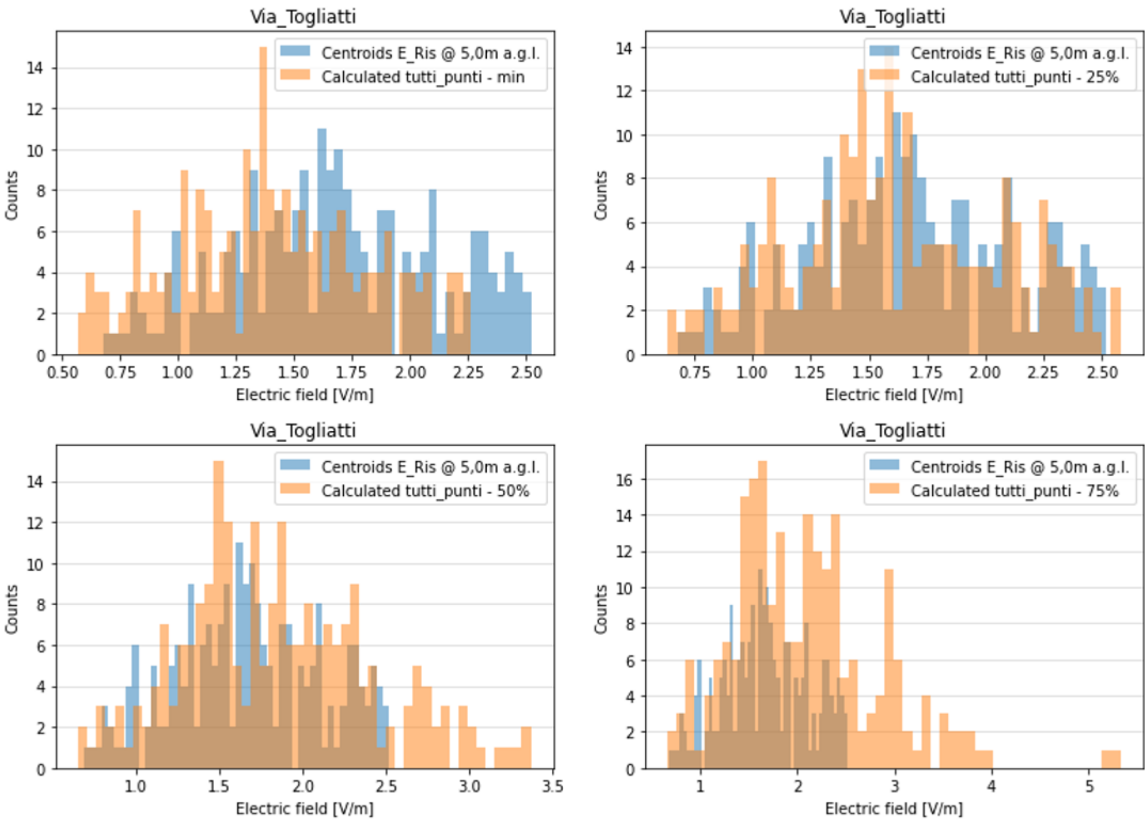

Figure B.9: "Via Togliatti" area of interest. Comparison between the distribution of the simulated electric field values at the centroid points at a height of 5,0 m a.g.l. (light blue) with the distributions of the following statistical indicators obtained from the three-dimensional grids (orange): A - minimum value, B - 25th percentile, C - 50th percentile, D - 75th percentile.

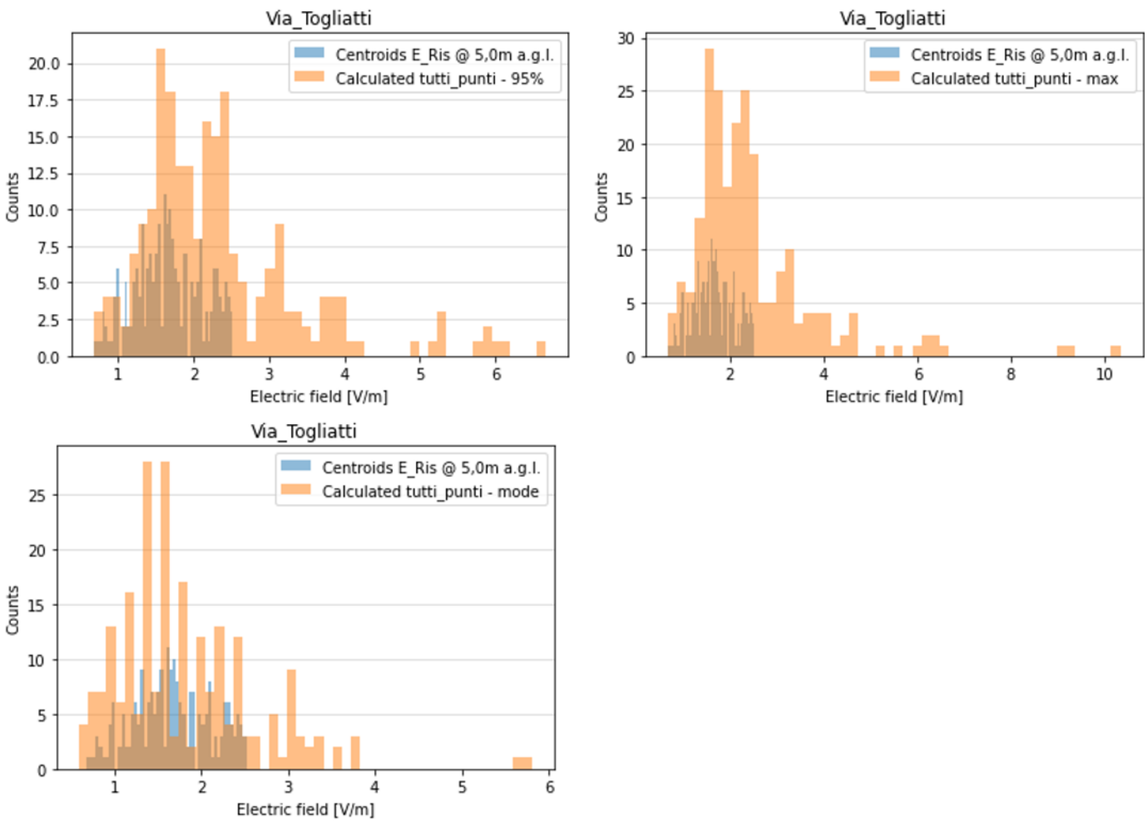

Figure B.10: "Via Togliatti" area of interest. Comparison between the distribution of the simulated electric field values at the centroid points at a height of 5,0 m a.g.l. (light blue) with the distributions of the following statistical indicators obtained from the three-dimensional grids (orange): A - 95th percentile, B - maximum value, C - mode.

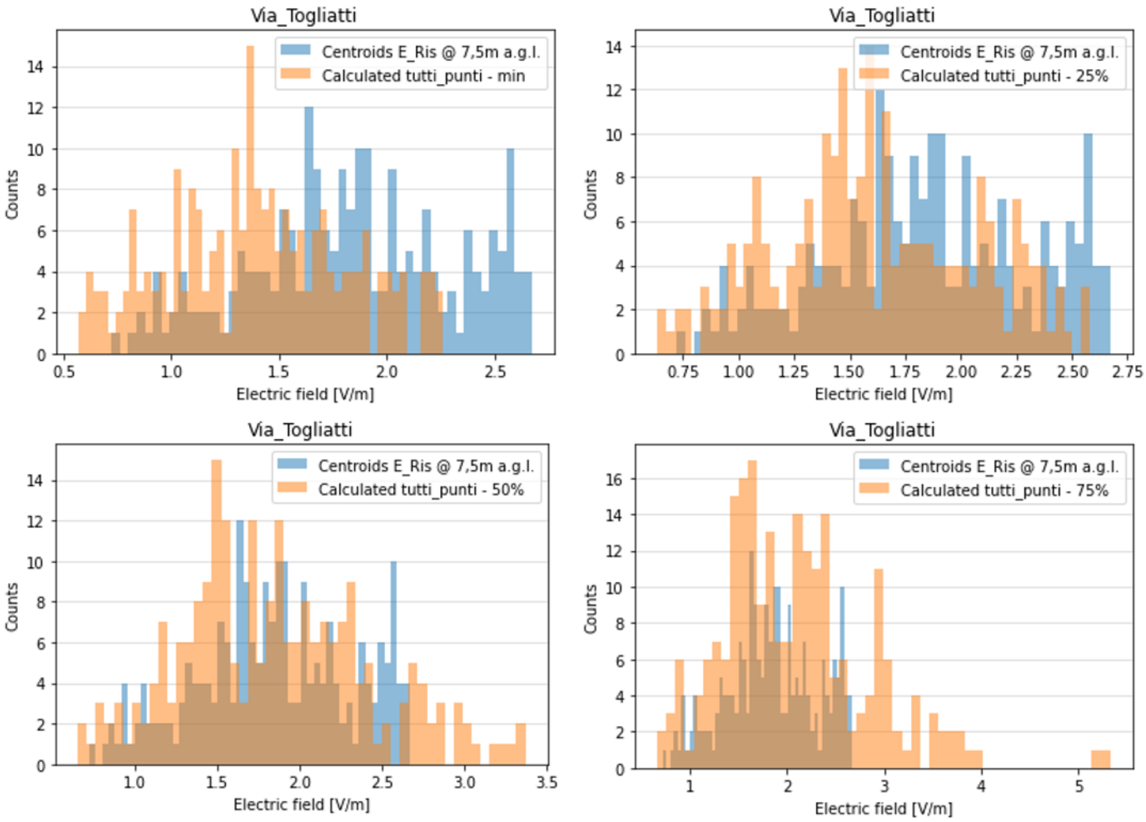

Figure B.11: "Via Togliatti" area of interest. Comparison between the distribution of the simulated electric field values at the centroid points at a height of 7,5 m a.g.l. (light blue) with the distributions of the following statistical indicators obtained from the three-dimensional grids (orange): A - minimum value, B - 25th percentile, C - 50th percentile, D - 75th percentile.

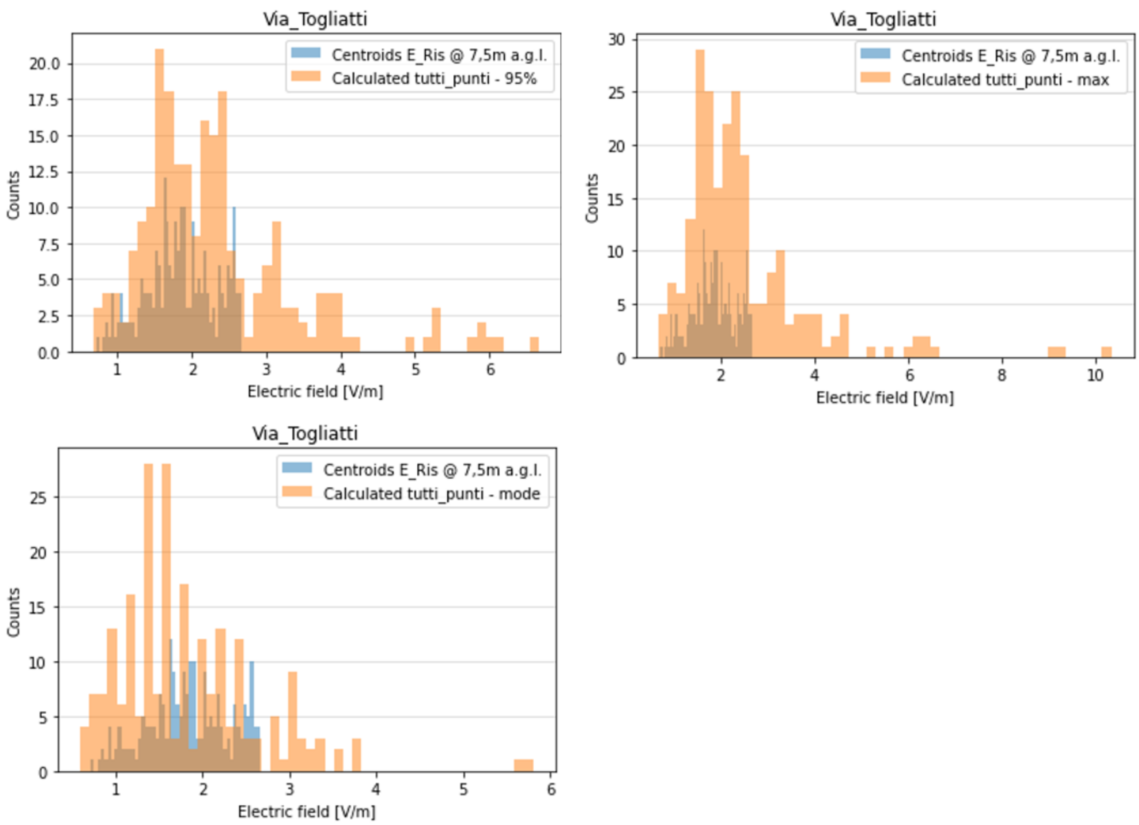

Figure B.12: “Via Togliatti” area of interest. Comparison between the distribution of the simulated electric field values at the centroid points at a height of 7,5 m a.g.l. (light blue) with the distributions of the following statistical indicators obtained from the three-dimensional grids (orange): A - 95th percentile, B - maximum value, C - mode.

Bibliography

[1] Ministero dell'Ambiente e della Sicurezza Energetica. *Programma di attività di ricerca CEM.* 2021, June 22th. URL: `https://www.mase.gov.it/pagina/programma-di-attivita-di-ricerca-cem`

[2] Fusillo G. *Appunti del Modulo di Fisica Ambientale - corso Chimica e Fisica Ambientale.* Università degli Studi di Urbino Carlo Bo, Corso di Laurea Scienze per l'Ambiente e la Natura. 2013.

[3] Lagorio S., Anglesio L., d'Amore G., Marino C., Scarfì M.R.. *Radiazioni a radiofrequenze e tumori: sintesi delle evidenze scientifiche* Istituto Superiore di Sanità Rapporti ISTISAN 19/11. 2019; ii; 111 p.

[4] IEC 62369-1:2008 *Evaluation of human exposure to electromagnetic fields from short range devices (SRDs) in various applications over the frequency range 0 GHz to 300 GHz - Part 1: Fields produced by devices used for electronic article surveillance, radio frequency identification and similar systems.* 1st ed. TC 106 - Methods for the assessment of electric, magnetic and electromagnetic fields associated with human exposurers. 2008, August 28th. 149 p.

[5] Curcuruto S., Baratta C., Logorelli M., d'Amore G., Anglesio L., Adda S. et all. *Documento istruttorio a supporto del legislatore per le modifiche del quadro normativo sui CEM-RF elaborato da ISPRA-ARPA e FUB.* Istituto Superiore per la Protezione e la Ricerca Ambientale. Rapporti 95/2013. 2013, November. 46 p.

[6] Anglesio L., Benedetto A., Bonino A., Colla D., Martire F., Saudino Fusette S., d'Amore G. *Population exposure to electromagnetic fields generated by radio base*

stations: evaluation of the urban background by using provisional model and instrumental measurements. Radiation protection dosimetry. 2001; 97(4), 355–358. URL: https://doi.org/10.1093/oxfordjournals.rpd.a006688

[7] Andreuccetti D. *Campi elettromagnetici ad alta frequenza.* Firenze. Istituto di Fisica Applicata Nello Carrara - Consiglio Nazionale delle Ricerce (IFAC-CNR). 2010.

[8] L'Angolo della Telefonia. *L'evoluzione della rete mobile.* URL: https://www.langolodellatelefonia.it/levoluzione-della-rete-mobile/ [Accessed 2023, October 1st]

[9] Wikipedia. *MIMO.* URL: https://en.wikipedia.org/w/index.php?title=MIMO&oldid=1179776316 [Accessed 2023, October 15th]

[10] Delibera n. 231/18/CONS *Procedure per l'assegnazione e regole per l'utilizzo delle frequenze disponibili nelle bande 694-790 MHz, 3600-3800 MHz e 26.5-27.5 GHz per sistemi terrestri di comunicazioni elettroniche al fine di favorire la transizione verso la tecnologia 5G, ai sensi della legge 27 dicembre 2017, n. 205.* AGCOM Agenzia per le Garanzie nelle Comunicazioni. 2018, May 8th.ì

[11] Bertin G., Buracchini E., Gianola P. *RF Sources – Exposure Assessment of Mobile Phone Base Stations: 5th-Generation Wireless Communication Systems.* Licitra G., d'Amore G., Magnoni M. (Eds.). *Physical Agents in the Environment and Workplace: Noise and Vibrations, Electromagnetic Fields and Ionizing Radiation.* 1st ed. CRC Press. 2018; (8): 167-178. URL: https://doi.org/10.1201/b22231

[12] Centro interuniversitario Interazioni tra Campo Elettromagnetici e Biosistemi ICEmB *Elettromagnetismo, innovazione tecnologica e salute.* Genova. 2018.

[13] IEC 62232:2022 *Determination of RF field strength, power density and SAR in the vicinity of base stations for the purpose of evaluating human exposure.* 3rd ed. TC 106 - Methods for the assessment of electric, magnetic and electromagnetic fields associated with human exposurers. 2022, October 14th. 736 p.

[14] IEC TR 62669:2019 *Case studies supporting IEC 62232 - Determination of RF field strength, power density and SAR in the vicinity of radiocommunication base stations for the purpose of evaluating human exposure.* 2nd ed. TC 106 - Methods for the

assessment of electric, magnetic and electromagnetic fields associated with human exposurers. 2019, April 5th. 124 p.

[15] Chiaraviglio L., Bartoletti S., Blefari-Melazzi N., Lodovisi C., Moretti A., Zampognaro F., Alouini M.S. *Measuring EMF and Throughput Before and After 5G Service Activation in a Residential Area.* IEEE Open Journal of the Communications Society. 2023; 4: 1179-1195. URL: https://doi.org/10.1109/OJCOMS.2023.3277782

[16] Mathiou M. *Misure di campo elettrico generato in ambiente di vita da Stazioni Radio Base UMTS e analisi della relazione con la potenza in antenna* [Tesi di Laurea Magistrale in Ingegneria delle Telecomunicazioni]. Politecnico di Torino, III Facoltà di Ingegneria dell'Informazione; 2011.

[17] CEI 211-10 *Guida alla realizzazione di una Stazione Radio Base per rispettare i limiti di esposizione ai campi elettromagnetici in alta frequenza.* CEI-CT106. 2004, January; issue num. 7184: 28 p.

[18] Leeka I. K., Gordon L. H., Gail L. B. *The precautionary principle and EMF: implementation and evaluation.* Journal of Risk Research. 2001; 4:2: 113-125. URL: https://doi.org/10.1080/136698701750128042

[19] Treccani. *SAR.* URL: https://www.treccani.it/enciclopedia/sar/ [Accessed 2023, October 17th]

[20] Calderari S. *Campi Elettromagnetici a Radiofrequenza e Radioprotezione* [Tesi di Laurea in Ingegneria dell'Informazione]. Università degli Studi di Padova, Dipartimento di Ingegneria dell'Informazione; 2020.

[21] Santagiustina M. *Appunti del corso Campi Elettromagnetici e Propagazione.* Università degli Studi di Padova, Laurea in Ingegneria dell'Informazione. 2019.

[22] Moccaldi R. *Effetti sulla salute in relazione ai campi elettromagnetici a radiofrequenza (telefonia mobile).* Consiglio Nazionale delle Ricerche - Servizio di Prevenzione e Protezione. 1997.

[23] IARC Working Group on the Evaluation of Carcinogenic Risks to Humans. *Non-Ionizing Radiation, Part 2: Radiofrequency Electromagnetic Fields.*

Lyon (FR): International Agency for Research on Cancer; (*IARC Monographs on the Evaluation of Carcinogenic Risks to Humans*, No. 102.). 2013. URL: https://www.ncbi.nlm.nih.gov/books/NBK304630/

[24] World Health Organization *Radiation: Electromagnetic fields Q&A*. WHO. 2016, August 4th. URL: https://www.who.int/news-room/questions-and-answers/item/radiation-electromagnetic-fields

[25] Treccani. *Radioprotezione*. URL: https://www.treccani.it/enciclopedia/radioprotezione/ [Accessed 2023, October 19th]

[26] International Commission on Non-Ionizing Radiation Protection ICNIRP. *Guidelines for Limiting Exposure to Electromagnetic Fields (100 kHz to 300 GHz)*. Health Physics. 2020, May; 118(5): 483-524. URL: https://doi.org/10.1097/HP.0000000000001210

[27] D.P.C.M. 8 luglio 2003 *Fissazione dei limiti di esposizione, dei valori di attenzione e degli obiettivi di qualità per la protezione della popolazione dalle esposizioni a campi elettrici, magnetici ed elettromagnetici generati a frequenze comprese tra 100 kHz e 300 GHz*. Gazzetta Ufficiale Serie Generale n.199 del 28-08-2003.

[28] Legge 17 dicembre 2012, n. 221 *Conversione in legge, con modificazioni, del decreto-legge 18 ottobre 2012, n. 179, recante ulteriori misure urgenti per la crescita del Paese*. Gazzetta Ufficiale n.294 del 18-12-2012 - Suppl. Ordinario n. 208, URL: https://www.normattiva.it/uri-res/N2Ls?urn:nir:stato:legge:2012-12-17;221

[29] Legge 22 febbraio 2001, n. 36 *Legge quadro sulla protezione dalle esposizioni a campi elettrici, magnetici ed elettromagnetici*. Gazzetta Ufficiale n.55 del 07-03-2001. URL: https://www.normattiva.it/uri-res/N2Ls?urn:nir:stato:legge:2001-02-22;36!vig=

[30] CEI 211-7/E *Guida per la misura e per la valutazione dei campi elettromagnetici nell'intervallo di frequenza 10 kHz - 300 GHz, con riferimento all'esposizione umana. Appendice E: Misura del campo elettromagnetico da stazioni radio base per sistemi di*

comunicazione mobile (2G, 3G, 4G, 5G). CEI-CT106. 2019, November; issue num. 17160: 36 p.

[31] D.M. 7 dicembre 2016 *Approvazione delle Linee guida, predisposte dall'ISPRA e dalle ARPA/APPA, relativamente alla definizione delle pertinenze esterne con dimensioni abitabili*. Gazzetta Ufficiale Serie Generale n.19 del 24-01-2017.

[32] D. Lgs. 1 agosto 2003, n. 259 *Codice delle comunicazioni elettroniche*. Gazzetta Ufficiale n.214 del 15-09-2003 - Suppl. Ordinario n. 150. URL: `https://www.normattiva.it/uri-res/N2Ls?urn:nir:stato:decreto.legislativo:2003-08-01;259`

[33] D.M. 2 dicembre 2014 *Linee guida, relative alla definizione delle modalita' con cui gli operatori forniscono all'ISPRA e alle ARPA/APPA i dati di potenza degli impianti e alla definizione dei fattori di riduzione della potenza da applicare nelle stime previsionali per tener conto della variabilita' temporale dell'emissione degli impianti nell'arco delle 24 ore*. Gazzetta Ufficiale Serie Generale n.296 del 22-12-2014.

[34] Legge 28 giugno 2016, n. 132 *Istituzione del Sistema nazionale a rete per la protezione dell'ambiente e disciplina dell'Istituto superiore per la protezione e la ricerca ambientale*. Gazzetta Ufficiale n.166 del 18-07-2016. URL: `https://www.normattiva.it/uri-res/N2Ls?urn:nir:stato:legge:2016;132~art2`

[35] Smeets E., Weterings R. *Environmental indicators: typology and overview*. European Environment Agency EEA, Technical report No 25/1999. 1999, September 7th. URL: `https://www.eea.europa.eu/ds_resolveuid/ZATOEJRPDX`

[36] Arpa FVG. *La logica DPSIR*. URL: `https://www.arpa.fvg.it/temi/temi/modellistica-ambientale-crma/imparia mo-insieme/la-logica-dpsir/` [Accessed 2023, October 20th]

[37] Arpa Piemonte. *Indicatori nello schema DPSIR*. URL: `https://www.arpa.piemonte.it/reporting/indicatori-on_line/indicatori-nello-schema-dpsir` [Accessed 2023, October 20th]

[38] Decreto Direttoriale MATTM 156-RIN del 16 novembre 2018 *Programma di promozione di attività di ricerca e di sperimentazione tecnicoscientifica, nonché di coordinamento dell'attività di raccolta, di elaborazione e di diffusione dei dati al fine di approfondire i rischi connessi all'esposizione a campi elettromagnetici a bassa e alta frequenza.* 2018.

[39] Scientific Committee on Emerging Newly Identified Health Risks SCENIHR. *Opinion on potential health effects of exposure to electromagnetic fields.* Bioelectromagnetics. 2015; 36(6): 480–484. URL: `https://doi.org/10.1002/bem.21930`

[40] Poli S., Trotti F., Ugolini R., Adda S., d'Amore G., Facta S. *Popolamento dell'indicatore di esposizione della popolazione ai campi elettromagnetici (ELF/RF): strumenti, procedure, esempi.* APAT - Agenzia per la Protezione dell'Ambiente e per i servizi Tecnici - Dipartimento Stato dell'Ambiente e Metrologia Ambientale. RTI CTN_AGF 2/2005. 2005; 60 p.

[41] Adda S., d'Amore G., Facta S., Poli S., Trotti F., Ugolini R. *Indicatore di esposizione della popolazione ai campi elettromagnetici (ELF/RF): costruzione e popolamento.* Atti dell'evento Controllo ambientale degli agenti fisici: dal monitoraggio alle azioni di risanamento e bonifica, Sessione Campi Elettromagnetici - Strumenti di gestione del controllo ambientale. 2006. URL: `https://www.arpa.piemonte.it/arpa-comunica/events/eventi-2006/controllo-ambientale-degli-agenti-fisici-dal-monitoraggio-alle-azioni-di-risanamento-e-bonifica/`

[42] Baglioni O., Consalvi M.G., Tosti C. *Valutazione della popolazione esposta a campi elettromagnetici a radiofrequenza.* Micron Arpa Umbria. 2008, May; V(9): 46-49.

[43] Wikipedia. *Storey.* URL: `https://en.wikipedia.org/w/index.php?title=Storey&oldid=1174585735` [Accessed 2023, September 9th]

[44] Comune di Bologna - Sistema Informativo Territoriale (SIT) *CARTA TECNICA COMUNALE - Edifici volumetrici.* Open Data Comune di Bologna. URL: `https://opendata.comune.bologna.it/explore/dataset/c_a944ctc_edifici_pl/information/?disjunctive.descrizion&disjunctive.origine` [Accessed 2023, October 22th]

[45] Unione Valle del Savio - Servizio SIT-Statistica *Edifici del Comune di Cesena*. Open Data Unione dei Comuni Valle del Savio. URL: https://dati.unionevallesavio.it/opendata/17 [Accessed 2023, November 2nd]

[46] Geoportale e governo del territorio - Città di Torino. *Dati di base - Carta Tecnica - Immobili e Antropizzazioni*. URL: http://geoportale.comune.torino.it/geocatalogocoto/?sezione=catalogo [Accessed 2023, September 30th]

[47] QGIS.org *QGIS Geographic Information System. Open Source Geospatial Foundation Project*. 2023. URL: http://qgis.org

[48] Geoportale Regione Piemonte. *BDTRE: La Base Dati Territoriale di Riferimento degli Enti piemontesi*. URL: https://www.geoportale.piemonte.it/cms/bdtre/bdtre-2 [Accessed 2023, September 30th]

[49] Istituto Nazionale di Statistica ISTAT. *Censimento permanente della popolazione e delle abitazioni*. URL: https://esploradati.censimentopopolazione.istat.it/ [Accessed 2023, October 1th]

[50] Istituto Nazionale di Statistica ISTAT. *Dati per sezioni di censimento*. URL: https://www.istat.it/it/archivio/285267 [Accessed 2023, October 2nd]

[51] Istituto Nazionale di Statistica ISTAT. *Basi territoriali e variabili censuarie*. 2017, January 14th. URL: https://www.istat.it/it/archivio/104317 [Accessed 2023, October 3rd]

[52] Direzione Centrale delle Rilevazioni Censuarie e Registri Statistici (DCCR). *5 - Le sezioni di censimento*. Balistreri A. (A cura di), Atti del 9° Censimento generale dell'industria e dei servizi e Censimento delle istituzioni non profit. Istituto Nazionale di Statistica ISTAT. 2015; p. 17-20. URL: https://www.istat.it/it/files//2016/02/Atti-CIS_Fascicolo_5.pdf

[53] Portale CEM - campi elettromagnetici in Piemonte, Arpa Piemonte. *Campi elettromagnetici - La mappa degli impianti, i risultati del monitoraggio e i progetti in*

Piemonte. URL: https://webgis.arpa.piemonte.it/secure_apps/portale_cem/ [Accessed 2023, September 30th]

[54] Arpa Piemonte. *Portale CEM sui campi elettromagnetici: pubblicati nuovi dati*. URL: https://www.arpa.piemonte.it/news/portale-sui-campi-elettromagnetici-ora-disponibili-i-dati-tecnici-degli-impianti-per-telecomunicazione-e-la-valutazione-teorica-dei-campi-elettrici [Accessed 2023, October 5th]

[55] Portale CEM - campi elettromagnetici in Piemonte, Arpa Piemonte. *Arpa Piemonte - Campi elettromagnetici ad alta frequenza - Metadati*. 2020, February 24th. URL: https://webgis.arpa.piemonte.it/gpserver_arpa/catalog/search/resource/details.page?uuid=arlpa_to:S_CEM_RF_2020-02-24-14:16 [Accessed 2023, October 5th]

[56] Adda S., Chiaraviglio L., Franci D., Lodovisi C., Pasquino N., Pavoncello S., Pedroli C., Pelosini R. *High Noon for Mobile Networks: Short-Time EMF Measurements to Capture Daily Exposure. IEEE Transactions on Instrumentation and Measurement*. 2023; vol. 72: pp. 1-10, Art no. 5504410. www.doi.org/10.1109/TIM.2023.3324354